

**Towards Scalable, Flexible, and Interpretable
Self-Supervised Learning for Multiview
Biomedical Data**

by

James Chapman

December 2023

PhD Thesis

i4health CDT

University College London

Declaration

I, James Chapman, confirm that the work presented in my thesis is my own. Where information has been derived from other sources, I confirm that this has been indicated in the thesis.

Abstract

Biomedical data are critical for enhancing our understanding and practices in medicine and healthcare. Yet, the complexity, heterogeneity, high-dimensionality, and label scarcity in these datasets present significant analytical challenges. This thesis introduces innovative approaches to self-supervised learning (SSL), focusing on multiview SSL, where data are represented by multiple distinct feature groups or modalities. To overcome these challenges, self-supervised learning (SSL) has emerged as a promising paradigm for learning from unlabeled data by leveraging inherent structures or patterns in the data. SSL methods can exploit different forms of supervision signals derived from the data itself, such as contrastive learning, reconstruction, prediction, or clustering. SSL methods can also benefit from deep neural networks that can learn expressive and flexible representations from complex and high-dimensional data. Central to this thesis are four research questions addressing the enhancement of multiview SSL: (1) How can regularization or prior knowledge be integrated into subspace learning methods for improved quality and robustness? (2) How can the data generation process aid in interpreting multiview models and validating their quality? (3) How can subspace learning methods be scaled up to large datasets using gradient-based optimization techniques? (4) How can these methods be extended to nonlinear functions with deep neural networks? Our contributions include: A framework for incorporating various forms of regularization or prior knowledge into subspace learning, enhancing the quality and robustness of these methods. A unification of simulated data generation literature for multiview learning, facilitating model interpretation and quality validation. A scalable and flexible subspace learning method for multiview SSL, adaptable to large-scale datasets through modern optimization techniques. An innovative extension of subspace learning to nonlinear functions using deep neural networks. A high quality open source software implementation of the canonical correlation analysis family of methods, enabling reproducible research and facilitating adoption by the community.

This research advances the field of biomedical data analysis by providing scalable, flexible, and interpretable solutions for multiview SSL challenges, harnessing the power of modern computational techniques and deep learning and making them accessible through open source software.

Impact Statement

The theoretical contributions of this thesis will allow researchers to scale canonical correlation analysis methods to much larger datasets. This will be of huge benefit as access to large biomedical datasets becomes more readily available. Through high quality open source implementations of a number of canonical correlation analysis methods, this thesis will also facilitate reproducible research and adoption by the Python community, which will be of huge benefit as the Python programming language is becoming the de facto standard for data science and machine learning. Through this mechanism, work in this thesis has already had an impact in fields as diverse as process monitoring, geothermal flow, and medical imaging.

List of Publications

First Author Peer Reviewed Conference Proceedings

Chapman, James, Lennie Wells, and Ana Lawry Aguila (2023). *Efficient Algorithms for the CCA Family: Unconstrained Objectives with Unbiased Gradients*. arXiv: 2310.01012 [cs.LG].

First Author Peer Reviewed Conference workshop and Abstract

Chapman, James and Lennie Wells (2023). “CCA with Shared Weights for Self-Supervised Learning”. In: *NeurIPS 2023 Workshop: Self-Supervised Learning - Theory and Practice*. URL: <https://openreview.net/forum?id=7rYseRZ7Z3>.

James Chapman Janaina Mourao-Miranda, John Shawe-Taylor (n.d.). *A Framework for Regularised Canonical Correlation Analysis by Alternating Least Squares*.

First Author Pre-Print

Chapman, James, Ana Lawry Aguila, and Lennie Wells (2022). “A Generalized EigenGame with Extensions to Multiview Representation Learning”. In: *arXiv preprint arXiv:2211.11323*.

Co-Authored Peer Reviewed Journal

Mihalik, Agoston, James Chapman, et al. (2022). “Canonical correlation analysis and partial least squares for identifying brain-behaviour associations: a tutorial

and a comparative study". In: *Biological Psychiatry: Cognitive Neuroscience and Neuroimaging*.

Co-Authored Peer Reviewed Conference Proceedings

Lawry Aguila, Ana, James Chapman, and Andre Altmann (2023). "Multi-modal Variational Autoencoders for Normative Modelling Across Multiple Imaging Modalities". In: *International Conference on Medical Image Computing and Computer-Assisted Intervention*. Springer Nature Switzerland Cham, pp. 425–434.

Lawry Aguila, Ana, James Chapman, Mohammed Janahi, et al. (2022). "Conditional VAEs for Confound Removal and Normative Modelling of Neurodegenerative Diseases". In: *International Conference on Medical Image Computing and Computer-Assisted Intervention*. Springer Nature Switzerland Cham, pp. 430–440.

Software

Mihalik, Agoston, Nils Winter, et al. (Oct. 2022). *CCA/PLS Toolkit*. Version 1.0.0. URL: https://github.com/anaston/cca_pls_toolkit.

Townsend, Florence, James Chapman, and James Cole (Nov. 2023). *florencejt/fusilli: Fusilli v1.0.0*. Version v1.0.0. DOI: 10.5281/zenodo.10228564. URL: <https://doi.org/10.5281/zenodo.10228564>.

LIST OF FIGURES

II.1	Independent and Dependent Variable Model of Mental Health	25
II.2	Latent Variable Model of Mental Health.....	26
II.3	The Wisdom of Crowds.....	28
III.1	Comparison of the effect of OLS, Ridge, and PCA regularisation on the eigenvalues of the covariance matrix.....	51
III.2	HCP: Comparative out-of-sample canonical correlations among PCA, RCCA, ElasticNet, PLS, and SPLS models. The bars represent the correlation coefficients, indicating that Ridge CCA and Elastic Net models have superior performance over PLS and SPLS in capturing holdout correlation.....	61
III.3	HCP: Behavioural weights highlighting the top-8 positive and neg- ative non-imaging weights. Each subfigure represents a distinct model's weight distribution across various behavioural domains such as cognition, emotion, personality, substance use, alertness, and psy- chiatric and life function. The variations in the weight profiles across models reflect differing patterns of association with the behavioural traits considered in the study.....	68
III.4	HCP: Brain connectivity weights visualized through chord diagrams for multiple models. Each diagram portrays the 8 strongest positive (red to blue gradient) and negative (blue to red gradient) weights, grouped by the Yeo 7 network parcellation.....	69
III.5	HCP: Pairwise correlation matrix of brain representations across different models. The high correlation coefficients between PCA, PLS, and SPLS indicate a significant overlap in the brain representations they produce, suggesting a bias of PLS toward principal components. Contrarily, the Ridge CCA and Elastic Net models show notably lower correlations with PCA, indicating that these models capture brain representations beyond the first principal components.	70

III.6 HCP: Pairwise correlation matrix of the brain and behaviour weights used by each model. Similar to the brain representations, PCA, PLS, and SPLS show a high correlation in their weights, indicating similarity in the factors they consider significant. The lower correlations observed for Ridge CCA and Elastic Net with PCA suggest that these models give importance to different aspects of the data, potentially capturing more nuanced relationships.....	71
III.7 ADNI: Comparative out-of-sample canonical correlations among PCA, RCCA, ElasticNet, PLS, and SPLS models. The bars represent the correlation coefficients, indicating that the Elastic Net models has superior performance over Ridge CCA, PLS, and SPLS in capturing holdout correlation.	71
III.8 ADNI: Bar plots of the behaviour weights for each model.	72
III.9 ADNI: Statistical maps of brain structure weights for each model.	73
III.10 ADNI: Correlation between the brain and behaviour representations for each model.....	74
III.11 ADNI: Correlation between the brain and behaviour weights for each model.	74
III.12 Time taken to fit each model.....	75
IV.1 Forward and Backward Multiview Models	79
IV.2 Example instances of correlated covariance matrices.	98
IV.3 Bar plots of the true and estimated weights and loadings for data generated from the implicit latent variable models with sparse weights. The left column shows the results for the identity covariance matrices, while the right column shows the results for the correlated covariance matrices.....	100
IV.4 Cosine similarity between the true and estimated weights and loadings for data generated from the implicit latent variable models with sparse weights. We plot each run as a point on a scatter plot with a log scale. The grey line indicates where the similarity between weights and loadings are equal.	101
IV.5 Bar plots of the true and estimated weights and loadings for data generated from the implicit latent variable models with sparse weights. The left column shows the results for the identity covariance matrices, while the right column shows the results for the correlated covariance matrices.....	103

IV.6	Cosine similarity between the true and estimated weights and loadings for data generated from the explicit latent variable models with sparse loadings. We plot each run as a point on a scatter plot with a log scale. The grey line indicates where the similarity between weights and loadings are equal.	104
IV.7	Varying signal to noise ratio with identity covariance matrices. We plot the performance of different levels of Regularized CCA from 0 (CCA) to 1 (PLS) for different sample sizes.	105
IV.8	Varying signal to noise ratio with correlated covariance matrices. We plot the performance of different levels of Regularized CCA from 0 (CCA) to 1 (PLS) for different sample sizes.....	105
V.1	Comparison of the complexity of PCA-CCA and CCA for varying numbers of samples and features.....	110
V.2	Comparison of the time taken to solve CCA using eigh and our CCA-EY method.	117
V.3	Stochastic CCA on MediaMill using PCC: Performance across varying mini-batch sizes. Shaded regions signify \pm one standard deviation around the mean of 5 runs.	119
V.4	Stochastic CCA on MediaMill: Training progress over a single epoch for mini-batch sizes 5, 100.....	119
V.5	Stochastic CCA on CIFAR using PCC: Performance across varying mini-batch sizes. Shaded regions signify \pm one standard deviation around the mean of 5 runs.	120
V.6	Stochastic CCA on CIFAR: Training progress over a single epoch for mini-batch sizes 5, 100.	121
V.7	Pearson correlations among PLS latent variables Z_k derived from UK Biobank data.....	123
V.8	Correlation between PLS brain representations Z and genetic risk scores for various disorders. AD=Alzheimer's disease, SCZ=Schizophrenia, BP=Bipolar, ADHD=Attention deficit hyperactivity disorder, ALS=Amyotrophic lateral sclerosis, PD=Parkinson's disease, EPI=Epilepsy. ns : $0.05 < p \leq 1$, * : $0.01 < p \leq 0.05$, ** : $0.001 < p \leq 0.01$, *** : $0.0001 < p \leq 0.001$	123
VI.1	Schematic of the DCCA approach highlighting the nonlinear transformation of data into correlated views.....	128

VI.2 Joint Embedding Data Generation Process	130
VI.3 Schematic of the encoder-projector setup in SSL	130
VI.4 Deep CCA on SplitMNIST: Comparison of methods across varying batch sizes.....	134
VI.5 Deep CCA on SplitMNIST: Learning progress over 50 epochs.	135
VI.6 Deep CCA on XRMB: Comparison of methods across varying batch sizes.....	135
VI.7 Deep CCA on XRMB: Learning progress over 50 epochs.	135
VI.8 Deep Multi-view CCA on mfeat: Comparison across various mini-batch sizes using the Validation TMCC metric.....	137
VI.9 Deep Multi-view CCA on mfeat: Learning progress over 100 epochs for batch sizes 50 and 100.....	138
VI.10 Learning curves for SSL-EY, Barlow Twins, and VICReg on CIFAR-100, depicting 1,000-epoch performance.....	139
VI.11 CIFAR 100 Projector Analysis: (a) Examining the impact of projector size on SSL-EY's performance. (b) Investigating the relationship between EY loss and classification accuracy.....	140
VI.12 Learning curves for SSL-EY, Barlow Twins, and VICReg on CIFAR-10, depicting 1,000-epoch performance.....	140
VI.13 CIFAR 10 Projector Analysis: (a) Examining the impact of projector size on SSL-EY's performance. (b) Investigating the relationship between EY loss and classification accuracy.....	141
VII.1 The CCA-Zoo compatibility map.....	145
VII.2 The CCA-Zoo pipeline	146
VII.3 Performance comparison for CCA methods	151
VII.4 Performance comparison for PLS methods.....	152
.1 Chord diagrams of the top 8 positive and negative brain loadings for each model.	161
.2 Statistical maps of brain structure loadings and weights for each model.	163

LIST OF TABLES

4.1	Employed CCA Variants.....	58
4.2	HCP Data Parameters	59
4.3	ADNI Data Parameters	59
4.4	Employed CCA Variants.....	60
5.1	HCP: Sparsity of models reflected by the count of non-zero weights. Elastic Net and SPLS demonstrate increased sparsity in the model weights for both brain and behaviour views, compared to PCA, RCCA, and PLS.....	62
5.2	ADNI: Number of non-zero weights for each model.	65
3.1	Covariance Structures in Data Generation Methods	83
3.2	Relationship Between Weights and Loadings in Population and Sam- ple Cases.....	84
6.1	Simulated Data Parameters for Weight and Loadings Recovery Ex- periments.....	97
6.2	Simulated Data Parameters for Brain-Behaviour Simulations	98
2.1	Definitions and dimensions of A and B for different subspace learning methods.....	109
4.1	Comparing the performance of SSL methods on CIFAR-10 and CIFAR-100.	138
3.1	Class Names and Method Names	147
3.2	Class Names and Method Names	148
3.3	Class Names and Method Names	153
3.4	Class Names and Method Names	154
3.5	Class Names and Method Names	155
3.6	Class Names and Method Names	155
3.7	Class Names and Method Names for Visualization in CCA-Zoo	156

Acronyms

ABCD Adolescent Brain Cognitive Development. 158

ADNI Alzheimer's Disease Neuroimaging Initiative. 15, 18, 44–46, 57, 59, 60, 64, 65, 67, 157, 162

CCA Canonical Correlation Analysis. 14, 23, 33–39, 43, 47, 79–81, 83, 84, 87, 88, 92, 94–96, 106, 108–110, 158

DCCA Deep Canonical Correlation Analysis. 35

FRALS Flexible Regularised Alternating Least Squares. 55–57, 60

GFA Group Factor Analysis. 83, 84

HCP Human Connectome Project. 15, 18, 44–46, 57, 58, 60, 64, 66, 67, 157, 160

KCCA Kernel Canonical Correlation Analysis. 110, 111

MCCA Multiset Canonical Correlation Analysis. 36

MRI Magnetic Resonance Imaging. 55

PCA Principal Component Analysis. 16, 29–31, 33, 107–110

PLS Partial Least Squares. 31, 33–35, 79, 80, 95, 96, 106, 108, 109

UKBB UK Biobank. 158

Glossary

latent variables Latent variables, also known as hidden variables, are unobserved variables used to model the relationships between observed variables.. 28

loadings The loadings of a latent variable or representation refer to the correlations between this latent variable or representation and the observed variables.. 8–10, 28, 87–90, 92, 94–96, 99–104, 106, 161, 163

representations In a multiview dataset, representations are functions of the observed variables that can be used as features in downstream tasks. Analogous to views, these representations are presumed to be interconnected within the context of multiview learning.. 8, 28, 63, 65, 74

views Views are the observed variables in a multiview dataset, which can be of the same or different data types. The core assumption in multiview learning is that these views are interconnected. For instance, in a dataset comprising images and text describing the same object, or images of the same object from various angles, the different modalities are related as they depict the same subject.. 24, 25, 27, 28, 31, 33, 43

weights The weights of a latent variable or representation are the coefficients in the linear combination of observed variables that constitute the factor.. 8, 10, 11, 28, 47, 48, 54, 62–65, 72, 74, 106, 163

CONTENTS

I	Introduction	19
1	Thesis Structure and Contributions.....	20
1.1	Chapter Summaries.....	21
II	Background: Multiview Machine Learning: Concepts, Methods, and Limitations	22
1	Introduction	23
2	Machine Learning and Multiview Learning.....	23
2.1	Multiview Machine Learning.....	24
2.2	Conditional Independence, Causality, and Multiview Learning	26
3	Learning Representations: Definitions and Notation	28
3.1	Generalized Eigenvalue Problems in linear algebra	29
3.2	Principal Components Analysis	29
3.3	Partial Least Squares	31
3.4	Canonical Correlation Analysis	33
3.5	Multiview CCA	36
3.6	Linear Discriminant Analysis LDA.....	37
3.7	Sample Covariance and Population Covariance	38
4	Practical Frameworks for Multiview Learning	39
4.1	Machine Learning and Statistical Inference.....	39
4.2	Components and Subspaces in CCA	40
5	Multiview Learning in Neuroimaging	42
5.1	Multiview Data in Neuroscience and Genetics	42
5.2	Applications of Multiview Learning in Neuroimaging	43
III	Regularisation of CCA Models: A Flexible Framework based on Alternating Least Squares	44
1	Introduction	45
2	Background: Regularisation for High-Dimensional and Structured Data	46

2.1	The Bias-Variance Tradeoff.....	46
2.2	Shrinkage Regularisation	47
2.3	Sparse Regularisation.....	52
3	Methods: Flexible Regularised Alternating Least Squares (FRALS)...	55
4	Experiment Design.....	57
4.1	Datasets	57
4.2	The Predictive Framework for CCA.....	57
4.3	The predictive framework for CCA	60
5	Experiment Results	60
5.1	HCP Results.....	60
5.2	ADNI Results.....	64
6	Discussion and Limitations	66
6.1	FRALS Limitations.....	66
6.2	Conclusion	67
IV	Insights From Generating Simulated Data for CCA	76
1	Introduction	77
2	Background: Weights and Loadings in Canonical Correlation Analysis	79
3	Unifying Generative Perspectives in CCA: Explicit and Implicit Latent Variable Models	80
3.1	Explicit Latent Variable Models: Probabilistic CCA and GFA ..	80
3.2	Implicit Latent Variable Models: The Joint Covariance Matrix Perspective.....	82
3.3	Summary of Data Generation Methods	82
3.4	Regularization and Generative Models.....	83
4	Proving the Invariance of Loadings in CCA.....	87
5	Efficient Sampling of Simulated CCA Data	92
5.1	Challenges with High-Dimensional Data.....	93
5.2	Sampling from Multivariate Normal Distributions	93
5.3	Using Low-Rank Covariance Matrices.....	94
5.4	Calculating the True Canonical Correlations.....	94
5.5	Calculating the True Weights (and Loadings)	94
6	Experiment Design.....	95
6.1	Exploring the Relationship Between Weights and Loadings in CCA Using Simulated Data	95
6.2	Assessing Information Recovery in CCA and PLS Models Under Varying Signal-to-Noise Ratios	96

6.3	Methodology for Constructing Correlated Covariance Matrices in CCA Simulations.....	97
7	Experiment Results	99
7.1	Exploring the Relationship Between Weights and Loadings in CCA Using Simulated Data	99
7.2	Assessing Information Recovery in CCA and PLS Models Under Varying Signal-to-Noise Ratios	102
8	Discussion	106
8.1	Limitations.....	106
8.2	Conclusion	106
V Efficient Algorithms for the CCA Family: Unconstrained Losses with Unbiased Gradients		107
1	Introduction	108
2	Background: Efficient CCA.....	108
2.1	Challenges in Solving Generalized Eigenvalue Problems	108
2.2	PCA-CCA.....	109
2.3	Kernel CCA	110
2.4	Stochastic PLS and CCA	111
3	Methods: Novel Objectives and Algorithms	113
3.1	Unconstrained objective for GEPs	113
3.2	Corresponding Objectives for the CCA family.....	114
3.3	Applications to (multi-view) stochastic CCA and PLS	116
4	Experiments and Results	116
4.1	Comparison to Scipy.....	116
4.2	Stochastic CCA.....	117
4.3	Stochastic PLS UK Biobank.....	120
5	Discussion	122
5.1	Limitations.....	122
5.2	Conclusion	124
VI Deep CCA and Self-Supervised Learning: Non-Linear Functions		125
1	Introduction	126
2	Background: Deep Representation Learning	127
2.1	Deep Learning	127
2.2	DCCA and Deep Multiview CCA.....	127
2.3	Self-Supervised Learning and Joint Embedding	129

3	Methods: Novel Objectives and Algorithms	132
3.1	Applications to (multi-view) stochastic CCA and PLS, and Deep CCA.....	132
3.2	Application to SSL.....	132
4	Experiments and Results	132
4.1	Deep CCA.....	132
4.2	Deep Multiview CCA: Robustness Across Different Batch Sizes	136
4.3	Self-Supervised Learning with SSL-EY	137
5	Discussion	141
5.1	Limitations.....	141
5.2	Conclusion	142
VII CCA-Zoo: A collection of Regularized, Deep Learning-based, Kernel, and Probabilistic methods in a scikit-learn style framework		143
1	Introduction	143
2	Background.....	144
3	Methods	144
3.1	API.....	145
3.2	Usage.....	145
3.3	Datasets	147
3.4	Model Selection Utilities	148
3.5	Linear	148
3.6	Deep	149
3.7	Probabilistic.....	149
3.8	Nonparametric	149
3.9	Visualization	149
3.10	Code Availability.....	149
4	Benchmarking	150
4.1	Canonical Correlation Analysis:.....	150
4.2	Partial Least Squares:.....	150
5	Discussion	151
5.1	Limitations.....	151
5.2	Conclusion	151
VIII Thoughts and Implications		157
1	Summary of findings.....	157
2	Implications	157

3	Future work	157
3.1	Applications	157
3.2	Methods	158
4	Closing Remarks	158
Appendices		159
1	HCP and ADNI Loadings	160
1.1	Human Connectome Project (HCP) Data	160
1.2	Alzheimer's Disease Neuroimaging Initiative (ADNI) Data.....	162
2	Eckhart-Young characterization of GEP subspace	164
2.1	Formal definitions	164
2.2	Standard Eckhart–Young inequality	164
2.3	Supporting Results	165
2.4	GEP-EY Objective	167
3	Tractable Optimization - no spurious local minima	168
3.1	Qualitative results	168
3.2	Quantitative results	171
4	Fast updates for (Multi-view) Stochastic CCA (and PLS)	174
4.1	Back-propagation for empirical covariances	174
5	Eckhart-Young loss recovers Deep CCA	178
5.1	Interlacing results	179

Chapter I

Introduction

In the middle of my PhD journey, in June 2021, I self-referred to the Community Living Well service in London, UK, for help with my mental health. I was assigned a therapist, who I met with weekly for 12 weeks. During our sessions, we discussed my mental health and the challenges I was facing. I was also asked to complete a questionnaire at the beginning and end of each session, which asked me to rate my mood and answer questions about my mental health. Each time I did this, I questioned how well these subjective numbers truly represented my feelings.

A keen sportsperson, I also wear a Garmin watch that tracks my heart rate, my sleep, and my activity levels. I use this data to monitor my health and fitness, and I have found it to be a useful tool in my training. Using a physical ‘stress level’ metric based on Heart Rate Variability (HRV), I can see how alcohol affects my sleep¹, how well I have slept, and I know I am about to get sick before I feel it.

Furthermore, as a type 1 diabetic, I rely on a continuous glucose monitor. This tool provides real-time blood sugar readings every five minutes, offering insights into trends and helping me fine-tune my insulin management.

These personal experiences underscore a broader issue in health data analysis: the challenge of integrating diverse health metrics, from subjective self-assessments to objective biometric readings, in a meaningful and interpretable way. This thesis focuses on methods to resolve this challenge using self-supervised learning. By applying these techniques to Brain-Behavior associations, I aim to demonstrate how integrating various health data streams can improve personal health management and understanding.

¹badly

1 Thesis Structure and Contributions

This thesis presents new methods that can scale multiview learning to large datasets, revolutionizing the analysis and comprehension of biomedical data. Using advancements in self-supervised and multiview learning, I explore the integration of diverse data sources, as exemplified by my mental health, physical activity, and diabetes management data.

A key goal is to develop practical, user-friendly methodological improvements. We focus on creating tools and methods that are not only theoretically sound but also intuitive for use in real-world scenarios. This will enable practitioners in biomedical research and other fields to focus on their domain expertise, rather than the technical details of the methods.

This thesis contributes in four ways:

- Developing a framework for regularised Canonical Correlation Analysis (CCA) using structured priors, like the Elastic Net, enhancing interpretability.
- Unifying proposed simulated data generation methods for CCA from the literature, demonstrating that they can all be viewed as latent variable models, and improving our ability to interpret CCA results.
- Formulating a new gradient descent approach for CCA and other fundamental generalised eigenvalue problems, tailored for large datasets.
- Extending the gradient descent approach to Deep CCA and Joint Embedding Self-Supervised Learning.

These contributions offer practical benefits. For instance, our regularised CCA framework allows practitioners to more accurately correlate brain imaging data with behavioral assessments and interpret the (possibly sparse) model parameters, aiding in the diagnosis and treatment of neurological disorders. Our perspective on simulated data generation methods for CCA will help researchers better understand the relationship between loadings and weights in CCA, and simplify the process of generating high-dimensional simulated data for CCA. The gradient descent approach for large datasets enables researchers to analyze extensive health databases, like the UK Biobank, more efficiently, leading to faster and more accurate health insights. Finally, the Deep CCA and Self-Supervised Learning extensions will allow researchers to integrate diverse data sources, such as images and text, using modern deep learning techniques.

1.1 Chapter Summaries

Chapter II reviews multiview and self-supervised learning techniques, focusing on their application in biomedical data.

Chapter III introduces a method to regularize CCA using structured priors, demonstrated with Human Connectome Project and Alzheimer's Disease Neuroimaging Initiative data.

Chapter IV examines the relationship between loadings and weights in CCA, using simulated data to show the advantages of loadings for interpretability.

Chapter V presents a new gradient descent algorithm for generalized eigenvalue problems, demonstrated with Multiview CCA and PLS. We show how our algorithm can be applied to large datasets, using the UK Biobank as an example.

Chapter VI extends the algorithm from Chapter V to deep learning, showing its application in scaling deep CCA. We demonstrate state-of-the-art results on CIFAR-10 and CIFAR-100 benchmarks, illustrating the potential of Deep CCA in Self-Supervised Learning.

Chapter VII introduces CCA-Zoo, a Python package implementing the methodologies of this thesis, and discusses its role in the Python ecosystem and biomedical research.

Chapter VIII discusses the implications, challenges, and future directions for the research presented in this thesis.

Through this thesis, I aspire to bridge the gap between the potential of biomedical data and the current capabilities of analytical methods, enhancing our ability to understand and manage personal health.

Chapter II

Background: Multiview Machine Learning: Concepts, Methods, and Limitations

Principal Component Analysis is a dimensionally invalid method that gives people a delusion that they are doing something useful with their data. If you change the units that one of the variables is measured in, it will change all the “principal components”! It’s for that reason that I made no mention of PCA in my book.

Professor David MacKay

Contents

1	Introduction.....	23
2	Machine Learning and Multiview Learning.....	23
2.1	Multiview Machine Learning	24
2.2	Conditional Independence, Causality, and Multiview Learning	26

3	Learning Representations: Definitions and Notation	28
3.1	Generalized Eigenvalue Problems in linear algebra	29
3.2	Principal Components Analysis.....	29
3.3	Partial Least Squares	31
3.4	Canonical Correlation Analysis	33
3.5	Multiview CCA.....	36
3.6	Linear Discriminant Analysis LDA	37
3.7	Sample Covariance and Population Covariance	38
4	Practical Frameworks for Multiview Learning	39
4.1	Machine Learning and Statistical Inference	39
4.2	Components and Subspaces in CCA.....	40
5	Multiview Learning in Neuroimaging	42
5.1	Multiview Data in Neuroscience and Genetics	42
5.2	Applications of Multiview Learning in Neuroimaging.....	43

1 Introduction

This chapter provides the foundational knowledge needed to understand the thesis as a whole, while the individual chapters will provide more specific background information as needed.

2 Machine Learning and Multiview Learning

Machine learning encompasses methods that enable models to learn patterns and make decisions from data. Machine learning methods are typically categorised by a training set of data, which is used to learn a model, and a test set of data, which is used to evaluate the model. Arguably the most common machine learning paradigm is supervised learning, where the training data consists of pairs of inputs and outputs, and the model learns to predict a function which maps the inputs to the outputs. This function is then used to predict the outputs for new inputs. The goal of supervised learning is to learn a function that generalizes well to new data, i.e. to make accurate predictions on unseen data. Unsupervised and self-supervised learning are common machine learning paradigms where the training data consists of inputs only, and the model learns to find patterns in the data. While the distinction between the two is sometimes blurred, unsupervised learning has been used to describe dimensionality

reduction, clustering, and generative modelling algorithms. Self-supervised learning (SSL) has been used to describe a special case of unsupervised learning, where labels are generated from the data itself, rather than being provided by an external source. SSL is a paradigm where the training signal is derived from the data itself, rather than relying on external labels (Balestrieri, Ibrahim, et al., 2023). The cornerstone of SSL is the concept of a ‘pretext task’, a learning task created from the data that trains the model to capture useful features or representations. Most famously, SSL is the backbone to the success of Large Language Models (Vaswani et al., 2017) and in particular ChatGPT (OpenAI, 2021), a language model trained on a pretext task of predicting masked words in a sentence. SSL methods have also recently been shown to outperform supervised methods for certain computer vision tasks for large datasets (Goyal et al., 2019).

2.1 Multiview Machine Learning

This thesis is focussed on multiview machine learning. Here, data from different sources or modalities, referred to as views, such as neuroimaging, genomics, and clinical records, are analyzed collectively to unveil underlying patterns. Multiview machine learning encompasses a variety of techniques aimed at learning from data that have multiple sources or modalities, also known as views. These techniques can also be broadly classified into supervised and self-supervised multiview learning, with some algorithms straddling the boundary between the two.

2.1.1 Supervised Multiview Learning

In supervised multiview learning, the goal is to integrate information from multiple distinct views or feature sets to improve the predictive performance of a model. This approach often involves using one view as the target, with other views serving as inputs. For instance, in the context of mental health, we can consider behavioural data as a dependent variable influenced by multiple independent variables like brain activity and demographics. Figure II.1 illustrates this concept, where behavioural patterns (y_1) are predicted based on features from brain activity (x_1) and demographic information (x_2).

Multiple Kernel Learning (MKL) (Gönen and Alpaydın, 2011) is a prominent example of supervised multiview learning, where the algorithm learns to combine kernel representations of the different views. This enhances the model’s predictive capabilities compared to using a single kernel. With the advent of deep learning, the underlying concept of MKL has been extended to deep learning architectures.

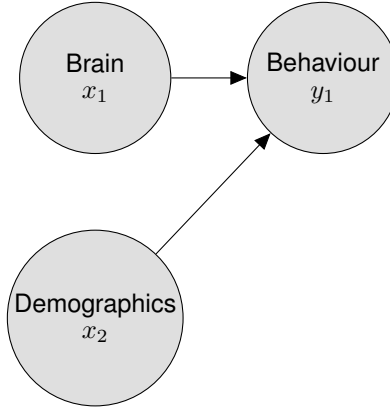


Figure II.1: Independent and Dependent Variable Model of Mental Health:
From this perspective, behavioural data is considered to be dependent on brain activity and demographics

These architectures enable the model to learn and combine representations from various views more effectively (Guo, J. Wang, and S. Wang, 2019). I contributed to this line of research through the software package Fusili (Townsend, Chapman, and Cole, 2023), which implements a number of deep-learning based multi-modal data fusion methods for supervised learning.

2.1.2 Self-Supervised Multiview Learning

In contrast to supervised multiview learning, where explicit labels guide the learning process, self-supervised multiview learning operates under the hypothesis that different views are manifestations of a shared, yet hidden, latent variable (Zong, Mac Aodha, and T. Hospedales, 2023). This approach, as evidenced in the latent variable model of mental health illustrated in Figure II.2, suggests that both neuroimaging and behavioural data are influenced by an underlying factor, such as the severity of a mental health condition, which remains unobserved.

A key challenge in self-supervised learning is designing pretext tasks to infer this latent source from the available views. A common approach is to estimate a common low-dimensional representation of the variance in the data from both views. In most objectives of this form, this amounts to identifying the mutual information between the views. These representations may be informative for their own sake, identifying common factors between the views, or they may be used as inputs to a downstream task, such as classification or regression.

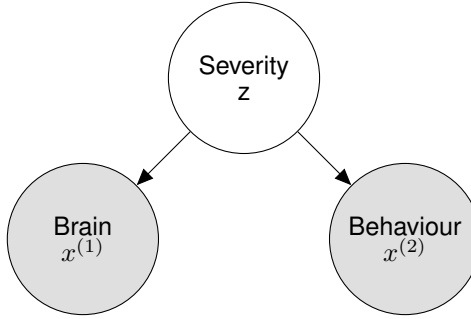


Figure II.2: Latent Variable Model of Mental Health: From this perspective the neuroimaging modality and behavioural data are both considered to have been generated with distributions conditioned on the severity of a mental health condition

2.2 Conditional Independence, Causality, and Multiview Learning

The graphical model in Figure II.1 represents the assumption that the brain and demographics are independent variables, and that the behaviour is a conditional variable, dependent on both the brain and demographics.

On the other hand, the graphical model in Figure II.2 represents the assumption that the brain and behaviour are conditionally independent given the severity of an unobserved ‘latent’ mental health condition.

Reichenbach (1956) introduced the eponymous Reichenbach’s principle, which states that if two variables are correlated, then either one causes the other, or both are caused by a third variable. While the relationship between conditional independence and causality is nuanced (Pearl, 2009), it is clear that our assumptions about the causal structure of the data can inform our choice of multiview learning algorithm. In particular, we could envision a number of causal structures that could give rise to the observed data in Figure II.2:

- direct causation (brain influencing behavior or vice versa or even both)
- both being influenced by a common, possibly unobserved, cause
- no direct causal link between them

In the first case, we might be more inclined to use a supervised multiview learning algorithm to predict one view from the other. In the second case, we might be more

inclined to use a self-supervised multiview learning algorithm to estimate the latent variable.

2.2.1 Complementary and Redundant Information

The nature of the information provided by different views (such as neuroimaging and behavioral data) is important for understanding multiview learning models. A particularly useful distinction is between complementary and redundant information (Nguyen and D. Wang, 2020; Lyu et al., 2021; M.-S. Chen et al., 2022). The complementary information in views offers unique insights into different aspects of the same subject. For instance, in mental health studies, neuroimaging might reveal structural changes in the brain that are not (yet) present in presented behavioural phenotypes, while behavioral data could be influenced by demographic factors that do not present as structural differences in the brain. Both these views together provide a more holistic understanding of a mental health condition. Conversely, redundant information in different views refers to overlapping or similar data presented from various angles. For instance, a specific mental health condition may manifest in both observable behavioral changes and detectable neuroimaging markers. While each view alone could suggest the presence of the condition, their combination, due to redundancy, can enhance the reliability of the diagnosis. This redundancy is not merely repetitive; it plays a crucial role in denoising and validating findings. In essence, if both neuroimaging and behavioral data independently point to the same diagnosis, the confidence in this diagnosis increases. The ‘Wisdom of Crowds’ phenomenon, where the collective average of multiple estimates tends to be more accurate than individual estimates, exemplifies the strength of redundant information (Galton, 1907), as illustrated in Figure II.3. This principle is akin to the redundancy in multiview data, where multiple views converge to a more accurate or robust conclusion than any single view alone.

In this thesis, we will explore Canonical Correlation Analysis, a multiview learning method predicated on the assumption that different views provide complementary information about latent variables. The following sections will establish a formal framework for representation learning and motivate the use of Canonical Correlation Analysis in harnessing complementary information from multiview data.



Figure II.3: *The Wisdom of Crowds*: The average of multiple noisy estimates of the weight of a cow is more accurate than any individual estimate.

3 Learning Representations: Definitions and Notation

Suppose we have a sequence of vector-valued random variables $X^{(i)} \in \mathbb{R}^{D_i}$ for $i \in \{1, \dots, I\}$. We want to learn meaningful K -dimensional representations

$$Z^{(i)} = f^{(i)}(X^{(i)}; \theta^{(i)}). \quad (\text{II.1})$$

For convenience, define $D = \sum_{i=1}^I D_i$ and $\theta = (\theta^{(i)})_{i=1}^I$. Without loss of generality take $D_1 \geq D_2 \geq \dots \geq D_I$. We will consistently use the subscripts $i, j \in [I]$ for views; $d \in [D_i]$ for dimensions of input variables; and $l, k \in [K]$ for dimensions of representations - i.e. to subscript dimensions of $Z^{(i)}, f^{(i)}$. Later on we will introduce total number of samples N .

In this report, when the functions f are linear, we will typically refer to u_k as weights, $Z_k = X_k u_k$ as representations or latent variables (noting that in the CCA literature they are sometimes referred to as canonical variables (Borga, 1998)), depending on the context. We will sometimes consider a matrix $U = (u_1, \dots, u_K) \in \mathbb{R}^{D \times K}$ of weights, and a matrix $Z = (Z_1, \dots, Z_K) \in \mathbb{R}^{N \times K}$ of representations. We will refer to the Pearson correlation between features and their respective latent variable $\text{Corr}(X_j^{(i)}, Z_k)$ as the loadings of $X_j^{(i)}$ on Z_k (Rosipal and Krämer, 2005; Alpert and R. A. Peterson, 1972; Borga, 1998), noting that the same concept has

also been referred to as structure correlations (Meredith, 1964).

We will use the notation $\Sigma_{ij} = \text{Cov}(X^{(i)}, X^{(j)})$ for the population covariance matrix between the random variables associated with view i and j . We will also use $\Sigma_{ii} = \text{Cov}(X^{(i)})$ for the population covariance matrix of the random variables associated with view i with each other.

3.1 Generalized Eigenvalue Problems in linear algebra

A Generalized Eigenvalue Problem (GEP) is defined by two symmetric matrices $A, B \in \mathbb{R}^{D \times D}$ (Stewart and J.-G. Sun, 1990)¹. They are usually characterized by the set of solutions to the equation:

$$Au = \lambda Bu \quad (\text{II.2})$$

with $\lambda \in \mathbb{R}$, $u \in \mathbb{R}^D$, called (generalized) eigenvalue and (generalized) eigenvector respectively. When B is positive definite, then the GEP becomes equivalent to an eigen-decomposition of the symmetric matrix $B^{-1/2}AB^{-1/2}$ (Ghojogh, Karray, and Crowley, 2019). In addition, one can find a basis of eigenvectors spanning \mathbb{R}^D . We define a top- K subspace to be one spanned by some set of eigenvectors u_1, \dots, u_K with the top- K associated eigenvalues $\lambda_1 \geq \dots \geq \lambda_K$. We say a matrix $U \in \mathbb{R}^{D \times K}$ defines a top- K subspace if its columns span one.

Uniqueness In GEPs, the eigenvectors u are not in general unique, but the generalized eigenvalues $1 \geq \lambda_1 \geq \lambda_2 \geq \dots \geq 0$ are unique (Mills-Curran, 1988).

3.2 Principal Components Analysis

Principal Components Analysis (Hotelling, 1933) (PCA) is a classical method in unsupervised machine learning for representation learning. It is widely used for dimensionality reduction and feature extraction. The primary goal of PCA is to transform the original high-dimensional data into a new coordinate system defined by orthogonal axes, capturing the most relevant aspects of the data.

In PCA, the representations are constrained to be linear transformations of the form:

$$Z_k = Xu_k, \quad (\text{II.3})$$

¹more generally, A, B can be Hermitian, but we are only interested in the real case

where u_k are orthonormal basis vectors such that:

$$u_k^\top u_k = 1, \quad u_k^\top u_l = \delta_{kl} \text{ for } k \neq l. \quad (\text{II.4})$$

The primary goal of PCA is to maximize the variance of the representations Z_k , finding the directions of maximal variance in the data.

3.2.1 Optimization and Solution

Mathematically, for the first principal component, this can be formulated as:

$$u_{\text{opt}} = \underset{u}{\operatorname{argmax}} (u^\top \Sigma u) \quad (\text{II.5})$$

subject to:

$$u^\top u = 1$$

Where $\Sigma = \mathbb{E}[X^\top X]$ is the population covariance matrix of the single view data X .

The Lagrangian for this problem is:

$$f(u, \lambda) = u^\top \Sigma u + \lambda(1 - u^\top u), \quad (\text{II.6})$$

where λ is the Lagrange multiplier. Differentiating the Lagrangian yields the first-order conditions:

$$\Sigma u = \lambda u, \quad (\text{II.7})$$

$$u^\top u = 1. \quad (\text{II.8})$$

Eigenvalue Problem This transforms the problem into an eigenvalue equation for the covariance matrix Σ , which can be efficiently solved using standard libraries such as scikit-learn (Pedregosa et al., 2011).

The first principal component therefore corresponds to the eigenvector associated with the largest eigenvalue λ . Subsequent components are the remaining eigenvectors ordered by their corresponding eigenvalues.

3.2.2 Limitations

There are two major limitations of PCA that are relevant to this thesis. The first is revealed by the epigraph of this chapter, which highlights the fact that PCA is not scale invariant. This means that the principal components are sensitive to the scale of the data, and therefore the units in which the data is measured. Furthermore, the interpretation of the principal components is challenging; they are linear combinations of all of the original features. For this reason, sparse variants of PCA have been developed (Zou, Hastie, and Robert Tibshirani, 2006; Zou and Xue, 2018), which aim to find sparse linear combinations of the original features; interpretable as a subset of the original features contributing to a significant proportion of the variance in the data. Another major limitation of PCA in the context of multiview learning is that it does not explicitly take advantage of either the redundancy or the complementary information in multiview data, even if we concatenate the views into a single random variable X . Nevertheless, PCA remains a popular tool in practice (Greenacre et al., 2022) and is a useful baseline for multiview learning methods, and we will use it as a point of comparison throughout this thesis.

3.3 Partial Least Squares

Partial Least Squares (PLS) (Wold, 1975) aims to maximize the shared covariance between two paired sets of data, referred to as views. PLS can be seen as a generalization of PCA, where PCA becomes a special case when the two views are identical.

PLS optimises for the dot product between the two views, a measure of similarity.

$$\langle u^{(1)}, \Sigma_{12}u^{(2)} \rangle = u^{(1)T}\Sigma_{12}u^{(2)} = \sqrt{u^{(1)T}\Sigma_{11}u^{(1)}}\sqrt{u^{(2)T}\Sigma_{22}u^{(2)}}\cos(\theta) \quad (\text{II.9})$$

Where θ is the angle between the two representations. In order to constrain the problem, we set the norms of the weights to 1.

3.3.1 Optimization and Solution

The constrained optimization problem for PLS can therefore be formulated as:

$$u_{\text{opt}}^{(1)} = \underset{u^{(1)}}{\operatorname{argmax}} \{ u^{(1)T} \Sigma_{12} u^{(2)} \} \quad (\text{II.10})$$

subject to:

$$u^{(1)T} u^{(1)} = 1$$

$$u^{(2)T} u^{(2)} = 1$$

The Lagrangian for this optimization problem can be formulated as:

$$f(u^{(1)}, \lambda) = u^{(1)T} \Sigma_{12} u^{(2)} + \lambda_1 (1 - u^{(1)T} u^{(1)}) + \lambda_2 (1 - u^{(2)T} u^{(2)}) \quad (\text{II.11})$$

Upon deriving the first order conditions, we get:

$$\Sigma_{21} u^{(1)} = \lambda_2 u^{(2)} \quad (\text{II.12})$$

$$\Sigma_{12} u^{(2)} = \lambda_1 u^{(1)} \quad (\text{II.13})$$

$$u^{(1)T} u^{(1)} = 1 \quad (\text{II.14})$$

$$u^{(2)T} u^{(2)} = 1 \quad (\text{II.15})$$

By substituting the constraint conditions into these equations, we find that $\lambda_1 = \lambda_2 = \lambda$ by symmetry. Further simplification yields:

$$\Sigma_{21} \Sigma_{12} u^{(2)} = \lambda^2 u^{(2)} \quad (\text{II.16})$$

$$\Sigma_{12} \Sigma_{21} u^{(1)} = \lambda^2 u^{(1)} \quad (\text{II.17})$$

Eigenvalue Problem Once again, we see that solving these equations will yield the $u^{(1)}$ and $u^{(2)}$ vectors as eigenvectors, this time of $\Sigma_{12} \Sigma_{21}$ and $\Sigma_{21} \Sigma_{12}$, respectively (Höskuldsson, 1988).

Generalized Eigenvalue Problem We can also represent the system of equations in matrix form as follows:

$$\begin{pmatrix} 0 & \Sigma_{12} \\ \Sigma_{21} & 0 \end{pmatrix} \begin{pmatrix} u^{(1)} \\ u^{(2)} \end{pmatrix} = \lambda I \begin{pmatrix} u^{(1)} \\ u^{(2)} \end{pmatrix} \quad (\text{II.18})$$

Which is of the form $Av = \lambda Bv$. PLS is therefore also defined by the solution to a single generalized eigenvalue problem.

Given the notions of uniqueness in GEPs, the weights u are not in general unique but we can write the vector of generalized eigenvalues $(\lambda_1, \dots, \lambda_K)$ representing covariances as:

$$\text{PLS}_K(X^{(1)}, X^{(2)}) := (\lambda_k)_{k=1}^K \quad (\text{II.19})$$

3.3.2 Limitations

Like PCA, a major problem with applying PLS to neuroimaging and behavioural modalities is that PLS is not scale invariant. This is because the dot product in equation II.9 is not scale invariant since it is not normalized by the norms of the representations. Since representations with larger norms will have larger dot products, PLS is biased towards larger representations. It is therefore also biased towards the largest principal components in the data (Helmer et al., 2020). This is particularly problematic when there is a low signal to noise ratio since PLS. Like PCA, another issue is the lack of sparsity in the PLS solution which has been an active area of research (Chun and Keleş, 2010; D. M. Witten, Robert Tibshirani, and Hastie, 2009).

3.4 Canonical Correlation Analysis

In Canonical Correlation Analysis (CCA), we aim to find the directions that maximize correlation, as opposed to maximizing covariance between two views of a dataset. As compared to PLS, CCA optimizes for the correlation between the two views, rather than the covariance. This can be viewed as maximizing the cosine similarity between the two views, rather than the dot product, as in PLS.

$$\cos(\theta) = \frac{\langle u^{(1)}, \Sigma_{12} u^{(2)} \rangle}{\sqrt{\langle u^{(1)}, \Sigma_{11} u^{(1)} \rangle} \cdot \sqrt{\langle u^{(2)}, \Sigma_{22} u^{(2)} \rangle}} = \frac{u^{(1)T} \Sigma_{12} u^{(2)}}{\sqrt{u^{(1)T} \Sigma_{11} u^{(1)}} \sqrt{u^{(2)T} \Sigma_{22} u^{(2)}}} \quad (\text{II.20})$$

By dividing by the norms of the representations, we can see that CCA is scale invariant, unlike PLS. All that matters is the angle between the representations, not their magnitude.

3.4.1 Optimization and Solution

The optimization problem for CCA can be expressed as:

$$u_{\text{opt}} = \underset{u}{\operatorname{argmax}} \{ u^{(1)T} X^{(1)T} X^{(2)} u^{(2)} \} \quad (\text{II.21})$$

subject to:

$$u^{(1)T} \Sigma_{11} u^{(1)} = 1$$

$$u^{(2)T} \Sigma_{22} u^{(2)} = 1$$

Although non-convex, numerous methods exist for solving the CCA problem, including eigendecomposition and generalized eigendecomposition solvers (Uurtio et al., 2017) and block coordinate descent via alternating least squares regressions (Golub and Zha, 1995; L. Sun, Ji, and Ye, 2008).

The first-order conditions derived in the same manner as the PLS case are:

$$\Sigma_{21} u^{(1)} = \lambda^{(2)} \Sigma_{22} u^{(2)} \quad (\text{II.22})$$

$$\Sigma_{12} u^{(2)} = \lambda^{(1)} \Sigma_{11} u^{(1)} \quad (\text{II.23})$$

$$u^{(1)T} \Sigma_{11} u^{(1)} = 1 \quad (\text{II.24})$$

$$u^{(2)T} \Sigma_{22} u^{(2)} = 1 \quad (\text{II.25})$$

Eigenvalue Problems Substituting the second two conditions into the first two, we get $\lambda^{(1)} = \lambda^{(2)} = \lambda$. Then, recognizing $X_i^\top X_i$ as the covariance matrix Σ_{ii} and $X_i^\top X_j$ as the cross-covariance matrix Σ_{ij} , we obtain another pair of eigenvalue problems:

$$\Sigma_{11}^{-1} \Sigma_{12} \Sigma_{22}^{-1} \Sigma_{21} u^{(1)} = \lambda^2 u^{(1)}$$

$$\Sigma_{22}^{-1} \Sigma_{21} \Sigma_{11}^{-1} \Sigma_{12} u^{(2)} = \lambda^2 u^{(2)}$$

An alternative form of the CCA problem can be developed by reparameterizing

$u^{(i*)} = \Sigma_{ii}^{-\frac{1}{2}} u^{(i)}$. The optimization problem then becomes:

$$u_{\text{opt}} = \underset{u}{\operatorname{argmax}} \{ u^{(1)T} \Sigma_{11}^{-\frac{1}{2}} \Sigma_{12} \Sigma_{22}^{-\frac{1}{2}} u^{(2)} \} \quad (\text{II.26})$$

subject to:

$$u^{(1)T} u^{(1)} = 1$$

$$u^{(2)T} u^{(2)} = 1$$

This reparameterized form will later underpin Deep Canonical Correlation Analysis (DCCA).

This form also shows that PLS and CCA can be made equivalent by whitening the data matrices before constructing the covariance matrix. When the number of features exceeds the number of samples ($p > n$), CCA becomes degenerate because the within-view covariance matrices cannot be inverted—contrasting with PLS, which is always computable.

Generalized Eigenvalue Problem We can also represent the system of equations in equation II.22 as a matrix equation:

$$\begin{pmatrix} 0 & \Sigma_{12} \\ \Sigma_{21} & 0 \end{pmatrix} \begin{pmatrix} u^{(1)} \\ u^{(2)} \end{pmatrix} = \lambda \begin{pmatrix} \Sigma_{11} & 0 \\ 0 & \Sigma_{22} \end{pmatrix} \begin{pmatrix} u^{(1)} \\ u^{(2)} \end{pmatrix} \quad (\text{II.27})$$

Which is once again of the form $Au = \lambda Bu$. CCA, like PLS, is therefore also defined by the solution to a single generalized eigenvalue problem.

Canonical Correlations In the case of CCA, the generalized eigenvalues λ are generally called canonical correlations (Hotelling, 1935; Hotelling, 1992). Given the notions of uniqueness in GEPs, the weights u are not in general unique but we can write the vector of generalized eigenvalues or canonical correlations as:

$$\text{CCA}_K(X^{(1)}, X^{(2)}) := (\rho_k)_{k=1}^K \quad (\text{II.28})$$

3.4.2 Limitations

Additionally, PLS assumes that the structures contributing to variance in both datasets are linearly related, which may not be the case in complex biological systems like the brain or in intricate behavioral patterns (Rosipal and Krämer, 2005).

The linearity assumption can sometimes be overly restrictive, failing to capture more complicated, nonlinear relationships between the data modalities.

3.5 Multiview CCA

Multiview CCA or MCCA is a straightforward extension of CCA to the case of 3-or more datasets. The goal is to find a set of directions $u^{(i)}$ such that the pairwise correlations between the views are maximized.

3.5.1 Optimization and Solution

The optimization problem for MCCA can be stated as:

$$u_{\text{opt}} = \underset{u}{\operatorname{argmax}} \sum_{i=1}^m \sum_{j=1, j \neq i}^m u^{(i)T} \Sigma_{ij} u^{(j)} \quad (\text{II.29})$$

subject to:

$$\sum_{i=1}^m u^{(i)T} \Sigma_{ii} u^{(i)} = 1$$

Generalized Eigenvalue Problem The generalized eigenvalue problem (GEP) for MCCA can be written in matrix form as follows:

$$\begin{pmatrix} 0 & \Sigma_{12} & \cdots & \Sigma_{1m} \\ \Sigma_{21} & 0 & \cdots & \Sigma_{2m} \\ \vdots & \vdots & \ddots & \vdots \\ \Sigma_{m1} & \Sigma_{m2} & \cdots & 0 \end{pmatrix} \begin{pmatrix} u^{(1)} \\ u^{(2)} \\ \vdots \\ u^{(m)} \end{pmatrix} = \lambda \begin{pmatrix} \Sigma_{11} & 0 & \cdots & 0 \\ 0 & \Sigma_{22} & \cdots & 0 \\ \vdots & \vdots & \ddots & \vdots \\ 0 & 0 & \cdots & \Sigma_{mm} \end{pmatrix} \begin{pmatrix} u^{(1)} \\ u^{(2)} \\ \vdots \\ u^{(m)} \end{pmatrix}. \quad (\text{II.30})$$

This GEP formulation of MCCA can be presented in a unified framework generalizing CCA and ridge-regularized extensions. Indeed, we now take $A, B_\alpha \in \mathbb{R}^{D \times D}$ to be block matrices $A = (A^{(ij)})_{i,j=1}^I, B_\alpha = (B_\alpha^{(ij)})_{i,j=1}^I$ where the diagonal blocks of A are zero, the off-diagonal blocks of B_α are zero, and the remaining blocks are defined by:

$$A^{(ij)} = \text{Cov}(X^{(i)}, X^{(j)}) \text{ for } i \neq j, \quad B_\alpha^{(ii)} = \alpha_i I_{D^{(i)}} + (1 - \alpha_i) \text{Var}(X^{(i)}) \quad (\text{II.31})$$

Where $\alpha \in [0, 1]^I$ is a vector of ridge penalty parameters: taking $\alpha_i = 0 \forall i$ recovers CCA and $\alpha = 1 \forall i$ recovers PLS. We may omit the subscript α when $\alpha = 0$ and we

recover the ‘pure CCA’ setting; in this case, following II.28 we can define

$$\text{MCCA}_K(X^{(1)}, \dots, X^{(I)}) \quad (\text{II.32})$$

to be the vector of the top- K generalized eigenvalues which are the average of the top- K correlations between each pair of views.

3.6 Linear Discriminant Analysis LDA

Linear Discriminant Analysis (LDA) can be viewed as a special case of Canonical Correlation Analysis (CCA) where $X^{(2)}$ is a one-hot encoded matrix representing the class labels. This allows us to draw a connection between the unsupervised learning framework of CCA and the supervised framework of LDA(Balakrishnama and Ganapathiraju, 1998; Riffenburgh, 1957), thus expanding the understanding of both algorithms.

Intuition: In LDA, the aim is to find a lower-dimensional subspace where the classes are maximally separated. This objective can be viewed through the lens of CCA, where the optimal directions $u^{(1)}$ and $u^{(2)}$ in the original and one-hot encoded spaces aim to maximize correlation. In the LDA context, $u^{(1)}$ would maximize the separation between classes.

3.6.1 Optimization and Solution

Mathematically, LDA is reduced to solving a generalized eigenvalue problem involving the between-class scatter matrix S_B and the within-class scatter matrix S_W :

$$\begin{aligned} \hat{S}_B &= \sum_{i=1}^c n_i(\mu_i - \mu)(\mu_i - \mu)^\top \\ \hat{S}_W &= \sum_{i=1}^c \sum_{x \in X_i} (x - \mu_i)(x - \mu_i)^\top \end{aligned}$$

Connection to CCA: When $X^{(2)}$ is the one-hot encoded matrix of class labels, the CCA problem effectively tries to maximize the correlation between the feature vectors and their corresponding labels. This turns out to be equivalent to maximizing the between-class variance in LDA while minimizing the within-class variance. Thus, LDA can be thought of as a constrained form of CCA, tailored to classification tasks.

This perspective unifies the two algorithms and shows that the core objective—finding meaningful relationships or directions in the data—is shared between both CCA and LDA.

3.7 Sample Covariance and Population Covariance

In the previous sections, the methods were described in terms of population covariance matrices such as $\Sigma_{11} = \mathbb{E}[X^{(1)T} X^{(1)}]$, $\Sigma_{22} = \mathbb{E}[X^{(2)T} X^{(2)}]$, and $\Sigma_{12} = \mathbb{E}[X^{(1)T} X^{(2)}]$. These population covariances assume an underlying probability distribution from which the data are drawn.

Sample Covariance: In practical settings, we often do not have access to the entire population but only to a sample. Hence, we can use the Sample Average Approximation to estimate these covariances:

$$\hat{\Sigma}^{(12)} = \frac{1}{b-1} \bar{\mathbf{X}}^{(1)} \bar{\mathbf{X}}^{(2)T}$$

Here, b denotes the size of the minibatch, and $\mathbf{X}^{(1)} \in \mathbb{R}^{p \times b}$ and $\mathbf{X}^{(2)} \in \mathbb{R}^{q \times b}$ are the data matrices for the samples from $X^{(1)}$ and $X^{(2)}$, respectively. The bar over $\mathbf{X}^{(1)}$ and $\mathbf{X}^{(2)}$ signifies that these are centered versions of the matrices, i.e., the mean has been subtracted from each column.

Practical Implications: Using sample covariance matrices introduces some estimation error but allows us to apply the methods in real-world scenarios where population-level data are unattainable. Additionally, the use of minibatches provides a computationally efficient way to estimate these covariances in large-scale problems, at the cost of some additional statistical noise.

Connection to Previous Methods: The use of sample covariance matrices is directly applicable to algorithms like CCA and LDA. When replacing the population covariances $\Sigma^{(ij)}$ with sample estimates, the optimization problems remain structurally similar but are solved using the sample data.

This dual perspective—considering both population and sample covariance matrices—enables a more robust and flexible approach to the methods discussed, bridging the gap between theoretical analysis and practical application. It will be particularly useful in the context of chapter IV where we will use population variables as ground truth while estimating the models using sample data.

4 Practical Frameworks for Multiview Learning

At this point, we have introduced the theoretical foundations of multiview learning, including CCA and its variants. However, it is not yet clear how we should apply these methods to real-world datasets.

4.1 Machine Learning and Statistical Inference

Canonical Correlation Analysis (CCA) has been studied from both machine learning and statistical inference perspectives. At its core, machine learning focuses on prediction, while statistical inference focuses on understanding the underlying data structure(Ij, 2018). However, these two approaches are not mutually exclusive, and statistical learning theory has emerged as a unifying framework for both perspectives (Vapnik, 1999; Hastie et al., 2009). In this section, we will review the differences between these two approaches and their implications for multiview learning.

4.1.1 Statistical Inference Evaluation Framework

Statistical inference approaches provide a contrasting perspective to machine learning methods, focusing on understanding and quantifying the underlying data structure:

Parameter Estimation In statistical inference, parameter estimation involves estimating model parameters and their uncertainties. This process is fundamental to understanding the data and the model's fit.

Hypothesis Testing Hypothesis testing assesses the statistical significance of the relationships found by the model. It tests whether the observed data patterns are likely to have occurred under the null hypothesis.

Confidence Intervals Confidence intervals provide ranges within which the true parameter values are likely to fall, considering uncertainty. They are essential for understanding the reliability of parameter estimates.

Permutation Testing Permutation testing is a non-parametric method that evaluates the significance of models. It compares model performance on the original data with performance on randomly shuffled data, helping to ascertain the results' robustness.

4.1.2 Machine Learning Evaluation Framework

Training, Validation, and Test Sets In machine learning, data is typically partitioned into training, validation, and test sets, each serving a specific purpose in the model development process:

- Training Set: Used for fitting the model.
- Validation Set: Assists in model parameter tuning.
- Test Set: Evaluates the model's generalization capability.

Cross-Validation A fundamental technique in machine learning, cross-validation involves dividing the training dataset into smaller subsets for training and validation. This approach provides insights into the model's performance across different data segments.

Holdout Method The holdout method involves using a separate dataset, not involved in training or validation, for final model assessment. This ensures an unbiased performance evaluation.

Out of Sample Correlation Specific to canonical correlation analysis, this involves measuring the correlation between latent variables in new datasets, assessing the model's ability to uncover relationships in unseen data.

Downstream Tasks Evaluating model performance on downstream tasks like classification or prediction can offer practical insights into the utility of the learned representations.

4.2 Components and Subspaces in CCA

4.2.1 Context: Eigenvalue Problems in CCA

While our focus so far has primarily been on the top-1 eigenvector-eigenvalue pair, it's important to note that the methodology also extends to the top-k subspace problem. This broader approach involves identifying the top-k eigenvectors and their corresponding eigenvalues.

4.2.2 Addressing the Top-k Problem

Transitioning from a focus on the top-1 component to exploring the top-k subspace introduces additional complexities. One common method to solve the top-k problem is to identify the top-1 component and then apply a deflation process to find subsequent orthogonal components. Deflation involves removing the top-1 component from the data and then repeating the process to find the next top-1 component. This process is repeated until the desired number of components is found. For instance, Hotelling's Deflation (Hotelling, 1933) involves removing the top-1 component from the data, while Projection Deflation (Mackey, 2008) involves projecting the data onto the orthogonal complement of the top-1 component. Different deflation methods enforce different forms of orthogonality, which can impact the resulting components and their interpretation, particularly when the first component is not a true eigenvector.

4.2.3 Non-Uniqueness of Components

Furthermore, non-uniqueness is a significant challenge in CCA, particularly when eigenvectors have repeated eigenvalues. Imagine a scenario where the top-1 eigenvalue is repeated k times. In this case, there are k possible eigenvectors that can be associated with the top-1 eigenvalue. While this is unlikely to occur in practice, the eigenvalues can in practice be very close to each other, leading to numerical instability and non-uniqueness in the components. Particularly true in cross-validation settings, this non-uniqueness can lead to instability in the components, complicating their interpretation and comparison. For example, the top-1 component in one analysis might be the second component in another analysis, making it difficult to compare the results.

This non-uniqueness also has a grounding in the probabilistic perspectives on PCA and CCA, where the latent variables are considered unique only up to a rotation. This perspective further reinforces the subspace approach, emphasizing the identification of a subspace rather than specific directions within it.

Thesis Approach: Concentrating on the Top-1 Component In this thesis, we focus on the top-1 component in CCA to align with and facilitate comparison with typical componentwise studies in brain-behavior research. This choice is driven by the complexity associated with the top-k problem and the variety of methods available

to address it. Under the assumption of a significant eigengap², the first component can be considered equivalent to the top-1 subspace. This equivalence allows for a clear and interpretable analysis, making the top-1 subspace a straightforward and reliable choice for studying multivariate data. It is important to note that while we focus on the top-1 component, the later sections of the thesis introduce a method for simultaneously solving the complete subspace, addressing broader subspace analyses.

5 Multiview Learning in Neuroimaging

5.1 Multiview Data in Neuroscience and Genetics

In neuroscience and genetics, two specific types of multiview studies are particularly relevant to this thesis: brain-behavior studies and imaging-genetics. Both involve the integration of data from multiple sources, offering rich insights into complex phenomena.

Brain-behavior studies typically involve pairing neuroimaging data, such as that obtained from Structural MRI (sMRI) or Functional MRI (fMRI), with non-imaging data like responses from questionnaires, cognitive test results, and other behavioral assessments. sMRI provides detailed anatomical brain images, essential for understanding brain structure and neurological disorders (Kanai and Rees, 2011), while fMRI focuses on brain function by mapping activity during cognitive tasks (Miranda et al., 2021). The integration of these imaging techniques with behavioral data offers a comprehensive view of how brain structures and functions correlate with behavioral and cognitive patterns (Rypma and D'Esposito, 2001; Genon, Eickhoff, and Kharabian, 2022).

Imaging-Genetics, another critical multiview approach, combines neuroimaging data with genetics and omics information (Lê Cao et al., 2008). This interdisciplinary field seeks to understand the genetic influences on brain structure and function, thereby illuminating the genetic basis of neuropsychiatric disorders and cognitive traits (R. Bogdan et al., 2017). Studies in this area can explore how specific genetic variations correlate with differences in brain morphology or activity patterns observed in neuroimaging (J. Liu and Calhoun, 2014).

²An 'eigengap' refers to the difference in magnitude between consecutive eigenvalues in an eigenvalue problem. A significant eigengap between the first and second eigenvalues suggests that the first eigenvalue (and its corresponding eigenvector) is distinctly more significant than the next, lending credence to its uniqueness and importance.

Together, these multiview approaches are fundamental in advancing our understanding of the brain's structure, function, and its interactions with genetic and behavioral factors. They represent key applications of SSL in neuroscience and genetics, providing comprehensive insights that underpin developments in these fields.

5.2 Applications of Multiview Learning in Neuroimaging

There have been a number of applications of CCA and related methods to multiview problems in neuroimaging. Using resting state fMRI data, modes of correlation have been found that relate to differences in sex and age relating to drug and alcohol abuse, depression and self harm (Mihalik, Ferreira, Rosa, et al., 2019). A similar mode relating to 'positive-negative' wellbeing has been found across studies (Stephen M Smith et al., 2015) suggesting that mental wellbeing has a relationship (though not necessarily causally) with functional connectivity between networks in the brain. Later in this dissertation we will replicate and build on the findings from this paper by using regularised and non-linear CCA methods. Owing to the high dimensionality of neuroimaging data, regularisation has been a particular focus of multiview learning in neuroimaging. Mihalik, Chapman, Rick A Adams, et al. (2022a) reviews the application of CCA to neuroimaging data and highlights the importance of regularisation in this context. Bilenko and Gallant (2016) CCA has also been used as a preprocessing step in order to identify groups of subjects in the latent variable space.

In particular, CCA and clustering have been used to identify depression using fMRI data (Dinga et al., 2019; Drysdale et al., 2017). CCA has also been used in the manner we described to denoise two views of a dataset such as separate measures of neuroimaging data (Zhuang, Yang, and Cordes, 2020) to remove artefacts. Deep CCA has recently been used to extract features for the diagnosis of schizophrenia(Qi and Tejedor, 2016).

Chapter III

Regularisation of CCA Models: A Flexible Framework based on Alternating Least Squares

Contents

1	Introduction.....	45
2	Background: Regularisation for High-Dimensional and Structured Data	46
2.1	The Bias-Variance Tradeoff	46
2.2	Shrinkage Regularisation.....	47
2.3	Sparse Regularisation	52
3	Methods: Flexible Regularised Alternating Least Squares (FRALS)	55
4	Experiment Design	57
4.1	Datasets.....	57
4.2	The Predictive Framework for CCA.....	57
4.3	The predictive framework for CCA.....	60
5	Experiment Results.....	60
5.1	HCP Results	60
5.2	ADNI Results	64
6	Discussion and Limitations.....	66
6.1	FRALS Limitations	66
6.2	Conclusion.....	67

Preface

In this chapter, I build upon my earlier work presented at the OHBM conference and the insights gained from a tutorial paper I co-authored, which included a series of simulations (Mihalik, Chapman, Rick A Adams, et al., 2022a).

1 Introduction

This chapter introduces a novel approach for analyzing large-scale neuroimaging datasets, such as the Human Connectome Project (HCP (Van Essen et al., 2013)) and Alzheimer's Disease Neuroimaging Initiative (ADNI), to understand the relationship between brain structure, function, and behavior (Stephen M. Smith and Thomas E. Nichols, 2018; Bzdok and B.T. Thomas Yeo, 2017; H.-T. Wang et al., 2020). These datasets are characterized by a disproportion between the number of subjects and the volume of features, posing a challenge for Canonical Correlation Analysis (CCA) models due to the risk of overfitting and spurious correlations (H.-T. Wang et al., 2018). For example, the HCP dataset used in this chapter contains 1003 subjects and 19,900 features in the functional MRI (fMRI) view alone while the ADNI dataset contains 592 subjects and 168,130 features in the structural MRI (sMRI) view alone.

In response to the reproducibility crisis in neuroscience (Button et al., 2013), this chapter focuses on enhancing the generalizability of CCA models through regularization, a technique that introduces a bias towards more interpretable and generalizable models (Engl, Hanke, and Neubauer, 1996; Bzdok, Thomas E Nichols, and Stephen M Smith, 2019). Existing regularization methods in CCA, such as 'sparse CCA' with Partial Least Squares (PLS) objectives (Lê Cao et al., 2008; D. M. Witten, Robert Tibshirani, and Hastie, 2009; Lindenbaum et al., 2021), are limited by their inherent bias towards the largest principal components (Mihalik, Chapman, Rick A. Adams, et al., 2022b).

To overcome these limitations, we propose the Flexible Regularised Alternating Least Squares (FRALS) framework for CCA based on the Alternating Least Squares form of CCA (Golub and Zha, 1995). FRALS allows for the integration of various regularized least squares solvers, particularly emphasizing the elastic net penalty, which combines L2 and L1 penalties. This method controls bias and promotes sparsity in model weights, advancing beyond previous sparse Brain-Behavior analysis methods.

Our application of the FRALS framework with Elastic Net regularization to the HCP and ADNI datasets showcases its effectiveness in enhancing out-of-sample canonical correlation compared to traditional CCA models. Additionally, FRALS uncovers new modes of variation in brain-behavior relationships.

In essence, this chapter presents FRALS as a robust, innovative solution for the analysis of high-dimensional neuroimaging datasets, significantly improving the reliability and interpretability of Brain-Behavior correlations.

2 Background: Regularisation for High-Dimensional and Structured Data

In this section, we review a number of regularisation techniques that have been applied to CCA and related methods.

2.1 The Bias-Variance Tradeoff

A key principle in machine learning is the bias-variance tradeoff (Curth, Jeffares, and Schaar, 2023; Hastie et al., 2009). This concept posits that a tradeoff exists between the bias and variance of a model: high-bias models typically exhibit low variance, and vice versa. High-bias models are generally simpler and more stable, but they might oversimplify the problem, leading to underfitting. Conversely, low-bias, complex models are sensitive to data changes and prone to overfitting. As the number of features increases, there are more parameters to estimate, and models tend to become more complex, leading to higher variance and lower bias. This relationship highlights the importance of balancing model complexity to avoid overfitting, particularly in high-dimensional scenarios with a low signal-to-noise ratio (McIntosh, 2021)¹. Regularisation can be understood as a method for reducing the variance of a model by introducing a bias towards simpler models. This means regularisation can improve the generalizability of models in high-dimensional settings.

Implicit and Explicit Regularisation We can implement regularisation in two different ways. Explicit regularisation is achieved by adding a penalty term to the objective function. This weights the objective function against a term that penalises complexity.

¹It's worth noting that the number of model parameters, often used as a proxy for complexity, does not always directly correlate with model behavior, as illustrated by the 'double descent' phenomenon.

Implicit regularisation is achieved by changing the optimisation algorithm and can include dimensionality reduction, as well as certain optimisation procedures like using stochastic gradient descent in place of gradient descent (Ali, Dobriban, and Ryan Tibshirani, 2020), and early stopping of optimization routines (Yao, Rosasco, and Caponnetto, 2007)

2.2 Shrinkage Regularisation

Shrinkage regularisation is a form of regularisation that penalises the magnitude of the model parameters. This technique is particularly effective in enhancing the performance of linear models in situations characterised by high dimensionality, multicollinearity, or low signal-to-noise ratios.

In high-dimensional situations where the number of features exceeds the number of observations in either view, Like Linear Regression, Canonical Correlation Analysis is non-identifiable, meaning there is no unique solution. This is because we can find perfectly correlated latent variables using a linear combination of the features, but there are many different linear combinations that will achieve this. Some of these linear combinations will generalize better than others, but there is no way to distinguish between them using the training data alone.

Even in low-dimensional situations, if features exhibit multicollinearity, they can also be non-identifiable or, at best, estimates of the parameters are unstable. Mathematically, this is because in both cases the covariance matrix of the features is not full rank and therefore is not invertible (non-identifiable) or ill-conditioned (matrix inversion is unstable). To capture this intuition, if two features are perfectly correlated, the model is not identifiable (has no unique solution) because we can arbitrarily swap the weights between the two features without changing the latent variables (CCA) or the predictions (regression). In practice, features are rarely perfectly correlated, but even when features are highly correlated, the model can be unstable (Mihalik, Ferreira, Moutoussis, et al., 2020), and small changes in the data can lead to large changes in the model parameters. Once again, some of these linear combinations will generalize better than others, but we might expect a model to generalize better if it spreads the weights across the correlated features rather than concentrating them on a single feature.

Finally, even in low-dimensional settings with little multicollinearity, the model parameters can be sensitive to noise in the data, and once again small changes in the data can lead to large changes in the model parameters. For example, parameters associated with noisy features might ‘cancel out’ in the training set, but

not in the test set, leading to poor generalisation.

The premise of shrinkage regularisation in all these cases is that the latent variables or predictions are too sensitive to small changes in the data because the model parameters are too large. Shrinkage regularisation works by shrinking the model parameters towards zero, so that small changes in the data do not lead to large changes in the model estimates.

PLS as Shrinkage Regularisation PLS can be interpreted as a form of shrinkage regularisation applied to CCA. We can explain this by considering an analogy between CCA and Linear Regression².

In Linear Regression, the ridge regression solution is given by:

$$\hat{\beta}_{\text{ridge}} = ((1 - c)\Sigma_{X,X} + cI)^{-1}\Sigma_{X,y} \quad (\text{III.1})$$

Where c is the regularisation parameter between 0 and 1³. The ridge penalty acts in three important ways:

- It shrinks the weights towards zero.
- It shrinks the weights of correlated features towards each other.
- It biases the solution to high covariance directions rather than high correlation directions.

As c becomes large, $\lim_{c \rightarrow \infty} (\Sigma_{X,X} + cI)^{-1} = (cI)^{-1}$, so that $\hat{\beta}_{\text{ridge}} = \frac{\Sigma_{X,y}}{c}$, which is precisely the covariance of the features of X with Y scaled by c (and shrunk towards zero for $c \geq 1$). Notice that the ridge regression solution is no longer sensitive to the correlation of features in X . Additionally, notice that for sufficiently large c , $(\Sigma_{X,X} + cI)$ is invertible even if $\Sigma_{X,X}$ is not invertible, so that ridge regression is always identifiable even when the number of features exceeds the number of observations.

Now consider the CCA problem. Firstly, recall that PLS and CCA are equivalent up to a scaling when the covariance matrices are identity matrices, a similar relationship to the relationship between Linear and Ridge Regression. Consider the well-known form of CCA given in equation III.2(Mihalik, Chapman, Rick A Adams, et al., 2022a) (formed by reparameterizing $u^{(i)} = (\Sigma_{ii})^{-\frac{1}{2}}u^{(i)}$):

²indeed Linear Regression is a special case of CCA where $X^{(2)}$ has one feature

³It is more common to see $(\Sigma_{X,X} + cI)^{-1}\Sigma_{X,y}$ but these are equivalent up to a scalar factor and this form helps us later on

$$u_{\text{opt}} = \underset{u}{\operatorname{argmax}} \{ u^{(1)T} (\Sigma_{11} + cI)^{-\frac{1}{2}} \Sigma_{12} (\Sigma_{22} + cI)^{-\frac{1}{2}} u^{(2)} \} \quad (\text{III.2})$$

subject to:

$$u^{(1)T} u^{(1)} = 1, u^{(2)T} u^{(2)} = 1$$

As we increase c , $\lim_{c \rightarrow \infty} (\Sigma_{ii} + cI)^{-\frac{1}{2}} = (cI)^{-1}$ so that the objective approaches:

$$u_{\text{opt}} = \underset{u}{\operatorname{argmax}} \{ u^{(1)T} (cI)^{-1} \Sigma_{12} (cI)^{-1} u^{(2)} \} \quad (\text{III.3})$$

subject to:

$$u^{(1)T} u^{(1)} = 1, u^{(2)T} u^{(2)} = 1$$

Which is precisely the PLS objective and constraints with an arbitrary scaling of the covariance matrix Σ_{12} by $\frac{1}{c^2}$. For this reason, we can consider PLS as an explicit shrinkage method for CCA, equivalent to adding a maximal ridge regularisation term. The downside of using PLS as a regularised CCA is precisely its very high bias. By strongly guiding the model towards high covariance solutions, it strongly biases the solution towards only the largest principal components. But what if the correlation between the views is not concentrated in the largest principal components? Although one would rarely resort to maximally regularised ridge regression except in extremely low sample sizes or high-dimensional data, it has become almost standard practice to use PLS in neuroimaging and genetics (Cruciani et al., 2022; Krishnan et al., 2011). One of the core contributions of this chapter will be to demonstrate that PLS is usually a poor choice for regularisation even in these very high-dimensional settings and that more nuanced regularisation methods can offer significant improvements in performance and interpretability. PLS is evidently not a nuanced tool for regularisation because it offers no control over the degree of regularisation applied.

Ridge Regularisation For this reason, Vinod (1976) proposed the Canonical Ridge or Ridge CCA, which combined the PLS and CCA constraints in a single constrained optimisation:

$$u_{\text{opt}}^{(1)} = \underset{u^{(1)}}{\operatorname{argmax}} \{ u^{(1)T} \hat{\Sigma}_{12} u^{(2)} \} \quad (\text{III.4})$$

subject to:

$$(1 - c_1) u^{(1)T} \hat{\Sigma}_{11} u^{(1)} + c_1 u^{(1)T} u^{(1)} = 1$$

$$(1 - c_2) u^{(2)T} \hat{\Sigma}_{22} u^{(2)} + c_2 u^{(2)T} u^{(2)} = 1$$

Where c_1 and c_2 are the ridge regularisation parameters for the first and second views respectively. By tuning these parameters, we can control the degree of regularisation applied to each view independently. If we set c_1 and c_2 to zero, we recover the standard CCA objective while if we set c_1 and c_2 to one, we recover the PLS objective. This allows us to interpolate between the two extremes, allowing us to control the level of shrinkage and therefore the level of bias towards the largest principal components. Ridge CCA has been shown to be effective for neuroimaging data for both CCA (A. Tenenhaus and M. Tenenhaus, 2011; Tuzhilina, Tozzi, and Hastie, 2023; Hardoon, Szedmak, and Shawe-Taylor, 2004) and Kernel CCA (Hardoon, Mourao-Miranda, et al., 2007).

PCA-CCA PCA can be used as an implicit regularisation method for CCA.

Most obviously, by using only the first k principal components of each view as the input to CCA, we can reduce the dimensionality of the data and therefore reduce the number of parameters in the model. Moreover, by working with the principal components, we remove the correlation between the features, which can improve the conditioning of the problem. While PCA and Independent Component Analysis (ICA) are often used as preprocessing steps for CCA, they can also be used as regularisation methods in their own right. Of particular note in neuroimaging are studies with a data-driven approach to the PCA step, where the number of principal components is chosen based on the data (Z. Liu et al., 2022; Mihalik, Chapman, Rick A. Adams, et al., 2022b).

A Visual Comparison of Shrinkage Techniques The distinct effects of Ridge and PCA on the eigenvalues of the effective covariance matrices can be clearly visualised with a simple visualisation. We plot the eigenvalues of covariance matrices

as perceived by models with different regularisation techniques⁴. As shown in Figure III.1, Ridge regularisation reduces the magnitude of the largest eigenvalues in the effective covariance matrix towards 1, and increases the magnitude of the smallest eigenvalues towards 1. On the other hand, PCA-CCA, leaves the largest eigenvalues unchanged, and ignores the smallest eigenvalues (we could have represented this by setting them to infinity).

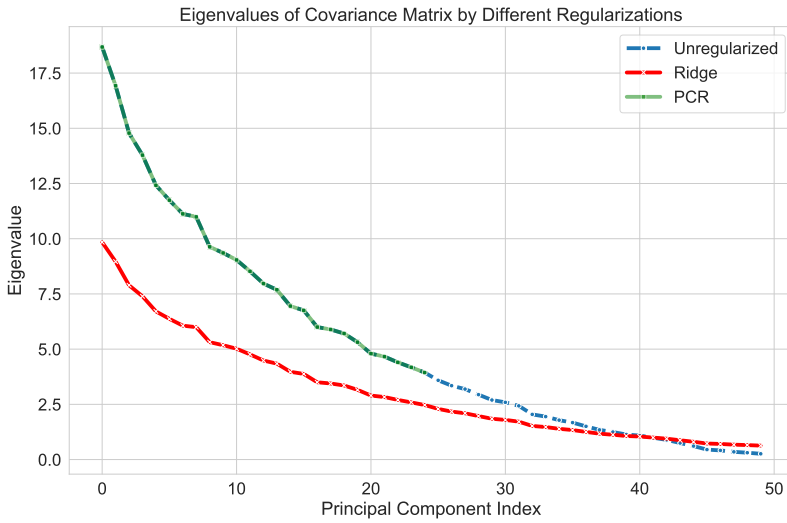


Figure III.1: Comparison of the effect of OLS, Ridge, and PCA regularisation on the eigenvalues of the covariance matrix.

When these effective covariance matrices are inverted to form the CCA objective, these effects are reversed. Ridge regularisation increases the magnitude of the weights associated with the largest eigenvalues and decreases the magnitude of the smallest eigenvalues. PCA maintains the weights associated with the largest eigenvalues and sets the weights associated with the smallest eigenvalues to zero. The visualisation underscores the intrinsic nature of each regularisation method:

- **Unregularised:** Presents the unaltered spectrum, making it susceptible to noise but preserving potential subtle patterns.
- **Ridge:** Warps the spectrum, shrinking the largest eigenvalues and expanding the smallest eigenvalues, potentially missing subtle patterns but offering a cleaner representation of stronger associations.

⁴e.g. the eigenvalues of $(1 - c_i)\hat{\Sigma}_{ii} + c_i I$ for ridge and $\hat{\Sigma}_{ii}$ truncated to include only the largest k principal components for PCA

- **PCA:** Truncates the spectrum, ignoring the smallest eigenvalues and preserving the largest eigenvalues, potentially missing subtle patterns but offering a cleaner representation of stronger associations.

However, while these shrinkage techniques can improve the performance of CCA, they do not obviously improve the interpretability of the results. Weights are shrunk towards zero, but they are not set to zero. This means that the model still uses all the features, and the results are not sparse.

2.3 Sparse Regularisation

Sparse regularisation is a powerful tool for improving the performance and interpretability of linear models. Sparse regularisation encourages the model to use only a subset of the features, which can both help to avoid overfitting and improve the interpretability of the model. Sparse regularisation works on the premise that only a subset of the features are relevant to the model. Sparsity is typically achieved by adding either an L1 penalty or constraint⁵. The L1 penalty is defined as:

$$\|u\|_1 = \sum_i |u_i| \quad (\text{III.5})$$

Intuitively, this is the sum of the absolute values of the elements of the vector. Now, with a foundational understanding of sparse regularisation, we review a number of approaches to adding sparsity to the CCA problem.

Sparse PLS: Penalised Matrix Decomposition Penalised Matrix Decomposition (PMD) (D. M. Witten, Robert Tibshirani, and Hastie, 2009) provides an approximate solution to the sparse CCA problem by altering the constraints of the classical CCA formulation. Specifically, PMD replaces the constraints $u^{(i)T} \hat{\Sigma}_{ii} u^{(i)} = 1$ with the PLS constraints $u^{(i)T} u^{(i)} = 1$ and additionally imposes $\|u^{(i)T}\|_1 \leq \tau$. The optimisation problem for PMD is then given by:

⁵The L0 norm of the weight vector is the number of non-zero elements in the vector and is arguably a closer match to the goal, but the L0 norm is (a) not a proper norm in the mathematical sense and (b) not convex and so is difficult to optimize.

$$u^{opt} = \underset{u}{\operatorname{argmax}} \{ u^{(1)T} \hat{\Sigma}_{12} u^{(2)} \} \quad (\text{III.6})$$

subject to:

$$u^{(1)T} u^{(1)} = 1, u^{(2)T} u^{(2)} = 1$$

$$\|u^{(1)}\|_1 \leq \tau_1, \|u^{(2)}\|_1 \leq \tau_2$$

This Sparse PLS (SPLS) approximation has been highly influential as a form of Sparse CCA because it is extremely computationally efficient method⁶. Like the relationship between PLS and CCA, PMD and a form of CCA with constrained L1 norm are equivalent only when the covariance matrices are identity matrices. There are a number of other sparse CCA methods that employ the PLS approximation (Parkhomenko, Tritchler, and Beyene, 2009; Waaijenborg, Witt Hamer, and Zwinderman, 2008; Lindenbaum et al., 2021). However, while the PLS approximation is efficient, it means these methods inherit a bias towards the largest principal components from PLS.

To address these problems and truly tackle the sparse CCA optimisation, another class of approaches have adopted a penalised least squares approach.

Sparse CCA: Least Squares Approaches It is well known that the CCA problem can be formulated as a constrained least squares problem with the intuition that for $X^{(1)}u^{(1)} = 1$ and $X^{(2)}u^{(2)} = 1$, correlation is maximised when the squared distance between $X^{(1)}u^{(1)}$ and $X^{(2)}u^{(2)}$ is minimised. (Golub and Zha, 1995) proved the convergence of a simple algorithm which alternates between solving the least squares problem for $u^{(1)}$ and $u^{(2)}$ while keeping the other fixed.

With this intuition, Wilms and Croux, 2015 and Mai and Zhang, 2019 separately proposed iterative penalised least squares methods for sparse CCA.

$$u^{opt} = \underset{u}{\operatorname{argmin}} \left\{ \|X^{(1)}u^{(1)} - X^{(2)}u^{(2)}\|_2^2 + P(u) \right\} \quad (\text{III.7})$$

subject to:

$$u^{(1)T} \hat{\Sigma}_{11} u^{(1)} = 1$$

$$u^{(2)T} \hat{\Sigma}_{22} u^{(2)} = 1$$

⁶it can be solved by a variant of the power method; iteratively multiplying $u^{(1)}$ by $\hat{\Sigma}_{12}$ and soft-thresholding

Where $P(u)$ is a penalty function. The penalty term can be any function that penalises the norm of the vector u . (Mai and Zhang, 2019) proved that solving the subproblems where one of $u^{(i)}$ is fixed is easy for one-homogenous P where $P((\mu + 1)\theta) = (\mu + 1)P(\theta)$ which notably includes the lasso penalty. This means a sparse CCA based on alternating lasso regressions can be solved relatively efficiently using existing solvers. However, the one homogenous penalty in practice limits the flexibility of the method. For example, the elastic net penalty is not one-homogenous and therefore cannot be used with this method. Chi et al. (2013) and Mullins et al., 2021 added ridge penalties to the subproblems to improve the conditioning of the problem in a way that could be considered a form of elastic net regularisation but the subproblems no longer correctly optimize the global objective⁷.

Sparse CCA: Proximal Gradient Descent and ADMM Kanatsoulis et al. (2018) proposed solving equation III.7 for more general classes of P using the alternating direction method of multipliers (ADMM) (Boyd et al., 2011). Fu et al., 2017 propose a regularised CCA based on an alternative classical CCA formulation, sometimes called the MAXVAR formulation, which views the problem as a constrained least squares with an auxiliary representation T (Carroll, 1968; Kettenring, 1971).

$$\operatorname{argmin}_{U,T} \left\{ \sum_i \|X^{(i)}U^{(i)} - T\|_F^2 \right\} \quad (\text{III.8})$$

$$\text{subject to: } T^\top T = I \quad (\text{III.9})$$

$$(\text{III.10})$$

In this formulation, $U^{(i)}$ represents the weights for the i^{th} view, and T denotes the latent variable matrix. The premise is that when T closely mirrors $X^{(i)}U^{(i)}$ across all i , the scores correlate. Notably, this method is adaptable to multiple views. The authors employed proximal gradient descent for regularisation, specifically suited for penalties like the lasso. While these methods are flexible, they don't have the plug-and-play nature of the penalised least squares methods. Not just a matter of convenience, this means that these methods are not compatible with existing solvers for regularised least squares problems like for example total variation regularisation solvers in nilearn, which are often highly optimised for specific problems and modalities.

⁷when rescaling the penalised solutions back to unit variance

Structured Regularisation As highly structured data, linear models using both structural MRI and fMRI data have been shown to benefit from structured regularisation methods but notably these methods have not been applied to CCA. Total variation regularisation, which biases spatially neighboring weights to be similar, has been shown to improve the performance of PCA (De Pierrefeu et al., 2017) and regression (Michel et al., 2011; Dohmatob et al., 2014; Baldassarre, Mourao-Miranda, and Pontil, 2012). Similarly, Laplacian (or GraphNet) regularisation, which induces a similar spatial bias with additional smoothness, has been shown to improve the performance of CCA on functional MRI data (Groenick et al., 2013; Cuingnet et al., 2012).

Having discussed the benefits of both shrinkage (e.g., PCA-CCA, Ridge CCA, PLS), sparsity (SPLS, Sparse CCA), and structure (Total Variation, Laplacian) in handling high-dimensional, noisy, and structured data, a natural progression is to integrate these advantages. Specifically, the challenge lies in creating a framework that allows for users to match the regularisation method to their data and research question, enhancing the interpretability and performance of Brain-Behaviour association models. This led us to propose the Flexible Regularised Alternating Least Squares (FRALS).

3 Methods: Flexible Regularised Alternating Least Squares (FRALS)

The primary goal of our Flexible Regularised Alternating Least Squares framework is to provide a versatile and user-friendly interface for Canonical Correlation Analysis (CCA). This is achieved by designing the framework to be compatible with any scikit-learn compatible regularised least squares solver. This compatibility is pivotal as it allows researchers and practitioners to leverage the extensive range of solvers available in scikit-learn, a popular machine learning library in Python.

This approach marks a significant departure from traditional methodologies in CCA, which often focused on developing or utilizing specific solvers tailored for particular types of data or computational constraints. By contrast, FRALS democratises access to advanced CCA techniques, allowing users to select solvers that best fit their specific data characteristics, computational needs, or familiarity. Such flexibility is particularly advantageous in interdisciplinary fields like neuroimaging, where diverse datasets and varying levels of technical expertise are common.

For example, users dealing with high-dimensional, sparse neuroimaging data

could opt for solvers optimised for such datasets, while those needing parallel computation for large data sets might choose solvers with GPU acceleration capabilities. In principle, FRALS can even be used with Neural Network-based solvers, which are becoming increasingly popular in machine learning⁸. This adaptability enhances FRALS' accessibility and future-proofs the framework against evolving computational technologies and data analysis needs.

In the FRALS framework, we consider the formulation for a single latent variable t with regularisation $\lambda_i P_i$ on the weights $u^{(i)}$:

$$\begin{aligned} \operatorname{argmin}_u & \left\{ \sum_i \|X^{(i)} u^{(i)} - t\|_2^2 + \lambda_i P_i(u^{(i)}) \right\} \\ & \text{subject to: } t^\top t = 1 \end{aligned} \quad (\text{III.11})$$

This problem can be decomposed into three subproblems. The first subproblem for the auxiliary variable t :

$$\begin{aligned} \operatorname{argmin}_t & \left\{ \sum_i \|X^{(i)} u^{(i)} - t\|_2^2 \right\} \\ & \text{subject to: } t^\top t = 1 \end{aligned} \quad (\text{III.12})$$

is a standard least squares problem and can be solved in closed form by averaging $X^{(i)} u^{(i)}$ and normalizing i.e. $t = \frac{\sum_i X^{(i)} u^{(i)}}{\|\sum_i X^{(i)} u^{(i)}\|_2}$. As shown earlier this makes t an estimate of the latent variables of a generative CCA model.

The subproblems for the weights $u^{(i)}$:

$$\operatorname{argmin}_{u^{(i)}} \left\{ \|X^{(i)} u^{(i)} - t\|_2^2 + \lambda_i P_i(u^{(i)}) \right\} \quad (\text{III.13})$$

are regularised least squares problems that can be solved using any suitable regularised least squares solver⁹.

In this chapter, we illustrate the power of the FRALS framework by implementing the well-tested Elastic Net solver from the `scikit-learn` package (Pedregosa et al., 2011), where $P_i = \alpha_i \times \text{l1_ratio} \|u^{(i)}\|_1 + \alpha_i \times (1 - \text{l1_ratio}) \|u^{(i)}\|_2^2$, allowing for

⁸Though for reasons that will later become clear, we do not recommend this!

⁹We could also in principle replace $X^{(i)} u^{(i)}$ with $f(X^{(i)})$ for any function f including kernels, neural networks, or random forests

independent tuning of shrinkage and sparsity of the weights in both views.

In summary, the FRALS framework is a flexible and user-friendly interface for CCA that allows users to combine scikit-learn compatible regularised least squares solvers to solve regularised CCA problems.

4 Experiment Design

This section outlines the methodologies used in our study to explore the Flexible Regularized Alternating Least Squares (FRALS) and associated techniques in Canonical Correlation Analysis (CCA). We focus on fitting a single latent dimension for the analyses.

4.1 Datasets

For this chapter, we chose the HCP and the ADNI datasets to facilitate comparison with two influential brain-behaviour studies (Stephen M Smith et al., 2015; João M Monteiro et al., 2016) as well as the tutorial paper that this chapter is loosely related to (Mihalik, Chapman, Rick A Adams, et al., 2022a). We are particularly interested in the performance of an Elastic Net FRALS on these datasets as Ridge CCA has been shown to outperform PLS (Mihalik, Chapman, Rick A Adams, et al., 2022a), implying that shrinkage regularisation is beneficial, and Sparse PLS has been shown to outperform PLS (João M Monteiro et al., 2016), implying that sparsity is beneficial. We therefore expect that Elastic Net FRALS will outperform PLS, Ridge CCA, and Sparse PLS on these datasets.

4.2 The Predictive Framework for CCA

Our evaluation of CCA models used a standard predictive framework, dividing the data into an 80:20 ratio for training and testing. This method ensures fitting the model on the training set without incorporating information from the test set.

4.2.1 Model Comparisons

The experiment aims to demonstrate the effectiveness of tunable shrinkage and sparsity in CCA models, enabled by the FRALS framework. We compare the performance of Elastic Net FRALS with other CCA variants such as PCA, PLS, Ridge CCA, SPLS, and Elastic Net CCA, particularly in the context of high-dimensional datasets like HCP and ADNI.

Table 4.1: Employed CCA Variants

Model	Abbreviation	Hyperparameters	Hyperparameter Range
Principal Component Analysis	PCA	-	-
Regularised CCA	RCCA	c_1, c_2	0-1 (log scaled)
FRALS - Elastic	Elastic	$\alpha_1, \alpha_2, l_{11}, l_{12}$	(1e-5, 1e-1), (0-1)
Partial Least Squares	PLS	-	-
Sparse PLS	SPLS	τ_1, τ_2	0-1 (log scaled)

4.2.2 Model Selection

For models that require hyperparameter tuning, a grid search was employed to find the best hyperparameters. We used 5-fold cross-validation to assess the performance of each model with various hyperparameters across different training data splits. The optimization goal was to achieve the highest average out-of-sample correlation.

4.2.3 The Human Connectome Project (HCP)

The HCP offers publicly available resting-state functional MRI (rs-fMRI) and non-imaging measures like demographics, psychometrics, and other behavioral measures. Specifically, we sourced data from 1003 subjects out of the 1200-subject data release of the HCP. The rs-fMRI data provided brain connectivity matrices. These were derived from pairwise partial correlations between subject components obtained through group independent component analysis (ICA), utilizing 25 components. This resulted in 300 brain variables, corresponding to the lower triangle of the connectivity matrix. In our analysis, 145 non-imaging subject measures were incorporated, similar to prior studies, with the exception of 13 measures (ASR_Aggr_Pct, ASR_Attn_Pct, ASR_Intr_Pct, ASR_Rule_Pct, ASR_Soma_Pct, ASR_Thot_Pct, ASR_Wtd_Pct, DSM_Adh_Pct, DSM_Antis_Pct, DSM_Anxi_Pct, DSM_Avoid_Pct, DSM_Depr_Pct, DSM_Somp_Pct) that were unavailable in the 1200-subject data release. Furthermore, nine confounding variables, including the acquisition reconstruction software version, a summary statistic of head motion during rs-fMRI acquisition, weight, height, systolic and diastolic blood pressure, hemoglobin A1C level, and cube-root of total brain and intracranial volumes as estimated by FreeSurfer, were regressed out from both data types. More details can be found in Stephen M Smith et al. (2015) and Mihalik, Chapman, Rick A Adams, et al. (2022a). We summarize the parameters of the HCP data in table 4.2.

Table 4.2: HCP Data Parameters

Parameter	Value
Number of samples (n)	1003
Number of features in View 1 (p)	300
Number of features in View 2 (q)	145

Table 4.3: ADNI Data Parameters

Parameter	Value
Number of samples (n)	592
Number of features in View 1 (p)	168130
Number of features in View 2 (q)	31

4.2.4 The Alzheimer’s Disease Neuroimaging Initiative (ADNI)

Accessible at adni.loni.usc.edu, the ADNI database was initiated in 2003. Its primary aim is the examination of how well serial MRI, PET (Positron Emission Tomography), biological markers, along with clinical and neuropsychological assessments, track the progression of Mild Cognitive Impairment (MCI) and the early stages of Alzheimer’s disease. In our study, we utilised data from a subset of 592 unique individuals, comprising 309 males (average age 74.68 ± 7.36 SEM) and 283 females (average age 72.18 ± 7.50 SEM). This subset included 147 healthy controls, 335 individuals with Mild Cognitive Impairment (MCI), and 110 diagnosed with dementia. T1 weighted structural MRI (sMRI) scans were the source of whole-brain voxel-based grey matter volumes. The sMRI data underwent preprocessing with SPM12 (Ashburner et al., 2014), which involved segmentation, normalisation using DARTEL, reslicing to a resolution of $2 \times 2 \times 2 \text{ mm}^3$, and spatial smoothing using a Gaussian kernel with 2 mm full width at half maximum (FWHM). A grey matter voxel selection mask, with a threshold of $\geq 10\%$, was applied to all participants’ scans, resulting in 168,130 brain variables. The Mini-Mental State Examination (MMSE) is a widely recognised neurocognitive test comprising 30 questions across five cognitive domains (M. F. Folstein, S. E. Folstein, and McHugh, 1975): orientation (questions 1-10), registration (questions 11-13), attention and calculation (questions 14-18), recall (questions 19-21), and language (questions 22-30). An additional item was included in our study to account for the number of attempts a subject needed to correctly respond to the registration domain questions, leading to a total of 31 variables. As in João M Monteiro et al. (2016), no confounds were removed from these data. We summarize the parameters of the ADNI data in table 4.3.

4.3 The predictive framework for CCA

To evaluate the performance of CCA models, we employ a standard predictive framework. We split the data into training and test sets using a 80:20 split, and use the training set to fit the model. We then use the test set to evaluate the model's performance. Where relevant, pre-processing is performed on the training set and the same pre-processing is applied to the test set. This is important to avoid data leakage, where information from the test set is used to fit the model.

4.3.1 Model Comparisons

In the experiments in this section, we are interested in illustrating the effects of tunable shrinkage and sparsity on the performance and interpretability of CCA models, enabled by the FRALS framework. To this end, we compare the performance of Elastic Net FRALS with other CCA variants, including PCA, PLS, Ridge CCA, Sparse PLS, and Elastic Net CCA. Since the HCP and ADNI data are high-dimensional, we drop CCA from the analysis since it would produce random results.

Table 4.4: Employed CCA Variants

Model	Abbreviation	Hyperparameters	Hyperparameter Range
Principal Component Analysis	PCA	-	-
Regularised CCA	RCCA	c_1, c_2	0-1 (log scaled)
FRALS - Elastic	Elastic	$\alpha_1, \alpha_2, l1_1, l1_2$	(1e-5, 1e-1), (0-1)
Partial Least Squares	PLS	-	-
Sparse PLS	SPLS	τ_1, τ_2	0-1 ¹⁰ (log scaled)

4.3.2 Model Selection

For the models that require hyperparameter tuning, we use a grid search to find the best hyperparameters. Specifically, we use 5-fold cross-validation to evaluate the performance of a model with a given set of hyperparameters on 5 different splits of the training data with non-overlapping validation sets. We optimise for the hyperparameters that give the best average out of sample correlation.

5 Experiment Results

5.1 HCP Results

Next, we consider the results of applying the various CCA variants to the HCP data.

5.1.1 Out of Sample Correlation

Both Ridge CCA and Elastic Net outperformed PLS and SPLS in terms of holdout correlation captured (Figure III.2). This suggests that tunable L2 regularisation is important, even for very high-dimensional data, and that resorting to PLS is suboptimal. On the other hand, while the additional sparsity improved SPLS over PLS (consistent with previous work João M Monteiro et al., 2016), it did not improve the performance of the Elastic Net model over Ridge CCA.

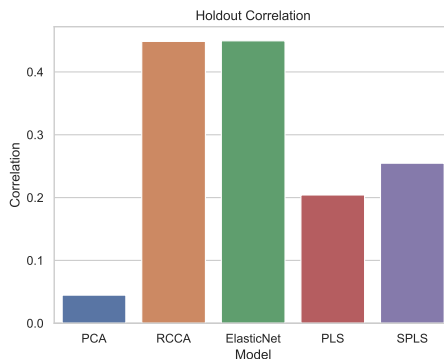


Figure III.2: HCP: Comparative out-of-sample canonical correlations among PCA, RCCA, ElasticNet, PLS, and SPLS models. The bars represent the correlation coefficients, indicating that Ridge CCA and Elastic Net models have superior performance over PLS and SPLS in capturing holdout correlation.

Nonetheless, the Elastic Net model demonstrated a more sparse representation than the Ridge CCA model, with the Elastic Net model utilizing 241 and 96 non-zero weights for the brain and behaviour views, respectively (Table 5.1). In contrast, the Ridge CCA model used 300 and 145 non-zero weights for the respective views. Moreover, the SPLS model achieved an even sparser solution with only 118 and 56 non-zero weights for the brain and behaviour views. Considering the comparable performance of the Elastic Net and Ridge CCA models, the former's sparsity may offer a preferable solution.

5.1.2 Behaviour Weights

Figure ?? presents the top eight positive and negative non-imaging weights for each model to visualize the behavioural data variations observed in the previous section. The PCA model emphasizes a mode of variation with positive correlations

Table 5.1: HCP: Sparsity of models reflected by the count of non-zero weights.
 Elastic Net and SPLS demonstrate increased sparsity in the model weights for both brain and behaviour views, compared to PCA, RCCA, and PLS.

Model	Brain Weights (out of 300)	Behaviour Weights (out of 145)
PCA	300	145
RCCA	300	145
Elastic Net	241	96
PLS	300	145
SPLS	118	56

to psychiatric and life function tests, contrasting with negative correlations to certain emotion and personality tests. In comparison, the RCCA and Elastic Net models highlight a variation mode negatively correlated with the Line Orientation test and to a lesser extent, smoking, while showing positive correlations with other cognitive assessments. The PLS model's variation mode echoes the positive-negative pattern identified by Stephen M Smith et al., 2015, showing positive correlations with agreeableness, vocabulary tests, and life satisfaction, juxtaposed with strong negative correlations with smoking and antisocial behaviors. SPLS selects a similar mode but prioritizes vocabulary tests and smoking over rule-breaking and antisocial personality traits, aligning with the preprocessing steps described in Stephen M Smith et al., 2015 which incorporated a top-100 PCA projection of both brain and behavioural data.

5.1.3 Brain Connectivity Weights

In this section, we use two different methods to visualize the brain connectivity weights. The first method is to use chord diagrams to visualize the top 8 positive and negative brain weights for each model. This approach is inspired by the chord diagrams used in Stephen M Smith et al., 2015. The second method is to use surface maps to visualize the brain connectivity weights. This approach has been used by both Ferreira et al., 2022 and Stephen M Smith et al., 2015.

Chord Diagrams We grouped the nodes of the connectivity matrix of our data into 7 parcels according to the Yeo 7 network parcellation BT Thomas Yeo et al., 2011. This was achieved by assigning each node to the network with the highest voxelwise overlap. These are then arranged around the circumference of the chord diagram using the Nichord package (P. C. Bogdan et al., 2023). The plots then show

the 8 strongest positive and negative weights for each model as ‘chords’. The chord diagrams in Figure III.4 show the top 8 positive and negative brain weights for each model.

- The **RCCA** model displays a diverse set of connections across all networks, with especially prominent weights in the **somatomotor** and **default mode** networks.
- The **ElasticNet** model presents similar connections between the **somatomotor** and **default mode** networks.
- The **PLS** model exhibits strong connections between the **frontoparietal** and **visual** networks.
- The **SPLS** model exhibits similar connections between the **frontoparietal** and **visual** networks.

This is perhaps consistent with the behaviour data as the somatomotor network is associated with motor function and sensory processing which is related to the Line Orientation test, requiring spatial reasoning and motor coordination.

The correlations made by the PLS and SPLS models between substance abuse and cognitive tests could be due to the significant role the frontoparietal network plays in executive function, which can be impaired by substance abuse. Likewise, the visual network is likely involved in a number of the cognitive tests and could be disrupted by substance abuse.

The RCCA and ElasticNet models might be detecting more integrative and possibly higher cognitive functions, while the PLS and SPLS models might be highlighting the more immediate cognitive processes that can be disrupted by substance abuse.

5.1.4 Model Similarity

In this section, we compare the models in terms of their similarity. We can measure the pairwise similarity between two models by comparing their weights and their representations. We can compare the weights by computing the correlation between the weights of the two models and we can compare the representations by computing the correlation between the representations of the two models.

In Figure III.5, we plot the correlation between the brain and behaviour representations for each model. We can see clearly that both PCA, PLS, and SPLS are all highly correlated in terms of their brain representations, revealing the bias of

PLS towards the largest principal components. On the other hand, in the behaviour space, the models are less correlated, with the exception of PLS and SPLS which are highly correlated with one another. There is however still substantial correlation between the PCA and PLS models. The very low correlation between the Ridge CCA and Elastic Net models with the PCA model is evidence that there are stronger correlations outside of the first principal components.

In Figure III.6, we similarly plot the correlation between the brain and behaviour weights for each model. The story is similar, albeit with marginally lower correlations between the PLS and PCA-based models. Finally, in the weights space, the Ridge CCA and ElasticNet models are even less correlated with the PCA model.

5.2 ADNI Results

We now turn to the ADNI data.

5.2.1 Out of Sample Correlation

In this experiment, the Elastic Net model outperformed all other models in terms of out-of-sample correlation (Figure III.7). The RCCA model also outperformed the PLS and SPLS models while SPLS outperformed PLS. Surprisingly, PCA performed almost as well as PLS. This suggests that there is value in both tunable shrinkage and sparsity in this dataset. It also reveals that the correlated signal between the brain structure and behavioural data is relatively much stronger than in the HCP data.

5.2.2 Sparsity of Weights

Table 5.2 once again shows the number of non-zero weights for each model. We can see that tuned SPLS and Elastic Net once again identify sparse weights. In this case, the difference in performance is more convincing and suggests that this sparsity is less spuriously induced than for the HCP data. This is supported by the fact that Elastic Net and SPLS models find a similar level of sparsity in the brain weights. On the other hand SPLS finds a much sparser set of behavioural weights.

5.2.3 Behaviour Weights

As for the HCP data, Figure III.8 plots the top 8 positive and negative non-imaging weights for each model. Some of the identified behavioural weights including a number of orientation tests are similar across all of the models, including even PCA.

Table 5.2: ADNI: Number of non-zero weights for each model.

Model	Brain Weights (out of 168130)	Behaviour Weights (out of 31)
PCA	168130	31
RCCA	168130	31
Elastic Net	59617	17
PLS	168130	31
SPLS	74995	10

This is indicative of the strong shared signal between the behavioural data and the brain structure data. SPLS and Elastic Net both emphasize the orientation and recall tests in the weight space. The RCCA and Elastic Net models are surprisingly different in the weight space, with the RCCA weights on a couple of attention and calculation tests in addition to the ubiquitous orientation and recall tests.

5.2.4 Brain Structure Weights

We plot the weights as a mosaic plot with 3 slices in each direction in Figure .2. Previous work using SPLS with the ADNI dataset identified the same striking pattern of weights with the model strikingly selecting the hippocampal weights (João M Monteiro et al., 2016). The Elastic Net has a less visually appealing selection of weights, with a honeycomb pattern near the edges of the brain and likewise for RCCA. It is noticeable that PCA, PLS and SPLS both weights in the same direction whereas RCCA and Elastic Net weight different regions with opposite signs.

5.2.5 Model Similarity

In this section, we once again compare the models in terms of their similarity. In Figure III.10, we can see that all of the models are highly correlated in terms of their behaviour representations. The brain representations are less correlated, but once again PCA, PLS, and SPLS are highly correlated with one another and less correlated with the Ridge CCA and Elastic Net models.

Surprisingly, in Figure III.11, we can see that the weights in both views are less correlated. This is particularly true for the brain weights where PCA exhibits a very low correlation with Ridge CCA and Elastic Net.

6 Discussion and Limitations

The Flexible Regularised Alternating Least Squares (FRALS) framework for CCA, introduced in this chapter, exhibits promising performance in terms of out-of-sample correlation. Our findings indicate that, while Elastic Net CCA generally outperforms other CCA variants, much of the benefit is derived from using properly tuned Ridge regularization. This is most obviously illustrated in the HCP dataset where sparsity does not appear to be beneficial in terms of out-of-sample correlation and therefore casts doubt on whether the sparsity of the model is interpretable or spurious. It also questions whether the additional computational cost of Elastic Net CCA is justified. Our experiments reveal that Ridge CCA typically outperforms PLS across both datasets. This observation is akin to the dynamics of regularized regression, where maximal ridge regularization is seldom necessary, even in high-dimensional contexts.

6.1 FRALS Limitations

The Flexible Regularised Alternating Least Squares (FRALS) framework, while effective in certain aspects, is notably limited by its computational inefficiency. This inefficiency arises from two main factors: the dynamic nature of regression targets and the intensive computation required for each iteration.

6.1.1 Changing Regression Targets

In FRALS, regression targets are not static but dynamically evolve during the algorithm's execution. These targets are essentially projections of the other view, and as they change, they alter the optimization landscape. Consequently, the algorithm must frequently recompute the least squares solution for each view. This process results in significant computational overhead and often leads to redundant calculations, thereby contributing to the inefficiency of the FRALS framework.

6.1.2 Computational Time

The primary computational challenge in FRALS is the repeated calculation of the least squares solution for each view in every iteration. This requirement is resource-intensive and is the main factor contributing to the slow speed of the FRALS algorithm. Empirical observations from our experiments show that FRALS operates at a pace approximately 10 times slower than Ridge CCA, varying with the specifics

of the experimental setup. This disparity in speed is particularly noteworthy given the popularity of SPLS due to its speed and convenience. Figure III.12 provides an estimate of the time taken to fit each model across complete training datasets over multiple runs. It is evident from the figure that Elastic Net CCA, despite being an iterative algorithm, is significantly slower than other models, particularly with the high-dimensional ADNI data. While SPLS demonstrates much faster processing, it is only marginally slower than PLS and RCCA, both of which employ optimized solvers in C and use PCA preprocessing for efficiency. Consequently, PCA emerges as the fastest model in these comparisons.

6.2 Conclusion

In this chapter, we introduced the Flexible Regularised Alternating Least Squares (FRALS) framework for CCA. We used the FRALS framework to implement Elastic Net CCA. We then compared the performance of Elastic Net CCA with other CCA variants on two datasets: the HCP and ADNI. We found that Elastic Net CCA outperformed other CCA variants on both datasets but that the performance of Elastic Net CCA was similar to Ridge CCA on the HCP dataset. However, we found that Elastic Net CCA was much slower than other CCA variants.

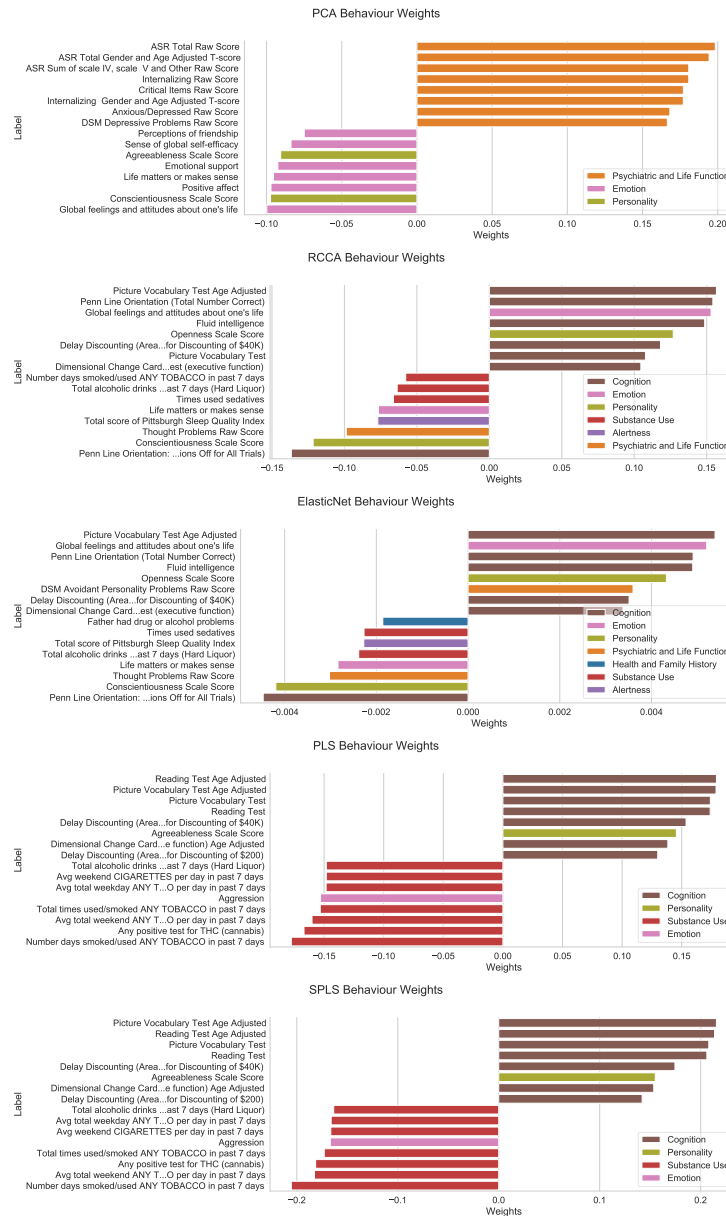


Figure III.3: HCP: Behavioural weights highlighting the top-8 positive and negative non-imaging weights. Each subfigure represents a distinct model's weight distribution across various behavioural domains such as cognition, emotion, personality, substance use, alertness, and psychiatric and life function. The variations in the weight profiles across models reflect differing patterns of association with the behavioural traits considered in the study.

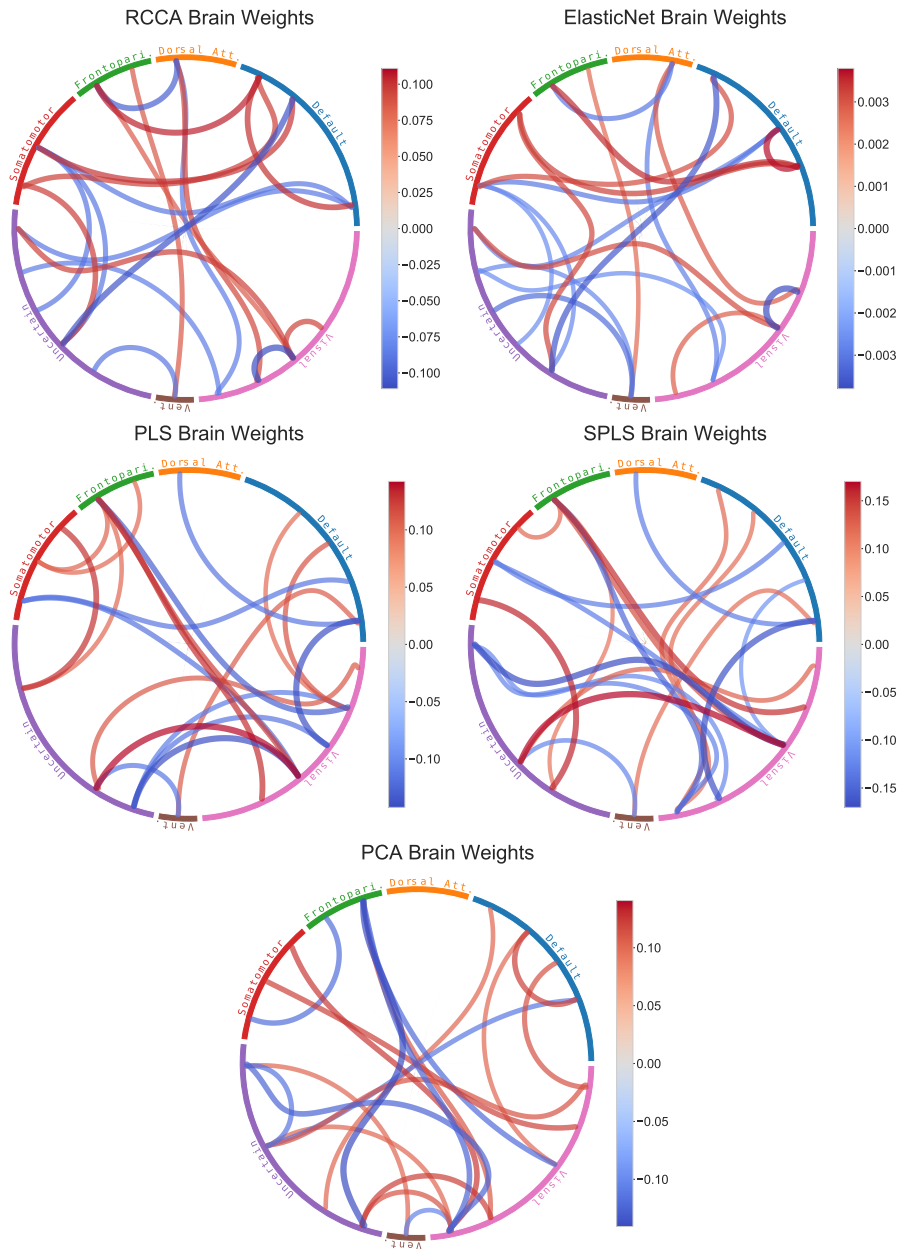


Figure III.4: HCP: Brain connectivity weights visualized through chord diagrams for multiple models. Each diagram portrays the 8 strongest positive (red to blue gradient) and negative (blue to red gradient) weights, grouped by the Yeo 7 network parcellation.

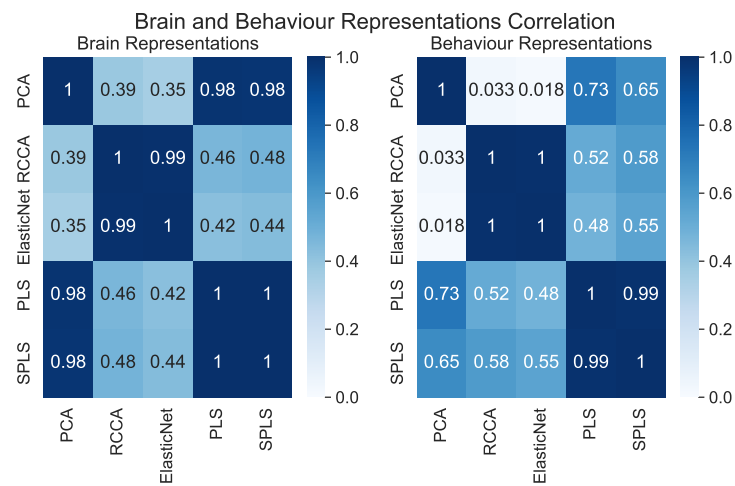


Figure III.5: HCP: Pairwise correlation matrix of brain representations across different models. The high correlation coefficients between PCA, PLS, and SPLS indicate a significant overlap in the brain representations they produce, suggesting a bias of PLS toward principal components. Contrarily, the Ridge CCA and Elastic Net models show notably lower correlations with PCA, indicating that these models capture brain representations beyond the first principal components.

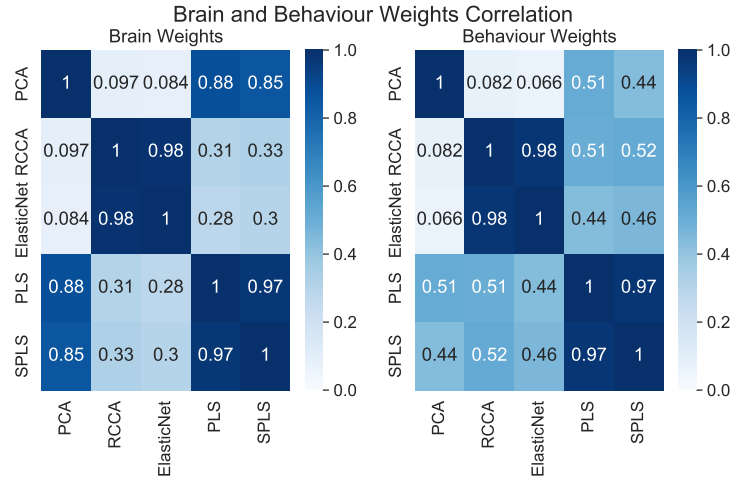


Figure III.6: HCP: Pairwise correlation matrix of the brain and behaviour weights used by each model. Similar to the brain representations, PCA, PLS, and SPLS show a high correlation in their weights, indicating similarity in the factors they consider significant. The lower correlations observed for Ridge CCA and Elastic Net with PCA suggest that these models give importance to different aspects of the data, potentially capturing more nuanced relationships.

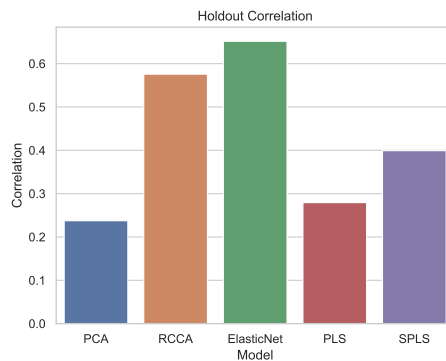
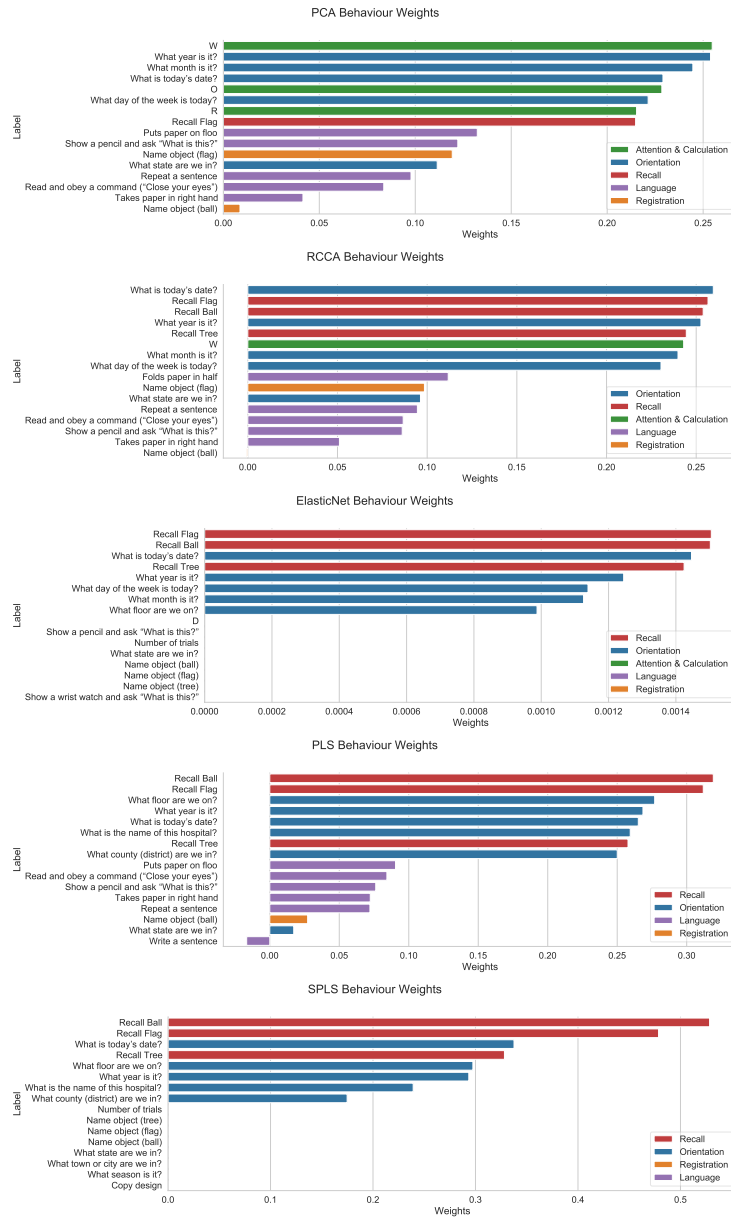


Figure III.7: ADNI: Comparative out-of-sample canonical correlations among PCA, RCCA, ElasticNet, PLS, and SPLS models. The bars represent the correlation coefficients, indicating that the Elastic Net models has superior performance over Ridge CCA, PLS, and SPLS in capturing holdout correlation.

**Figure III.8: ADNI:** Bar plots of the behaviour weights for each model.

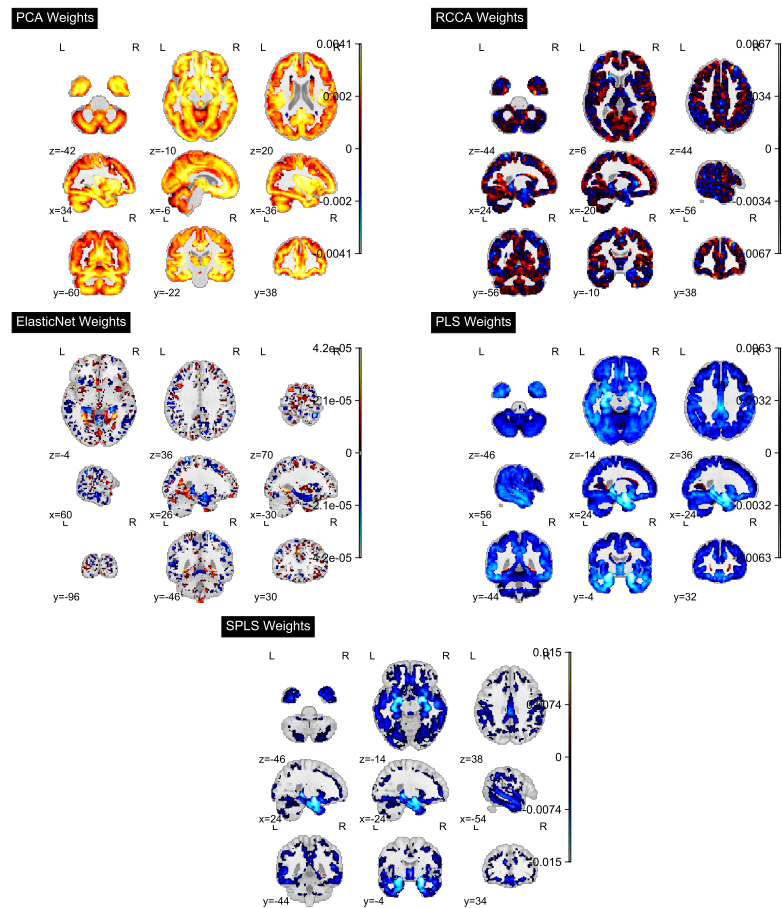


Figure III.9: ADNI: Statistical maps of brain structure weights for each model.

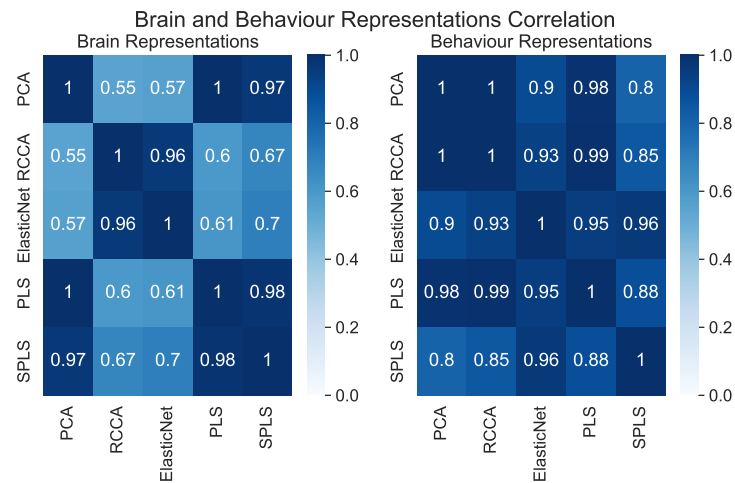


Figure III.10: ADNI: Correlation between the brain and behaviour representations for each model.

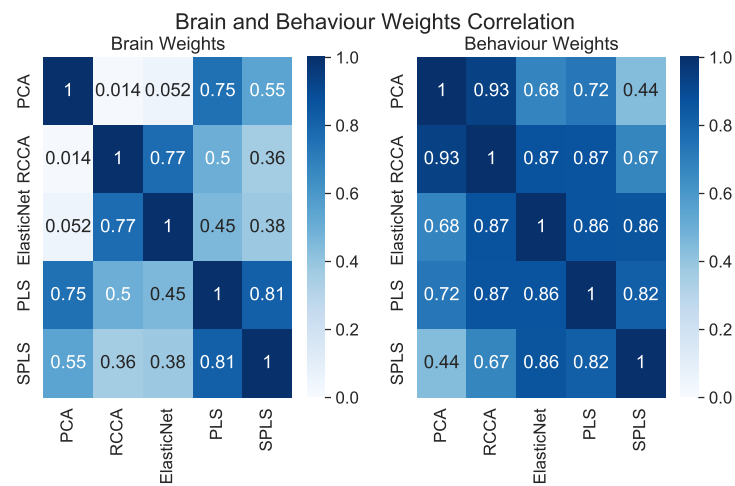


Figure III.11: ADNI: Correlation between the brain and behaviour weights for each model.

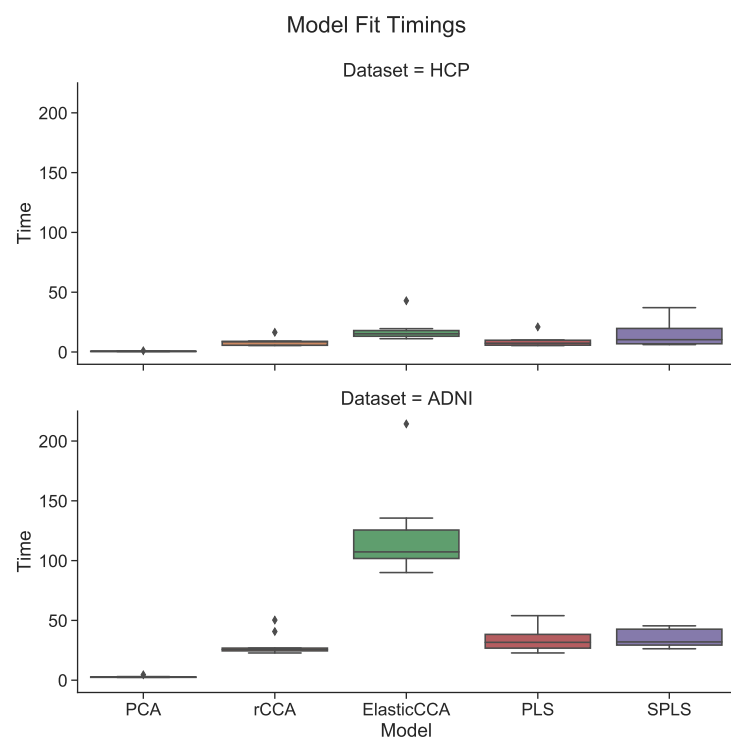


Figure III.12: Time taken to fit each model.

Chapter IV

Insights From Generating Simulated Data for CCA

All models are wrong, some are useful.

G. Box

Contents

1	Introduction.....	77
2	Background: Weights and Loadings in Canonical Correlation Analysis.....	79
3	Unifying Generative Perspectives in CCA: Explicit and Implicit Latent Variable Models	80
3.1	Explicit Latent Variable Models: Probabilistic CCA and GFA	80
3.2	Implicit Latent Variable Models: The Joint Covariance Matrix Perspective	82
3.3	Summary of Data Generation Methods.....	82
3.4	Regularization and Generative Models	83
4	Proving the Invariance of Loadings in CCA	87
5	Efficient Sampling of Simulated CCA Data	92
5.1	Challenges with High-Dimensional Data	93
5.2	Sampling from Multivariate Normal Distributions	93
5.3	Using Low-Rank Covariance Matrices	94

5.4	Calculating the True Canonical Correlations	94
5.5	Calculating the True Weights (and Loadings)	94
6	Experiment Design	95
6.1	Exploring the Relationship Between Weights and Loadings in CCA Using Simulated Data	95
6.2	Assessing Information Recovery in CCA and PLS Models Under Varying Signal-to-Noise Ratios.....	96
6.3	Methodology for Constructing Correlated Covariance Matrices in CCA Simulations	97
7	Experiment Results.....	99
7.1	Exploring the Relationship Between Weights and Loadings in CCA Using Simulated Data	99
7.2	Assessing Information Recovery in CCA and PLS Models Under Varying Signal-to-Noise Ratios.....	102
8	Discussion	106
8.1	Limitations	106
8.2	Conclusion.....	106

Preface

This chapter, deriving insights from various projects, primarily unpublished, delves into the application of loadings and weights for model interpretation in CCA models. However, the simulated data generation methods were used to generate simulated data in Mihalik, Chapman, Rick A Adams, et al. (2022a). The arguments for the use of loadings influenced our choice of loadings for the interpretation of the results in work under review R. Adams et al. (n.d.).

1 Introduction

In this chapter, we aim to address a significant debate within the Canonical Correlation Analysis (CCA) literature: the use of model weights versus loadings for model interpretation (Gu and Wu, 2018). This chapter combines insights mathematical insights from generative models of CCA along with empirical results from higher dimensionality simulated data than previously considered in the literature to generate insights into high-dimensional CCA studies.

We provide a novel categorization of methods for generating CCA simulated data, as documented in existing literature (D. M. Witten, Robert Tibshirani, and Hastie, 2009; M. Chen et al., 2013; Suo et al., 2017; Helmer et al., 2020), into explicit and implicit latent variable models. We suggest that latent variable models naturally reflect the hypothesis that latent factors influence the observed data, often made explicit in factor models (Ferreira et al., 2022; W. Cheng, P. Cheng, and Liou, 2013) and implicit in studies that interpret patterns through canonical variables (Mihalik, Ferreira, Rosa, et al., 2019; Mihalik, Ferreira, Moutoussis, et al., 2020). This distinction allows us to contrast the generative models in CCA literature with the generative model for linear regression, highlighting that in linear regression, regularization can be interpreted as prior on the weights, whereas in CCA, it is perhaps more natural to interpret regularization as a prior on the loadings. By adopting a number of computational tricks, we show how we are able to generate simulated data with significantly higher dimensions than previously considered in the literature (Helmer et al., 2020; Matković et al., 2023).

We also rigorously demonstrate that loadings are invariant to columnwise transformations in data matrices, unlike weights, a property that makes CCA unique compared to PCA or PLS. This of particular relevance in fields like brain-behavior studies, where data preprocessing often involves columnwise manipulation, with features such as questionnaire items routinely summarized into composite scores.

Our experimental design focuses on two main aspects: firstly, evaluating the ability of CCA models to accurately recover the true model weights and loadings, and secondly, examining the out-of-sample performance, which is often observed to be poor in practical datasets despite statistical significance, in particular for PLS-based models. Our experiments focus on two main aspects: firstly, evaluating the ability of CCA models to accurately recover the true model weights and loadings, and secondly, examining the out-of-sample performance, which is often observed to be poor in practical datasets despite statistical significance, in particular for PLS-based models. This observation led us to question whether the issue lies in poor model fit, or a lack of signal in the data with weak or biologically spurious correlations.

One of our most striking findings is the efficacy of Ridge Regularized CCA models as opposed to PLS models in identifying high correlations under anisotropic noise conditions. This complements earlier work (Helmer et al., 2020) that found that the number of samples needed to find high correlations increases with the dimensionality; our results suggest that the important variable is the dimensionality of the smaller view.

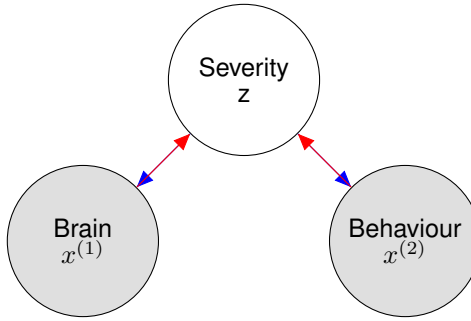


Figure IV.1: Forward and Backward Multiview Models: The **generative** and **discriminative** approaches in CCA.

2 Background: Weights and Loadings in Canonical Correlation Analysis

Canonical Correlation Analysis (CCA), as discussed in chapter II, finds linear combinations of variables in two datasets that exhibit the highest correlation. Introducing the concept of latent variables, especially in biomedical applications, helps uncover underlying factors influencing these observable data. This is crucial in understanding processes like gene expression or pathologies, and more broadly, in normative health distributions (Lawry Aguila, Chapman, and Altmann, 2023).

CCA's practical application revolves around two main approaches: the discriminative approach, which uses weights to estimate highly correlated latent variables from observed data, and the generative approach, focusing on the data generation process with loadings to describe the relationship between latent variables and observed data. The discriminative approach, represented as the 'backward model' in Figure IV.1, estimates the distribution $P(Z|X^{(1)}, X^{(2)})$. Conversely, the generative approach, the 'forward model', is concerned with $P(X^{(1)}, X^{(2)}|Z)$. Similar arguments have also been made in the context of PCA (Park, Ceulemans, and Van Deun, 2023) which also has both a generative (Tipping and Bishop, 1999) and discriminative (Hotelling, 1933) interpretation.

The ongoing debate in CCA research, highlighted by Gu and Wu (2018) and others, centers around the interpretation of models in terms of weights or loadings. Weights are often preferred for prediction, while loadings offer better interpretability (Z. Liu et al., 2022). This discussion is particularly relevant to our work in chapter III and various studies involving sparse CCA and PLS, where understanding the

meaning sparse loadings and weights becomes critical. Of particular importance to us given our work in chapter III, as well as a number of studies that employ variants of sparse CCA and sparse PLS is understanding the interpretation of sparse loadings and weights.

3 Unifying Generative Perspectives in CCA: Explicit and Implicit Latent Variable Models

This section categorizes the generative models in CCA literature into explicit and implicit latent variable types, each offering distinct insights into the data generation process and the relationship between weights and loadings.

3.1 Explicit Latent Variable Models: Probabilistic CCA and GFA

In explicit latent variable models, we assume each view is generated from a linear model with added noise, conditional on the latent variable. The distributions for the two views are given by:

$$z \sim \mathcal{N}(0, I) \tag{IV.1}$$

$$x^{(i)} \sim \mathcal{N}(W^{(i)}z + \mu^{(i)}, \Psi^{(1)}) \tag{IV.2}$$

Where z represents the latent variable, $x^{(i)}$ represents the i -th view, $W^{(i)}$ represents the model loadings, $\mu^{(i)}$ represents the mean, and Ψ_i represents the noise covariance matrix for the i -th view.

Bach and Jordan (2005) established that the maximum likelihood solution of this model relates the CCA weights to the loadings by the within-view covariance Σ_{ii} :

$$W^{(i)} = \Sigma_{ii} U^{(i)} R \tag{IV.3}$$

Where R is an arbitrary rotation matrix and $U^{(i)}$ is the matrix of CCA weights for the i -th view. For invertible covariance matrices, we can access an estimate of the ‘true’ CCA weights associated with the top-k subspace by multiplying the loadings by the inverse of the covariance matrix:

$$\hat{U}^{(i)} R = \Sigma_{ii}^{-1} W^{(i)} \quad (\text{IV.4})$$

We estimate the covariance matrices Σ_{ii} from the data using sample covariance matrices $\hat{\Sigma}_{ii}$. For Identity covariance matrices, the CCA weights are the same as the loadings.

In the Group Factor Analysis (GFA) model, we assume diagonal covariance, which aligns the marginal distribution of views with the probabilistic PCA model as the noise level decreases. This assumption enhances computational efficiency and supports extensions like sparsity on loadings:

$$z \sim \mathcal{N}(0, I) \quad (\text{IV.5})$$

$$x^{(i)} \sim \mathcal{N}(W^{(i)} z, \sigma_i^2 I) \quad (\text{IV.6})$$

The joint distribution of the two views with an explicit latent variable model is:

$$\begin{bmatrix} X^{(1)} \\ X^{(2)} \end{bmatrix} \sim \mathcal{N} \left(\begin{bmatrix} \mu^{(1)} \\ \mu^{(2)} \end{bmatrix}, \begin{bmatrix} W^{(1)} W^{(1)T} + \Psi^{(1)} & W^{(1)} W^{(2)T} \\ W^{(2)} W^{(1)T} & W^{(2)} W^{(2)T} + \Psi^{(2)} \end{bmatrix} \right) \quad (\text{IV.7})$$

Where $\Psi^{(i)}$ is the noise covariance matrix for the i -th view. Importantly, this shows us that the true covariance in each view is a function of the loadings and the noise covariance matrix. Specifically, the covariance matrix of the i -th view is given by:

$$\Sigma_{ii} = W^{(i)} W^{(i)T} + \Psi^{(i)} \quad (\text{IV.8})$$

When $W^{(i)} W^{(i)T}$ has large eigenvalues as compared to $\Psi^{(i)}$, Σ_{ii} is often called a ‘spiked covariance matrix’ (Johnstone, 2001). Interestingly, as the noise level approaches zero, the marginal distribution of the views aligns with the probabilistic PCA model for each view. In this case we don’t even need to model the data as a multiview problem to recover the latent variables, and suggests we should generally use PCA as a baseline.

3.2 Implicit Latent Variable Models: The Joint Covariance Matrix Perspective

The joint covariance matrix perspective, prevalent in sparse CCA literature (Suo et al., 2017; M. Chen et al., 2013), emphasizes covariance matrices over direct modeling of latent variables. This approach is advantageous for constructing data with known sparse weights and canonical correlations. This is achieved by constructing the joint covariance matrix of the distribution $P(X^{(1)}, X^{(2)})$:

$$\begin{bmatrix} X^{(1)} \\ X^{(2)} \end{bmatrix} \sim \mathcal{N} \left(\begin{bmatrix} 0 \\ 0 \end{bmatrix}, \begin{bmatrix} \Sigma_{11} & \Sigma_{12} \\ \Sigma_{21} & \Sigma_{22} \end{bmatrix} \right) \quad (\text{IV.9})$$

Where Σ_{11} and Σ_{22} are the within-view covariance matrices and Σ_{12} and Σ_{21} are the between-view covariance matrices.

For clarity and simplicity in our discussion, we refer to a single canonical correlation coefficient, ρ , without loss of generality. This allows us to focus on the structure of the covariance matrices without the complexity of multiple canonical correlations.

In constructing the between-view covariance matrices Σ_{12} and Σ_{21} , we control the true signal by setting active variables and correlations. Specifically, the between-view covariance matrix is constructed as follows:

$$\Sigma_{12} = \rho \Sigma_{11} u_1^{(1)} u_1^{(2)T} \Sigma_{22} \quad (\text{IV.10})$$

Here, ρ is the canonical correlation, and $u_1^{(i)}$ is the first column of the matrix of weights $U^{(i)}$ for the i -th view.

This perspective simplifies the structure of covariance matrices, focusing on the relationship between views as controlled by the canonical correlation coefficient, ρ , and the weights $u^{(i)}$.

3.3 Summary of Data Generation Methods

In the following tables, we compare the covariance structures and the relationship between weights and loadings across these data generation methods. These comparisons highlight key differences in modeling the relationships within and between views, and their implications for interpreting CCA in different scenarios.

Table 3.1 summarizes the joint covariance structures of each data generation

method.

Table 3.1: Covariance Structures in Data Generation Methods

	Method	Within-view Covariance Σ_{ii}	Between-view Covariance Σ_{12}
Explicit	Probabilistic CCA	$W^{(i)} W^{(i)T} + \Psi^{(i)}$	$W^{(1)} W^{(2)T}$
	GFA	$W^{(i)} W^{(i)T} + \sigma^{(i)2} I$	$W^{(1)} W^{(2)T}$
Implicit	Joint Covariance	Σ_{ii}	$\rho \Sigma_{11} u_1^{(1)} u_1^{(2)T} \Sigma_{22}$
	Joint Covariance (Identity)	I	$\rho u_1^{(1)} u_1^{(2)T}$

Table 3.2 summarizes the relationship between the weights and loadings in each data generation method, distinguishing between population and sample cases. This distinction is crucial, especially in scenarios where the population covariance matrix Σ is identity, but the sample covariance matrix $\hat{\Sigma}$ is only an approximation. An important observation is that for the implicit latent variable models, we can generate data with sparse weights but not, in general, sparse loadings. For the explicit latent variable models, we can generate data with sparse loadings but not, in general, sparse weights.

3.4 Regularization and Generative Models

In this section, we contrast the generative perspectives on Canonical Correlation Analysis (CCA) with the generative model for linear regression. We show that in linear regression, regularization can be interpreted as prior on the weights, whereas in CCA, we can interpret regularization as a prior on the loadings or the weights, with different implications for model interpretation. We also highlight the non-identifiability issue of the implicit latent variable model, where weights are not unique.

3.4.1 Regularization and the Generative Model for Linear Regression

Linear regression assumes data generation from a linear model with added noise:

$$y = xU + \epsilon, \quad \epsilon \sim \mathcal{N}(0, \sigma^2 I) \quad (\text{IV.11})$$

Table 3.2: Relationship Between Weights and Loadings in Population and Sample Cases

	Method	Case	Weights	Loadings
Explicit	Probabilistic CCA	Population	$(W^{(i)} W^{(i)T} + \Psi^{(i)})^{-1} W^{(i)}$	$W^{(i)}$
		Sample	$\hat{\Sigma}_{ii}^{-1} W^{(i)}$	$W^{(i)}$
	GFA	Population	$(W^{(i)} W^{(i)T} + \sigma^{(i)2} I)^{-1} W^{(i)}$	$W^{(i)}$
		Sample	$\hat{\Sigma}_{ii}^{-1} W^{(i)}$	$W^{(i)}$
Implicit	Joint Covariance (Non-Identity)	Population	$U^{(i)}$	$\Sigma_{ii} U^{(i)}$
		Sample	$U^{(i)}$	$\hat{\Sigma}_{ii} \hat{U}^{(i)}$
	Joint Covariance (Identity)	Population	$U^{(i)}$	$U^{(i)}$
		Sample	$U^{(i)}$	$\hat{\Sigma}_{ii} \hat{U}^{(i)}$

Here, y is the target variable, x the data matrix, U the regression coefficients, and ϵ represents i.i.d. Gaussian noise.

Lasso Regression The Lasso imposes a Laplace prior on the regression coefficients, leading to a double-exponential prior on weights:

$$U \sim \mathcal{L}(0, \lambda) \quad (\text{IV.12})$$

Ridge Regression Ridge regression, in contrast, employs a Gaussian prior on the regression coefficients, equivalent to a Gaussian prior on weights:

$$U \sim \mathcal{N}(0, \lambda) \quad (\text{IV.13})$$

3.4.2 Regularization and Generative Models for CCA

CCA models differ in their approach to regularization compared to linear regression.

Explicit Latent Variable Model Regularization in the context of the explicit latent variable naturally relates to priors on the loadings $W^{(i)}$. For example, sparsity in the loadings can be achieved by imposing a Laplace prior on the loadings:

$$W^{(i)} \sim \mathcal{L}(0, \lambda) \quad (\text{IV.14})$$

This expresses the prior belief that latent factors only explain the data through a small number of features. For example, in the context of latent factors in brain-behavior studies, this prior belief is equivalent to the assumption that a latent mode of variance (perhaps a subtype) is only expressed through a small number of brain regions.

Implicit Latent Variable Model In the implicit latent variable model of CCA, the joint likelihood of all observed x is modeled with Σ as a block covariance matrix, constructed based on the weights $U^{(i)}$. The covariance matrix Σ is structured to encapsulate both within-view variances and cross-covariances derived from the weights:

$$\Sigma = \begin{bmatrix} \Sigma_1 & \Sigma_1 U^{(1)} \rho U^{(2)T} \Sigma_2 \\ \Sigma_2 U^{(2)} \rho U^{(1)T} \Sigma_1 & \Sigma_2 \end{bmatrix} \quad (\text{IV.15})$$

Here, Σ_i represents the within-view covariance matrix for view i , and the off-diagonal blocks $\Sigma_1 U^{(1)} \rho U^{(2)T} \Sigma_2$ and its transpose represent the between-view covariance matrices. These matrices are functions of the weights $U^{(i)}$ and their interrelationships across different views of the data, modulated by ρ , the canonical correlation coefficients.

Here the regularization naturally relates to priors on the weights $U^{(i)}$. For example, sparsity in the weights can be achieved by imposing a Laplace prior on the weights:

$$U^{(i)} \sim \mathcal{L}(0, \lambda) \quad (\text{IV.16})$$

This expresses the more nuanced prior belief that the latent factors are expressed through a subset of features and then distorted by arbitrary rotations as well as the within-view covariance matrices. Manipulating equation IV.3, the conditional distribution of the implicit latent variable model we have:

$$x^{(i)}|z \sim \mathcal{N}(\Sigma_i U^{(i)} R z = W^{(i)} z, \Sigma_i - W^{(i)} W^{(i)T} = \Psi^{(i)}) \quad (\text{IV.17})$$

$$z \sim \mathcal{N}(0, I) \quad (\text{IV.18})$$

The arbitrary rotation matrix R means that for multidimensional $U^{(i)}$, even if $\Sigma_i = I$, and even if the true loadings are sparse, the weights may still not be sparse!

$$x^{(i)}|z \sim \mathcal{N}(U^{(i)} R z = W_{\text{sparse}}^{(i)} z, \Sigma_i - W_{\text{sparse}}^{(i)} W_{\text{sparse}}^{(i)T} = \Psi^{(i)}) \quad (\text{IV.19})$$

$$z \sim \mathcal{N}(0, I) \quad (\text{IV.20})$$

Alternatively, even if we know the true weights (i.e. $R = I$), the CCA model may not be able to recover them. This is to say they are not, in general, identifiable (Park, Ceulemans, and Van Deun, 2023). In other words there are multiple values of $W^{(i)}$ that can produce the same covariance structure.

We can illustrate this with a trivial example:

$$\Sigma_1 = \begin{bmatrix} 1 & 1 & 0 \\ 1 & 1 & 0 \\ 0 & 0 & 1 \end{bmatrix} \begin{bmatrix} 1 \\ 0 \\ 1 \end{bmatrix} = \begin{bmatrix} 1 & 1 & 0 \\ 1 & 1 & 0 \\ 0 & 0 & 1 \end{bmatrix} \begin{bmatrix} 0.5 \\ 0.5 \\ 1 \end{bmatrix} = \begin{bmatrix} 1 \\ 1 \\ 1 \end{bmatrix} \quad (\text{IV.21})$$

$$(\text{IV.22})$$

One practical implication of this observation is that it raises serious questions

about using stability selection, a common practice in the sparse CCA literature (Mihalik, Ferreira, Moutoussis, et al., 2020; Deng et al., 2021), to select the optimal regularization parameter. This is because different runs of the algorithm may result in different rotations of the weights, even if the representations are the same! This could lead to varying and potentially misleading interpretations.

Whereas priors on the loadings in the explicit latent variable model are intuitive, priors on the weights in the implicit latent variable model are evidently less so.

4 Proving the Invariance of Loadings in CCA

Building on these observations, we now shift our focus to a mathematical argument favoring the use of loadings over weights for the interpretation of CCA models. Specifically, we demonstrate that loadings are invariant to columnwise transformations of the data matrix, a property not shared by weights.

CCA can be solved in the principal component space. Consider the singular value decomposition (SVD) of the data matrices:

$$X^{(i)} = U^{(i)} \Sigma_i V^{i\top} \quad (\text{IV.23})$$

Here, $U^{(i)}$ and $V^{(i)}$ are the left and right singular vectors of $X^{(i)}$ respectively, and Σ_i is a diagonal matrix of singular values. The intuition behind this decomposition is that we are representing the data matrix in terms of its fundamental components: the directions of maximum variance (captured by $V^{(i)}$), the scale of these directions (captured by Σ_i), and the projections of the data onto these directions (captured by $U^{(i)}$). $U^{(i)}$ are the principal components of $X^{(i)}$.

Substituting Equation IV.23 into the CCA objective function, we have:

$$\max_{U^{(1)}, u^{(2)}} \text{Corr}(X^{(1)}U^{(1)}, X^{(2)}u^{(2)}) = \max_{U^{(1)}, u^{(2)}} \text{Corr}(U^{(1)}\Sigma_1 V^{1\top} U^{(1)}, U^{(2)}\Sigma_2 V^{2\top} u^{(2)}) \quad (\text{IV.24})$$

Reparameterizing the weights as $v^{(i)} = \Sigma_i V^{i\top} u^{(i)}$, we obtain:

$$\max_{v^{(1)}, v^{(2)}} \text{Corr}(U^{(1)}v^{(1)}, U^{(2)}v^{(2)}) \quad (\text{IV.25})$$

This reparameterization simplifies the optimization problem in two ways. Firstly, if the data matrices are low rank (which is guaranteed if the number of samples is less than the number of features), then the matrix of principal components $U^{(i)}$ is lower dimensional than the data matrix $X^{(i)}$, reducing the number of parameters in the optimization problem. Secondly, the reparameterization ensures that $v^{(1)T} U^{(1)T} U^{(1)} v^{(1)} = v^{(1)T} v^{(1)}$, making the constraints independent of the data. We can therefore solve the CCA problem by solving the simpler PLS problem in the principal component space, which is computationally more feasible but also gives us a convenient way to understand how the weights and loadings of CCA models change under different transformations of the data.

Definition: *Loadings* are defined using the reparameterized weights as follows:

$$w_j^{(i)} = \text{Corr}(X_j^{(i)}, U^{(i)} v^{(i)}) = \frac{\text{Cov}(X_j^{(i)}, U^{(i)} v^{(i)})}{\sqrt{\text{Var}(X_j^{(i)})} \sqrt{\text{Var}(U^{(i)} v^{(i)})}} \quad (\text{IV.26})$$

By convention, and without loss of generality, we standardize the latent variables to have unit variance so that:

$$w_j^{(i)} = \frac{\text{Cov}(X_j^{(i)}, U^{(i)} v^{(i)})}{\sqrt{\text{Var}(X_j^{(i)})}} \quad (\text{IV.27})$$

Intuitively, loadings measure how much each original feature contributes to the latent variables, providing insight into the structure of the data.

4.0.1 Scale Invariance of Loadings in CCA

First, we show that the loadings are invariant to column-wise scaling of the data matrix whereas the weights are not.

Effect of Scaling on Singular Vectors

Lemma 4.1. *Scaling the columns of the data matrix does not affect the left singular vectors $U^{(i)}$.*

Proof. Scale the columns of the data with a matrix C :

$$C = \begin{pmatrix} c_{11} & 0 & \cdots & 0 \\ 0 & c_{22} & \cdots & 0 \\ \vdots & \vdots & \ddots & \vdots \\ 0 & 0 & \cdots & c_{nn} \end{pmatrix} \quad (\text{IV.28})$$

where c_{ii} represents the scaling factor for the i -th column of the data matrix. For columns that are not scaled, $c_{ii} = 1$. This means that the corresponding column remains unchanged.

Since C is diagonal it can be represented by a diagonal matrix $S = C$ and an orthogonal matrix (the identity matrix) R . The transformed dataset is therefore $X^{(1')} = X^{(1)}C$:

$$X^{(1')} = U^{(i)}\Sigma_i V^{i\top} C = U^{(i)}(\Sigma_i S^{(i)})(^{(i)}V^{i\top} I) = \quad (\text{IV.29})$$

which makes clear that the left and right singular vectors $U^{(i)}$ and $V^{(i)}$ right remain unchanged. Therefore, the modified equation can be represented as:

$$X^{(1')} = U^i \Sigma_{i'} (V^{(i)})^T \quad (\text{IV.30})$$

where $\Sigma_{i'} = \Sigma_i S^{(i)}$. □

Noting that the CCA optimisation problem remains the same as in Equation IV.25, we can now show that the weights are not invariant to scaling of the data matrix but the loadings are.

Weights change From the earlier reparameterization, and given that $v^{(i')} = v^{(i)}$, the weights post-scaling are:

$$u^{(i')} = V^{(i)}(\Sigma_{i'})^{-1}v^{(i)} = V^{(i)}(\Sigma_{i'})^{-1}v^{(i)} = C^{(i)^{-1}}u^{(i)} \quad (\text{IV.31})$$

which are the original weights scaled by the inverse of the scaling matrix C . This means that the weights are not invariant to scaling of the data matrix. Furthermore it means we can set the weights to arbitrary values by scaling the data matrix.

Invariance to Linear Combinations in CCA Loadings Since loadings are correlations between the original features and the latent variables, they are invariant to scaling of the data. This follows from the definition of correlation and the unchanged latent variables:

$$w_j^{(i)} = \text{Corr}(X_j^{(i')}, U^{(i)}v^{(i)}) = \text{Corr}(c_{jj}X_j^{(i)}, U^{(i)}v^{(i)}) = \text{Corr}(X_j^{(i)}, U^{(i)}v^{(i)}) \quad (\text{IV.32})$$

Intuitively, the loadings remain the same because scaling the data does not change the relative contributions of each feature to the latent variables.

4.0.2 Invariance to Repeated Linear Combinations of Columns

We can also prove a more general result that the loadings are invariant to repeated linear combinations of columns of the data matrix. This is not as contrived as it sounds, since we often need to decide which features to include or exclude in a model, and when we work with highly correlated variables like survey questions, we may choose to use summary scores instead of individual questions.

Impact of Linear Combinations on Singular Vectors

Lemma 4.2. *Adding linear combinations of columns to the data matrix does not affect the left singular vectors $U^{(i)}$.*

Proof. Now, consider adding columns that are linear combinations of existing columns in $X^{(i)}$ to form $X^{(i'')}$. We can represent this using a transformation matrix A such that $X^{(i'')} = X^{(i)}A$:

$$A = \begin{pmatrix} 1 & 0 & \cdots & 0 & a_{11} & a_{12} & \cdots & a_{1m} \\ 0 & 1 & \cdots & 0 & a_{21} & a_{22} & \cdots & a_{2m} \\ \vdots & \vdots & \ddots & \vdots & \vdots & \vdots & \ddots & \vdots \\ 0 & 0 & \cdots & 1 & a_{n1} & a_{n2} & \cdots & a_{nm} \end{pmatrix} \quad (\text{IV.33})$$

where a_{ij} represents the weight of the j -th column in the i -th linear combination. The key is that we can still represent the transformed dataset as a product of the original left singular vectors $U^{(i)}$ and a new diagonal matrix $\Sigma_{i''}$ and right singular vectors $V^{(i'')}$.

$$X^{(i'')} = U^{(i)}(\Sigma_i V^{i\top} A) = U^{(i)}(\Sigma_{i'} V^{(i')\top}) \quad (\text{IV.34})$$

Where we know that the transformation is rank preserving because the first n columns of A are the identity matrix. The left singular vectors $U^{(i'')}$ therefore remain the same as $U^{(i)}$. \square

Weights are Underdetermined The weights $u^{(i'')}$ are underdetermined in the transformed space due to the added linear dependencies in the columns. The specific weights will depend on the SVD computation approach.

$$u^{(i'')} = V^{(i)}(\Sigma_{i''})^{-1}v^{(i)} \quad (\text{IV.35})$$

In the extreme case, if we have two identical columns in the data matrix, then we can use any weights we like for these columns provided that their sum is the same. The loadings, as before, remain unchanged because the original columns are unchanged and the latent variables are unchanged.

4.0.3 Summary

In this section, we have established the mathematical basis for preferring loadings over weights in interpreting CCA models. We demonstrated that loadings are invariant to columnwise transformations of the data matrix, a property not shared by weights. This distinction is not just of theoretical interest but has significant practical implications in the application of CCA.

Practical Implications While the identifiability of weights can be partially solved by the standardization of data, and while this is a common practice, it is not always necessary or desirable and always introduces assumptions. Additionally, in fields like psychometrics or social sciences, where survey data is often used, the decision to include or exclude specific features, or to use composite scores instead of individual items, can significantly affect the analysis. The invariance of loadings to such alterations in the data structure makes them a more robust choice for interpreting relationships between variables in these contexts.

In summary, the preference for loadings in the interpretation of CCA models is not only mathematically sound but also practically advantageous. It provides a more reliable and consistent framework for interpreting the relationships between variables in complex datasets, especially in interdisciplinary research, data preprocessing, and fields dealing with heterogeneous or transformed data.

5 Efficient Sampling of Simulated CCA Data

Efficient sampling from high-dimensional multivariate normal distributions is a critical step in simulating data for Canonical Correlation Analysis (CCA). Traditional methods can be computationally intensive and storage-demanding, especially for large datasets. This has in practice limited the dimensionality of simulated data, restricting the scope of research and analysis. For example Matkovic et al. (2023) simulate data with 8,000 observations and 100 features while Helmer et al. (2020) used at most 10,000 observations and 64 features. We were interested in the behavior of CCA in high-dimensional settings like voxel-wise MRI and connectivities, which can have hundreds of thousands of features (Jack Jr et al., 2008) and up to tens of thousands of observations (Sudlow et al., 2015). To address this challenge, we make the assumption that in biomedical data, the covariance matrix is low-rank and/or sparse, and use this to develop efficient methods for sampling from multivariate normal distributions.

5.1 Challenges with High-Dimensional Data

Direct sampling from a multivariate normal distribution is impractically slow for high-dimensional data¹. In particular, the implicit latent variable model requires storage of the full covariance matrix, which is prohibitive for high-dimensional data. This is because storing a covariance matrix with, for example, 100,000 dimensions would require 80GB of memory to store. This is impractical for many computers let alone laptops.

5.2 Sampling from Multivariate Normal Distributions

An efficient approach to sampling from a multivariate normal distribution is to use the Singular Value Decomposition (SVD) or cholesky decomposition of the covariance matrix. This approach involves decomposing the covariance matrix and then using the resulting components to transform samples from a standard multivariate normal distribution, thereby generating samples that conform to the desired high-dimensional distribution with reduced computational overhead.

$$Z \sim \mathcal{N}(0, I) \tag{IV.36}$$

$$X = \Sigma^{1/2} Z \tag{IV.37}$$

Where $\Sigma^{1/2}$ is a square root of the covariance matrix. Notice that this is exactly the same as the generative model for the explicit latent variable model, where $\Sigma^{1/2}$ is the matrix of loadings. Note that we can also add low rank noise by sampling from an independent multivariate normal distribution and adding it to the transformed samples. This means we only need to sample from a univariate normal distribution and perform a matrix multiplication of complexity $O(np^2)$. However, even with this approach, the computational complexity and storage requirements can still be prohibitive for high-dimensional data. In particular, the implicit latent variable model requires storage of the full covariance matrix. For example, a covariance matrix with 100,000 dimensions would require 80GB of memory to store. This is impractical for many computers let alone laptops.

¹This has been arguably *the* core research challenge for Monte Carlo methods (Mackay, 1998)

5.3 Using Low-Rank Covariance Matrices

The explicit latent variable model, offers us more efficient approaches. We employ two strategies: sparse and low-rank covariance matrices. For certain applications, sparse covariance matrices offer an additional avenue for efficiency. These matrices, with many zero entries, reduce both computational complexity and storage requirements, allowing for faster processing and less memory usage. For example, a sparse covariance matrix with 100,000 dimensions and 10% density would only require 8GB of memory to store. Using low-rank covariance matrices, we can reduce the complexity further by storing only the factorized rank- k components. In this way we can reduce the storage requirements to at most $O(kp)$. For example, a low-rank covariance matrix with 100,000 dimensions, 10% density and rank 1000 would only require 80MB of memory to store. We also only need to draw $O(kp)$ samples from a univariate normal distribution and perform a matrix multiplication with complexity $O(nkp)$ rather than $O(np^2)$ for the full rank case.

5.4 Calculating the True Canonical Correlations

We can also control the population canonical correlations by varying the signal-to-noise ratio (SNR) i.e. the ratio of the variance of the signal to the variance of the noise (the sum of the eigenvalues of the covariance matrices).

5.5 Calculating the True Weights (and Loadings)

We get the loadings for free (they are the low-rank square root of the covariance matrix). For the weights, we can use the relationship between the weights and the loadings in the explicit latent variable model to calculate the weights from the loadings and the covariance matrix. Recall that the weights are given by:

$$\hat{W}^{(i)} = \Sigma_{ii} \hat{U}^{(i)} R \quad (\text{IV.38})$$

Where R is an arbitrary rotation matrix and $\hat{U}^{(i)}$ is the matrix of CCA weights for the i th view. This implies that for invertible covariance matrices, we can access the ‘true’ CCA weights associated with the top- k subspace by multiplying the loadings by the inverse of the covariance matrix:

$$\hat{U}^{(i)} R = \Sigma_{ii}^{-1} \hat{W}^{(i)} \quad (\text{IV.39})$$

The apparent problem is that we need to invert the $O(p^2)$ covariance matrix, which is computationally expensive. However, we can use the Sherman-Morrison-Woodbury formula to calculate the inverse of the covariance matrix in $O(kp^2)$ time, where k is the rank of the covariance matrix. This is because the inverse of a rank- k matrix can be written as a rank-1 update of the inverse of a rank-($k-1$) matrix. This means that we can calculate the weights in $O(kp^2)$ time, which is much faster than the $O(p^3)$ time required to calculate the weights directly from the covariance matrix.

In the sections so far, we have discussed the mathematical properties of weights and loadings in CCA models and categorized the different generative models for CCA. We have also shown how to efficiently sample from these generative models. In the next section, we will present a number of experiments demonstrating the relationship between weights and loadings in simulated data.

6 Experiment Design

Our goal in this section is to empirically demonstrate the relationship between weights and loadings in CCA models as well as to better understand the behavior of CCA models in the high-dimensional settings that section 5 enables, and which are of interest in the neuroimaging community.

The first set of experiments illustrates the relationship between weights and loadings in simulated data using explicit latent variable models with identity and non-identity covariance matrices. The second set of experiments illustrates the amount of information that can be recovered from simulated data using CCA and PLS models with varying signal-to-noise ratios and sample sizes.

6.1 Exploring the Relationship Between Weights and Loadings in CCA Using Simulated Data

Our first experiment is designed to illustrate the challenges of recovering the true weights and loadings respectively in CCA models for explicit and implicit latent variable models with identity and non-identity covariance matrices.

We compare the true weights derived from the data generation model with the estimated weights of CCA, Ridge CCA, Elastic Net, PLS, and PCA models. We

expect that when the covariance matrix is identity, the weights and loadings will be identical. When the covariance matrix is non-identity, we expect that the weights and loadings will be different. Moreover, we expect that the estimated loadings will be more stable than the estimated weights for CCA models because the weights are not always identifiable. Under the explicit latent variable model, we expect that the weights will only be (close to) sparse when the covariance matrix is close to identity. This means we do not expect the Elastic Net model to improve on the Ridge CCA model since the Lasso regularizes the weights but not the loadings. Finally, we expect that when using the explicit latent variable model, for high signal-to-noise ratios, the PLS and even PCA models will recover the true weights and loadings because the majority of the variance is explained by the latent variables.

Detailed Parameters of Simulated Data for Weights and Loadings Analysis in CCA We generate data with 100 samples and 10 features in each view. We then generate data under two implicit latent variable models and two explicit latent variable models. The ridge penalty is coarsely tuned between 0.1 and 0.9 in order to illustrate the effect of regularization as we already show the corner cases of no regularization (CCA) and full regularization (PLS). For the Elastic Net model, we tune the l1 ratio between 0.1 and 0.9. This ensures that the Elastic Net has some sparsity as compared to the Ridge model, effectively avoiding the corner case of no sparsity where the Elastic Net is equivalent to the Ridge model. We summarize the parameters of these experiments in table 6.1.

6.2 Assessing Information Recovery in CCA and PLS Models Under Varying Signal-to-Noise Ratios

Our next experiment was motivated by the observation that PLS models (including sparse PLS) often exhibit low but non-zero out of sample correlations in real high-dimensional data. We want to understand how much of this is due to the fact that PLS models optimize covariance rather than correlation, and how much is due to the fact that the signal-to-noise ratio is too low. In order to understand this, we simulated data with varying signal-to-noise ratios and compared the out of sample correlations of PLS models with the out of sample correlations of Ridge CCA models with varying regularization. Since we are interested in studying these effects in high-dimensional data, we aimed to simulate data with similar numbers of features to real brain-behavior datasets. This means that we are only able to use our memory-efficient sampling methods for the explicit latent variable model.

Table 6.1: Simulated Data Parameters for Weight and Loadings Recovery Experiments

Parameter	Value
Number of samples (n)	100 train, 500 test
Number of features in View 1 (p)	10
Number of features in View 2 (q)	10
True Latent dimensions	1
Fraction of active features (explicit:loadings, implicit:weights) View 1	0.5
Fraction of active features (explicit:loadings, implicit:weights) View 2	0.5

Detailed Parameters of Simulated Data for Signal-to-Noise Simulations We simulated data with 1000 samples and between 100 and 10,000 features in one view and 100 features in the other. These are of the same order of magnitude as typical brain-behaviour datasets. We summarise these data properties in table 6.2.

6.3 Methodology for Constructing Correlated Covariance Matrices in CCA Simulations

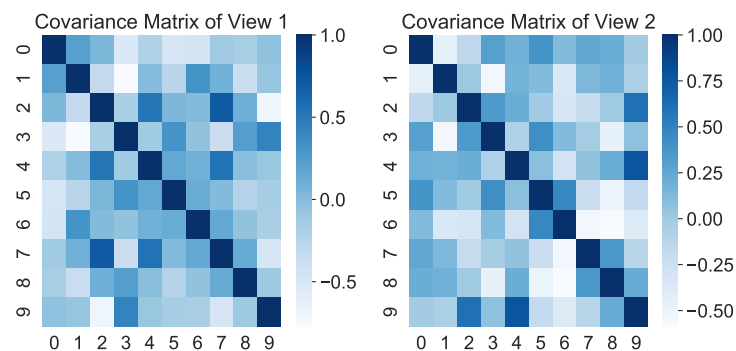
In both experiments, we construct correlated covariance matrices by generating a random matrix A with entries drawn from a uniform distribution between -1 and 1. We then construct the covariance matrix as $\Sigma = AA^\top$. This ensures that the covariance matrix is positive semi-definite and also tends to produce strong correlations.

We plot an example of the covariance matrices for correlated covariance matrices in both views in figure IV.2.

Recalling table 3.1, note that in the implicit latent variable models, these covariance matrices are precisely the population within-view covariance matrices. In the explicit latent variable models, these covariance matrices are just the covariance matrices of the noise to which we add the signal covariance matrices. Nonetheless,

Table 6.2: Simulated Data Parameters for Brain-Behaviour Simulations

Parameter	Value
Number of features in View 1 (p)	100-10000
Number of features in View 2 (q)	100-10000
True Latent dimensions	1
Fraction of active features View 1	1.0
Fraction of active features View 2	1.0
Signal-to-noise ratio	0.001-1

**Figure IV.2:** Example instances of correlated covariance matrices.

for strong enough noise, this process ensures that there are large correlations between features.

7 Experiment Results

7.1 Exploring the Relationship Between Weights and Loadings in CCA Using Simulated Data

We first present the results of the experiments demonstrating the relationship between weights and loadings in simulated data from explicit and implicit latent variable models with identity and non-identity covariance matrices.

For both cases, we plot the true weights and loadings along with the estimated weights and loadings for each model. We estimate model loadings by multiplying the model weights by the sample within-view covariance matrix following equation IV.3. This means that the estimated model loadings may not be sparse even when the estimated model weights are sparse and the *population* covariance matrix is identity.

7.1.1 Implicit Latent Variables (Sparse Weights)

Figure IV.3 shows the true and estimated weights and loadings for data generated from the implicit latent variable models with sparse weights. The Elastic net model exhibits no false negatives (i.e. where the true weight is non-zero but the estimated weight is zero) in both cases. This shows that the Elastic Net model is able to recover the true weights and that the Lasso penalty is indeed inducing sparsity in the weights. The CCA model appears recover spectrum of the true weights much better for the identity covariance matrices than for the correlated covariance matrices. This is likely because the multicollinearity introduced makes the learnt weights substantially less stable with respect to a change in the data.

We can also quantify the similarity between the true and estimated weights and loadings using the cosine similarity; a measure of the similarity between two vectors that is invariant to the scale of the vectors. The cosine similarity between two vectors is defined as the cosine of the angle between them (Luo et al., 2018). Since we are indifferent to the direction of the vectors, we take the absolute value of the cosine similarity. The absolute cosine similarity between two vectors is 1 if they are identical (up to a sign) and 0 if they are orthogonal. We plot the cosine similarity between the true and estimated weights and loadings for data generated from the implicit

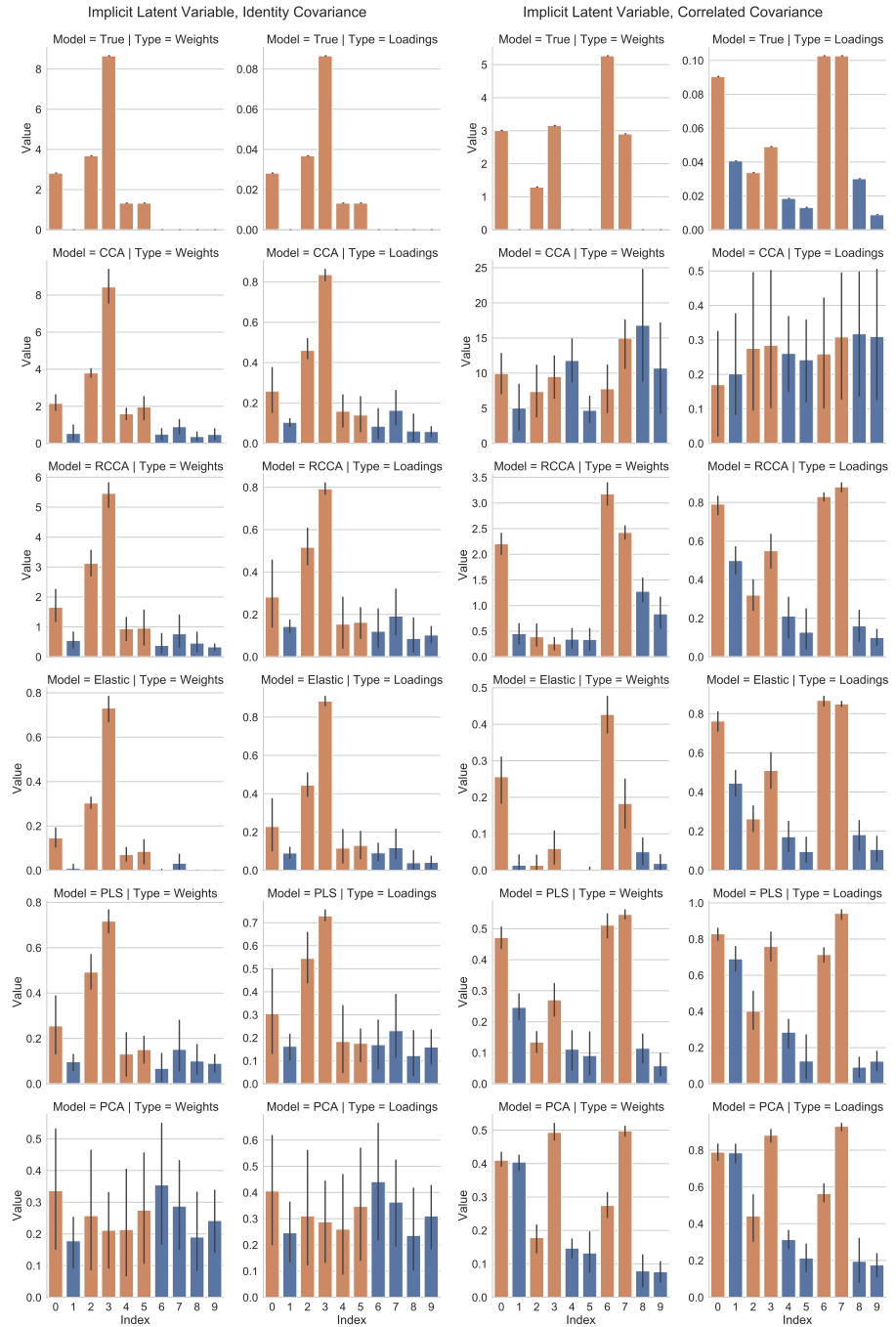


Figure IV.3: Bar plots of the true and estimated weights and loadings for data generated from the implicit latent variable models with sparse weights. The left column shows the results for the identity covariance matrices, while the right column shows the results for the correlated covariance matrices.

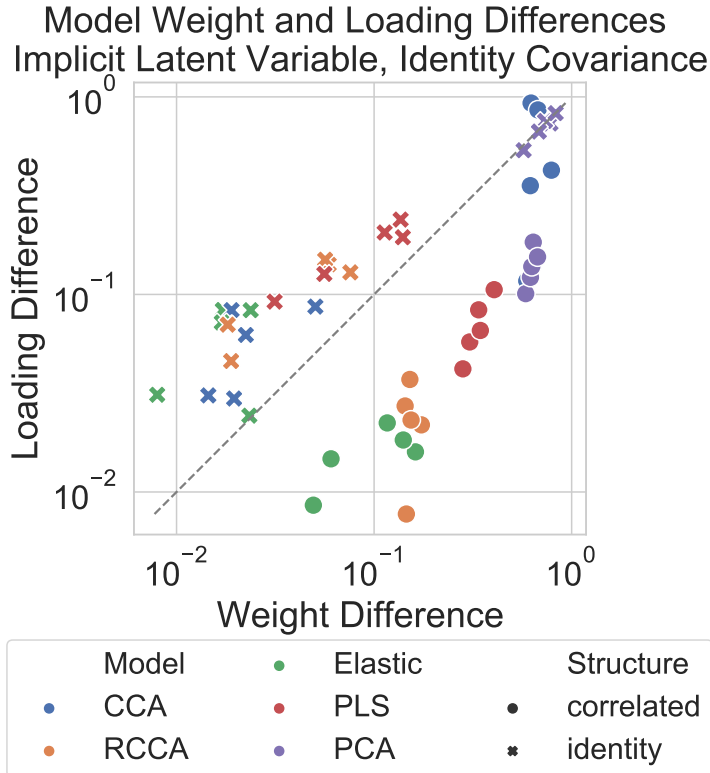


Figure IV.4: Cosine similarity between the true and estimated weights and loadings for data generated from the implicit latent variable models with sparse weights. We plot each run as a point on a scatter plot with a log scale. The grey line indicates where the similarity between weights and loadings are equal.

latent variable models with sparse weights in figure IV.4.

Interestingly, we see that for the identity covariance matrices, weight differences are smaller than loading differences. On the other hand for the correlated covariance matrices, the loading differences are smaller than the weight differences. This is evidence of the fact that the weights are not identifiable in the implicit latent variable model as suggested by our theory. Only when the covariance matrices are identity, and when there is only one latent variable, are the weights identifiable.

7.1.2 Explicit Latent Variables

Figure IV.5 shows the true and estimated weights and loadings for data generated from the explicit latent variable models with sparse loadings. The left column shows the results for the identity covariance matrices, while the right column shows the results for the correlated covariance matrices. Once again, the Elastic Net model exhibits no false negatives (i.e. where the true weight is non-zero but the estimated weight is zero) when the noise covariance matrix is identity such that both the weights and loadings are sparse.

Once again, we can quantify the similarity between the true and estimated weights and loadings using the cosine similarity (Figure IV.6).

Notably, when the noise covariance matrix is correlated, the difference in recovery of the weights is much larger than the difference in recovery of the loadings. Surprisingly, when the noise covariance matrix is identity, the PLS and PCA models appear to better recover the weights than the loadings in this case.

7.2 Assessing Information Recovery in CCA and PLS Models Under Varying Signal-to-Noise Ratios

In Figures IV.7 and IV.8 we plot the test correlation (score) varying the signal-to-noise ratio and the number of features under the identity and correlated noise covariance matrices respectively.

In figure IV.7, we can see that the PLS model outperforms all of the Ridge CCA models for all values of the signal-to-noise ratio and dimensionality, though only by a small margin. The unregularized CCA model is much worse than even the Ridge CCA model with the smallest regularization. In this experiment the performance of PLS is directly related to the signal-to-noise ratio.

In figure IV.8, we see a totally different picture. The PLS model is now outperformed by the Ridge CCA model with the smallest regularization. While CCA is still the worst performing model, PLS is now much worse across signal-to-noise ratios and dimensions than any of the Ridge CCA models. This suggests that the PLS model is not able to recover anything like the true signal when the covariance matrices are correlated.

In this experiment it is also clear that the signal-to-noise ratio must be higher to obtain the same performance with higher dimensional data. It is interesting that performance of the Ridge CCA improves across the board with lower regularization.

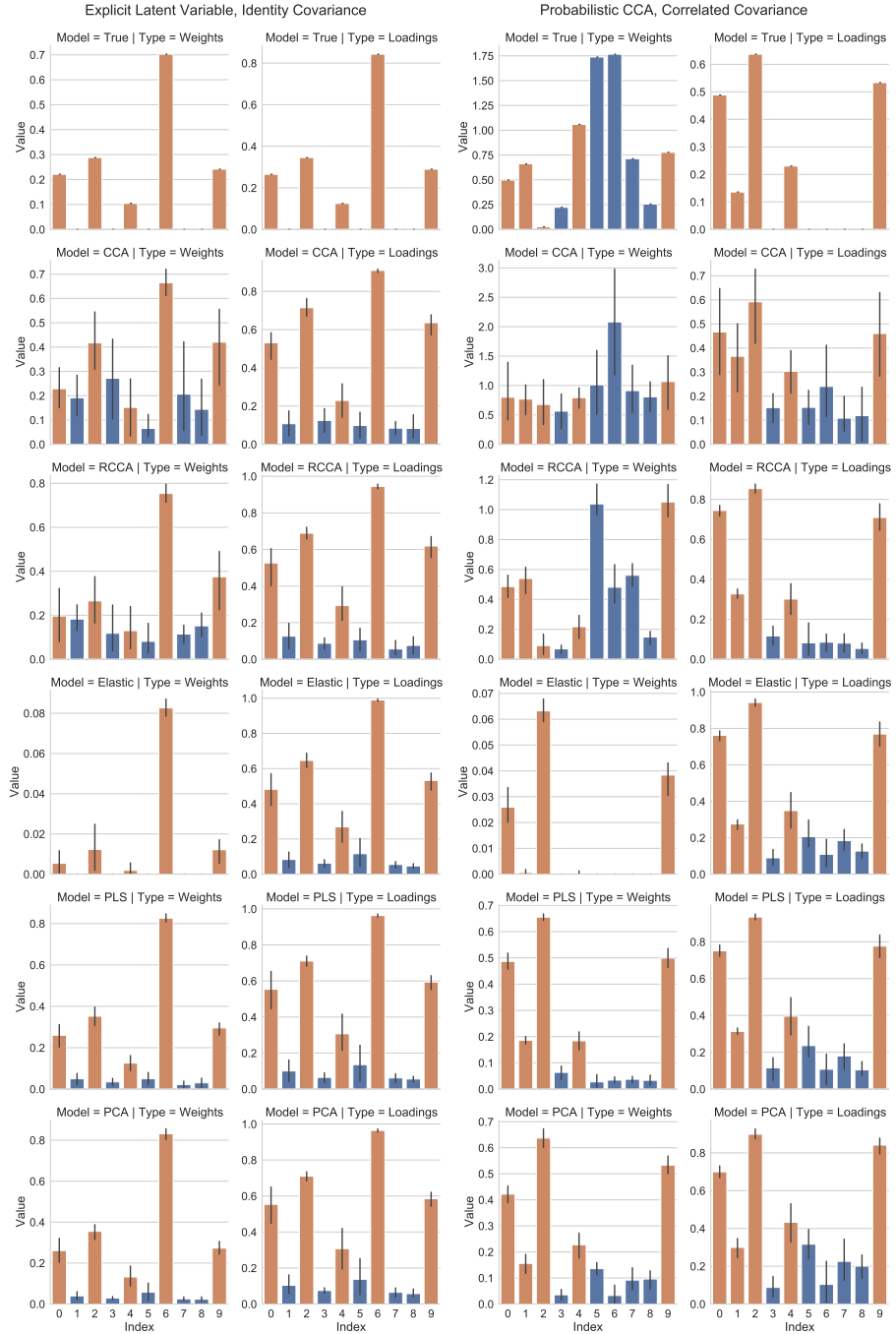


Figure IV.5: Bar plots of the true and estimated weights and loadings for data generated from the implicit latent variable models with sparse weights. The left column shows the results for the identity covariance matrices, while the right column shows the results for the correlated covariance matrices.

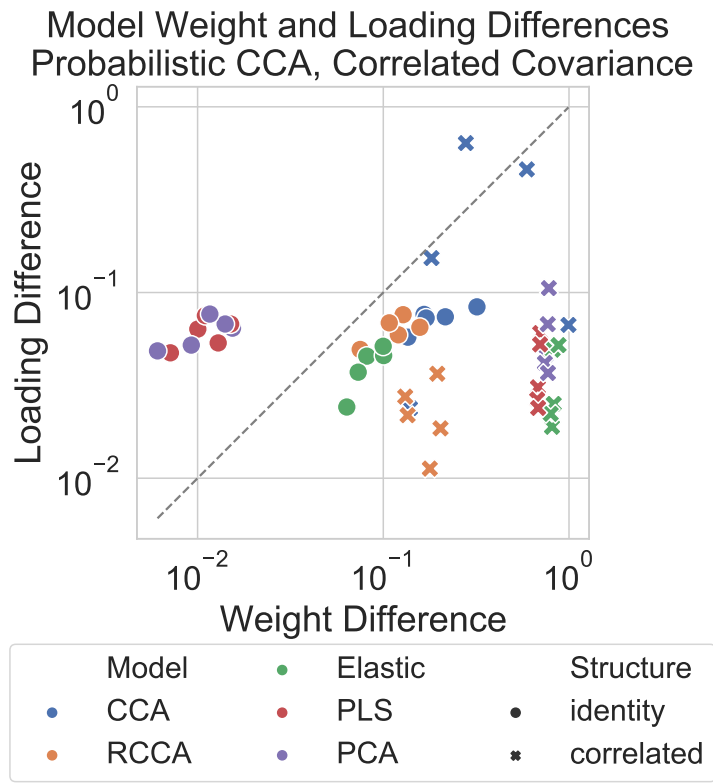


Figure IV.6: Cosine similarity between the true and estimated weights and loadings for data generated from the explicit latent variable models with sparse loadings. We plot each run as a point on a scatter plot with a log scale. The grey line indicates where the similarity between weights and loadings are equal.

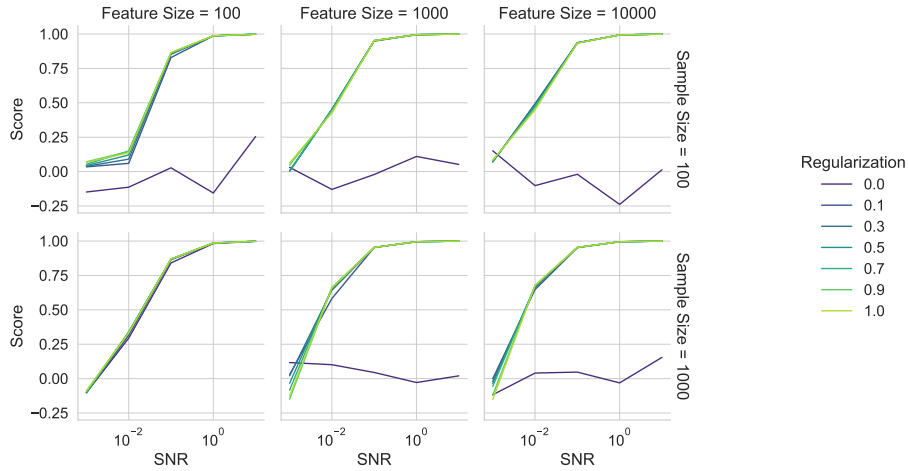


Figure IV.7: Varying signal to noise ratio with identity covariance matrices. We plot the performance of different levels of Regularized CCA from 0 (CCA) to 1 (PLS) for different sample sizes.

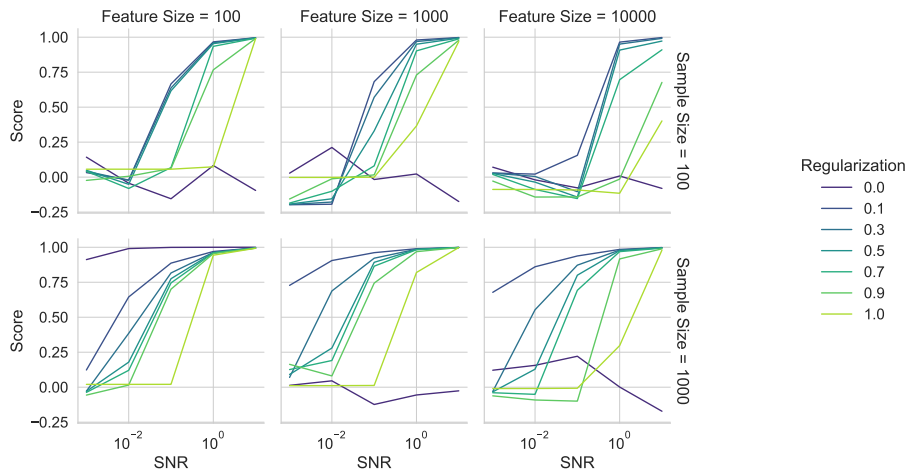


Figure IV.8: Varying signal to noise ratio with correlated covariance matrices. We plot the performance of different levels of Regularized CCA from 0 (CCA) to 1 (PLS) for different sample sizes.

8 Discussion

Given our theoretical observations in this chapter, a natural question to ask is whether we can construct a regularization functional that imposes sparsity on the loadings (instead of the weights). The answer is yes, but it is not straightforward and in the small sample setting, it is not clear that it is a good idea. The principle would be much the same as the Lasso, but we would need to use the sample covariance matrix to define the norm:

$$P(W) = \|W\|_1 \quad (\text{IV.40})$$

$$P(L) = \|\hat{\Sigma}U\|_1 \quad (\text{IV.41})$$

Which imposes an L1 penalty on the loadings via an L1 penalty on the weights multiplied by the sample covariance matrix. We could in principle apply the soft-thresholding operator to the estimated loadings. However we would need to be careful to ensure that the sample covariance matrix is invertible in order to get back to the weights. This is of course not guaranteed in the small sample setting.

8.1 Limitations

8.2 Conclusion

In this chapter, we unified methods for generating simulated multiview data from the generative perspectives of implicit and explicit latent variable models. We used this perspective to understand the relationship between weights and loadings in CCA models. Through a mathematical argument, we showed that the loadings are invariant to columnwise transformations of the data matrix, while the weights are not. This is a key advantage of loadings over weights for the interpretation of CCA models since it implies that weights are arbitrary and can be set to any value by scaling the data matrix or adding linear combinations of columns. Through a series of experiments, we showed how different simulated data generation models can enhance our understanding of the properties of CCA and PLS models.

Chapter V

Efficient Algorithms for the CCA Family: Unconstrained Losses with Unbiased Gradients

Contents

1	Introduction.....	108
2	Background: Efficient CCA.....	108
2.1	Challenges in Solving Generalized Eigenvalue Problems	108
2.2	PCA-CCA	109
2.3	Kernel CCA.....	110
2.4	Stochastic PLS and CCA	111
3	Methods: Novel Objectives and Algorithms	113
3.1	Unconstrained objective for GEPs	113
3.2	Corresponding Objectives for the CCA family	114
3.3	Applications to (multi-view) stochastic CCA and PLS....	116
4	Experiments and Results.....	116
4.1	Comparison to Scipy	116
4.2	Stochastic CCA	117

4.3	Stochastic PLS UK Biobank	120
5	Discussion	122
5.1	Limitations	122
5.2	Conclusion.....	124

Preface

The content of this chapter is based on a series of papers (Chapman, Aguila, and Wells, 2022; Chapman, Wells, and Aguila, 2023) as well as a NeurIPS workshop paper (Chapman and Wells, 2023). I am grateful to my co-authors Lennie Wells and Ana Lawry Aguila for their contributions to this work. In particular, Lennie’s mathematical expertise improved the theoretical grounding of the idea greatly and Ana’s access to the UK Biobank dataset enabled the application of our methods to a real-world biomedical dataset. In this thesis I include much of the work from these papers, but I exclude many of Lennie’s extensive proofs where I can make no claim to have contributed beyond proofreading.

1 Introduction

Classical algorithms for linear CCA methods require computing full covariance matrices and so scale quadratically with dimension, becoming intractable for many large-scale datasets of practical interest. There is therefore great interest in approximating solutions for CCA in stochastic or data-streaming settings (Arora, Cotter, et al., 2012).

2 Background: Efficient CCA

2.1 Challenges in Solving Generalized Eigenvalue Problems

The GEP is often represented as $Au = \lambda Bu$, where A and B are matrices. To generalize the dimensions of these matrices, let’s denote them as $m \times m$. This dimension m can vary based on the specific method in use. For instance, in Principal Component Analysis (PCA), represented as PCA, m would be equal to p since A and B are $p \times p$ matrices. In methods like Partial Least Squares (PLS) and Canonical Correlation Analysis (CCA), represented as PLS and CCA respectively, m would be $p_1 + p_2$, as A and B in these cases are $(p_1 + p_2) \times (p_1 + p_2)$.

Method	A	B	u	Dimensions
PCA	Σ_{11}	I	$u^{(1)}$	$p \times p$
LDA	S_B	S_W	$u^{(1)}$	$p \times p$
CCA	$\begin{pmatrix} \Sigma_{11} & \Sigma_{12} \\ \Sigma_{21} & \Sigma_{22} \end{pmatrix}$	$\begin{pmatrix} \Sigma_{11} & 0 \\ 0 & \Sigma_{22} \end{pmatrix}$	$\begin{pmatrix} u^{(1)} \\ u^{(2)} \end{pmatrix}$	$(p_1 + p_2) \times (p_1 + p_2)$
PLS	$\begin{pmatrix} 0 & \Sigma_{12} \\ \Sigma_{21} & 0 \end{pmatrix}$	I	$\begin{pmatrix} u^{(1)} \\ u^{(2)} \end{pmatrix}$	$(p_1 + p_2) \times (p_1 + p_2)$

Table 2.1: Definitions and dimensions of A and B for different subspace learning methods.

To solve the GEP, one common technique is to transform it into a standard eigenvalue problem $B^{-\frac{1}{2}}AB^{-\frac{1}{2}}y = \lambda y$, followed by eigendecomposition. However, this approach has computational complexity $\mathcal{O}((p_1 + p_2)^3)$ and may suffer from numerical instability.

2.2 PCA-CCA

One way to reduce the complexity of solving GEPs is to use the PCA-CCA method, which first applies PCA to the data and then solves the GEP in the reduced space. An important advantage of using PCA-CCA is computational efficiency, especially for high-dimensional data. The overall complexity of PCA-CCA involves two main steps. First, applying PCA has a complexity of $\mathcal{O}(p_1^3 + p_2^3)$, dominated by the larger of the two matrices. Second, solving the generalized eigenvalue problem in the reduced space with K components in each view leads to a complexity of $\mathcal{O}((2K)^3)$. Thus, the overall complexity of PCA-CCA is $\mathcal{O}(p_1^3 + p_2^3) + (2K)^3$, which is significantly lower than the complexity of solving the GEP directly. Since CCA, ridge CCA, and PLS can all be solved in the principal component space, PCA-CCA can be used to compute solutions efficiently *even if we keep all the principal components*. Most obviously, this is the case when the number of samples n is smaller than either of

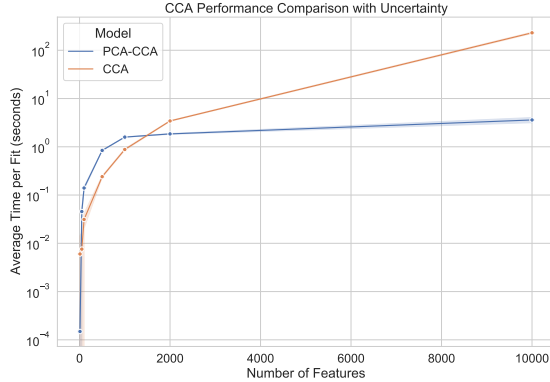


Figure V.1: Comparison of the complexity of PCA-CCA and CCA for varying numbers of samples and features.

the number of features p_1 or p_2 , i.e. $n < p_1$ or $n < p_2$. In this case the maximum number of principal components is $K = n$, and the complexity of PCA is $\mathcal{O}(n^3 + n^3)$ so that the overall complexity of PCA-CCA is thus $\mathcal{O}(2n^3 + (2n^3)^3) = \mathcal{O}(10n^3)$. For fat data where p_1 and p_2 are larger than n , we can reasonably expect $10n^3 < p_1^3 + p_2^3$ and thus PCA-CCA is still more efficient than solving the original GEP.

We illustrate this in a simple simulation study in Figure V.1¹.

This approach has been employed to great effect in neuroimaging but surprisingly is not used even in the scikit-learn implementation of CCA (Pedregosa et al., 2011). Nonetheless, for the large sample sizes (desirable for machine learning frameworks as well as statistical power), the complexity of even PCA-CCA can render the problems nearly intractable.

2.3 Kernel CCA

Kernel CCA (KCCA) also offers computational efficiency for high-dimensional data ($p_i > n$) as its complexity scales with the number of samples n , not the number of features p_i (Akaho, 2006). It casts the CCA optimisation as a dual problem:

¹This simulation was used to justify our pull request to scikit-learn (Pedregosa et al., 2011) implementing a PCA-PLS and PCA-CCA backend

$$\alpha_{\text{opt}} = \underset{\alpha}{\operatorname{argmax}} \{ \alpha^{(1)} K^{(1)T} K^{(2)} \alpha^{(2)} \} \quad (\text{V.1})$$

subject to:

$$\begin{aligned} \alpha^{(1)} K^{(1)T} K^{(1)} \alpha^{(1)} &= 1 \\ \alpha^{(2)} K^{(2)T} K^{(2)} \alpha^{(2)} &= 1 \end{aligned}$$

Where $\alpha^{(i)}$ are dual variables, $K^{(i)}$ are kernel matrices, and $K^{(i)T}$ are their transposes. The kernel matrices are defined as $K^{(i)} = \phi(X^{(i)})\phi(X^{(i)})^T$, where $\phi(\cdot)$ is a nonlinear mapping function. The kernel trick is used to avoid the explicit computation of the nonlinear mapping function $\phi(\cdot)$. The complexity of KCCA is $\mathcal{O}(n^3)$, which can be much lower than the complexity of solving the original GEP directly when $p_i > n$. However, a significant drawback of KCCA is the need for access to all training data at test time, which raises concerns about efficiency and scalability. Furthermore, when the number of samples is large, the kernel matrix can itself be too large to fit in memory.

2.4 Stochastic PLS and CCA

A number of algorithms have been proposed to approximate GEPs including PCA and PLS (Arora, Cotter, et al., 2012), and CCA specifically (K. Bhatia et al., 2018), in the ‘stochastic’ or ‘data-streaming’ setting; these can have big computational savings. Arora, Mianjy, and Marinov (2016) demonstrate that PLS can be approximated by applying a stochastic Power Method. For PLS, the iterations are computed by:

$$\begin{aligned} U_t^{(1)} &= \mathcal{P}_{\text{orth}} \left(U_{t-1}^{(1)} + \eta_t X_t Y_t^\top U_{t-1}^{(2)} \right), \\ U_t^{(2)} &= \mathcal{P}_{\text{orth}} \left(U_{t-1}^{(2)} + \eta_t Y_t X_t^\top U_{t-1}^{(1)} \right), \end{aligned}$$

where $\mathcal{P}_{\text{orth}}(\cdot)$ represents an orthogonal projection operator that projects a vector or matrix onto the space orthogonal to the current subspace. $\hat{U}_t^{(1)}$ and $\hat{U}_t^{(2)}$ are the current estimates of the left and right singular vectors for the two views, X_t and Y_t are the new data points at time t , and η_t is the learning rate at time t . The approach has low computational complexity, $\mathcal{O}(k(p_1 + p_2))$. However there are two main drawbacks to this approach. First, convergence is not guaranteed. Second, the orthogonal projection step does not extend naturally to the CCA problem where the constraint is $U^\top B U = I$ rather than $U^\top U = I$.

To the best of our knowledge, the state-of-the-art in Stochastic PLS and CCA are the subspace Generalized Hebbian Algorithm (SGHA) (Z. Chen et al., 2019) and γ -EigenGame (I. M. Gemp et al., 2020; I. Gemp, McWilliams, et al., 2021).

SGHA uses a Lagrange multiplier heuristic along with saddle-point analysis, albeit with limited convergence guarantees. Specifically, they form the constrained optimization problem for the top-k subspace as

$$\min_U -\text{Tr} U^T A U \quad \text{subject to} \quad U^T B U = I \quad (\text{V.2})$$

Transforming this into an unconstrained problem using Lagrange multipliers:

$$\min_U -\text{Tr} (U^T A U) + \lambda (U^T B U - I) \quad (\text{V.3})$$

Finally, they combine the primal and dual updates into a single update rule:

$$U_{t+1} = (1 - \eta_t) U_t + \eta_t (A U_t + \lambda_t B U_t) \quad (\text{V.4})$$

This algorithm is very simple to implement but because it is based on a heuristic primal-dual update rule rather than gradient descent, it is hard to use with more sophisticated optimizers such as Adam (Kingma and Ba, 2014).

γ -EigenGame is a stochastic algorithm for CCA which is based on the γ -Eigengame for PCA (I. M. Gemp et al., 2020). The EigenGame series of algorithms are based on the idea of eigenvectors competing to explain the data. They each maximize a utility function with reward and penalty terms:

$$\max_{u_i} \underbrace{\frac{u_i^T A u_i}{u_i^T B u_i}}_{\text{rewards}} - \sum_{j < i} \underbrace{\frac{(u_j^T A u_j)(u_i^T B u_j)^2}{(u_j^T B u_j)^2(u_i^T B u_i)}}_{\text{penalties}} \quad (\text{V.5})$$

Where player i only needs to maintain orthogonalization with respect to players $j < i$. By a few heuristic arguments, this can be moulded to an update rule in the full batch case:

$$u_i \leftarrow (u_i^T B u_i) A u_i - (u_i^T A u_i) B u_i - \sum_{j < i} (u_i^T A y_j) [(u_i^T B u_i) B y_j - (u_i^T B y_j) B u_i] \quad (\text{V.6})$$

Where $y_i = \frac{u_i}{\sqrt{u_i^T B u_i}}$. Finally, the stochastic version of this algorithm is obtained by replacing $B y_j$ with a rolling average of $B u_j$, necessitating an additional hyper-parameter γ which must be tuned. As with SGHA, this algorithm is also hard to combine with more sophisticated optimizers.

Further Benefits of Stochastic Algorithms Stochastic algorithms also introduce a form of implicit regularisation (S. L. Smith et al., 2021) which can be very helpful in these high-dimensional settings.

3 Methods: Novel Objectives and Algorithms

In this section, we introduce a novel class of objectives for GEPs, which we call the Eckhart–Young (EY) objectives. They can be applied to any GEP, including CCA, PLS, and PCA but we will focus on CCA.

3.1 Unconstrained objective for GEPs

First, we present proposition 3.1, a formulation of the top- K subspace of GEP problems, which follows by applying the Eckhart–Young–Minsky inequality (Stewart and J.-G. Sun, 1990) to the eigen-decomposition of $B^{-1/2} A B^{-1/2}$. However, making this rigorous requires some technical care which we defer to the proof in supplement 2.

Proposition 3.1 (Eckhart–Young inspired objective for GEPs). *The top- K subspace of the GEP (A, B) can be characterized by minimizing the following objective over $U \in \mathbb{R}^{D \times K}$:*

$$\mathcal{L}_{\text{EY-GEP}}(U) := \text{trace}(-2 U^T A U + (U^T B U)(U^T B U)) \quad (\text{V.7})$$

Moreover, the minimum value is precisely $-\sum_{k=1}^K \lambda_k^2$, where (λ_k) are the generalized eigenvalues.

This objective also has appealing geometrical properties. It is closely related to a wide class of unconstrained objectives for PCA and matrix completion which have

no spurious local optima (Ge, Jin, and Zheng, 2017), i.e. all local optima are in fact global optima. This implies that certain local search algorithms, such as stochastic gradient descent, should indeed converge to a global optimum.

Proposition 3.2. *[No spurious local minima] The objective \mathcal{L}_{EY-GEP} has no spurious local minima. That is, any matrix \bar{U} that is a local minimum of \mathcal{L}_{EY-GEP} must in fact be a global minimum.*

It is also possible to make this argument quantitative by proving a version of the strict saddle property from Ge, Jin, and Zheng, 2017; Ge, Huang, et al., 2015; we state an informal version here and give full details in Section 3.

Corollary 3.1 (Informal: Polynomial-time Optimization). *Under certain conditions on the eigenvalues and generalized eigenvalues of (A, B) , one can make quantitative the claim that: any $U_K \in \mathbb{R}^{D \times K}$ is either close to a global optimum, has a large gradient $\nabla \mathcal{L}_{EY-GEP}$, or has Hessian $\nabla^2 \mathcal{L}_{EY-GEP}$ with a large negative eigenvalue.*

Therefore, for appropriate step-size sequences, certain local search algorithms, such as sufficiently noisy SGD, will converge in polynomial time with high probability.

3.2 Corresponding Objectives for the CCA family

For the case of linear CCA we have $U^T A U = \sum_{i \neq j} \text{Cov}(Z^{(i)}, Z^{(j)})$, $U^T B U = \sum_i \text{Var}(Z^{(i)})$. To help us extend this to the general case of nonlinear transformations, Equation (II.1), we define the analogous matrices of total between-view covariance and total within-view variance

$$C(\theta) = \sum_{i \neq j} \text{Cov}(Z^{(i)}, Z^{(j)}), \quad V(\theta) = \sum_i \text{Var}(Z^{(i)}) \quad (\text{V.8})$$

In the case of linear transformations:

$$Z_k^{(i)} = \langle u_k^{(i)}, X^{(i)} \rangle. \quad (\text{V.9})$$

it makes sense to add a ridge penalty so we can define

$$V_\alpha(\theta) = \sum_i \alpha_i U^{(i)T} U^{(i)} + (1 - \alpha_i) \text{Var}(Z^{(i)}) \quad (\text{V.10})$$

This immediately leads to following unconstrained objective for the CCA-family of problems.

Definition 3.1 (Family of EY Objectives). *Learn representations $Z^{(i)} = f^{(i)}(X^{(i)}; \theta^{(i)})$ minimizing*

$$\mathcal{L}_{\text{EY}}(\theta) = -2 \operatorname{trace} C(\theta) + \|V_\alpha(\theta)\|_F^2 \quad (\text{V.11})$$

Unbiased estimates since empirical covariance matrices are unbiased, we can construct unbiased estimates to C, V from a batch of transformed variables \mathbf{Z} .

$$\hat{C}(\theta)[\mathbf{Z}] = \sum_{i \neq j} \widehat{\operatorname{Cov}}(\mathbf{Z}^{(i)}, \mathbf{Z}^{(j)}), \quad \hat{V}(\theta)[\mathbf{Z}] = \sum_i \widehat{\operatorname{Var}}(\mathbf{Z}^{(i)}) \quad (\text{V.12})$$

In the linear case we can construct $\hat{V}_\alpha(\theta)[\mathbf{Z}]$ analogously by plugging sample covariances into Equation (V.10). Then if \mathbf{Z}, \mathbf{Z}' are two independent batches of transformed variables, the batch loss

$$\hat{\mathcal{L}}_{\text{EY}}[\mathbf{Z}, \mathbf{Z}'] := -2 \operatorname{trace} \hat{C}[\mathbf{Z}] + \langle \hat{V}_\alpha[\mathbf{Z}], \hat{V}_\alpha[\mathbf{Z}'] \rangle_F \quad (\text{V.13})$$

gives an unbiased estimate of $\mathcal{L}_{\text{EY}}(\theta)$. This loss is a differentiable function of \mathbf{Z}, \mathbf{Z}' and so also of θ .

Simple algorithms: We first define a very general algorithm using these estimates in Algorithm 1. In the next section we apply this algorithm to multi-view stochastic CCA and PLS.

Algorithm 1: GEP-EY: General algorithm for learning correlated representations

Input: data stream of mini-batches $(\mathbf{X}(b))_{b=1}^\infty$ where each consists of M samples from the original dataset. Learning rate $(\eta_t)_t$. Number of time steps T . Class of functions $f(\cdot; \theta)$ whose outputs are differentiable with respect to θ .

Initialize: $\hat{\theta}$ with suitably random entries

for $t = 1$ **to** T **do**

- Obtain two independent mini-batches $\mathbf{X}(b), \mathbf{X}(b')$ by sampling b, b' independently
- Compute batches of transformed variables
- $\mathbf{Z}(b) = f(\mathbf{X}(b); \theta), \mathbf{Z}(b') = f(\mathbf{X}(b'); \theta)$
- Estimate loss $\hat{\mathcal{L}}_{\text{EY}}(\theta)$ using Equation (V.13)
- Obtain gradients by back-propagation and step with your favourite optimizer.

end for

3.3 Applications to (multi-view) stochastic CCA and PLS

Lemma 3.1 (Objective recovers GEP formulation of linear (multi-view) CCA). *When $f^{(i)}$ are linear, as in V.9, the population loss from Equation (V.11) recovers MCCA.*

Proof. By construction, for linear MCCA we have $C = U^T A U$, $V_\alpha = U^T B_\alpha U$, where (A, B_α) define the GEP for MCCA introduced in Equation (II.31). So $\mathcal{L}_{\text{EY}}(U) = \mathcal{L}_{\text{EY-GEP}}(U)$ and by Proposition 3.1 the optimal set of weights define a top- K subspace of the GEP, and so is a MCCA solution. \square

Moreover, by following through the chain of back-propagation, we obtain gradient estimates in $\mathcal{O}(MKD)$ time. Indeed, we can obtain gradients for the transformed variables in $\mathcal{O}(MK^2)$ time so the dominant cost is then updating U ; we flesh this out with full details in Section 4.

4 Experiments and Results

4.1 Comparison to Scipy

In a first simple experiment, we compare our method to solving the CCA Generalized Eigenvalue Problem using the `scipy` implementation of `eigh` (Virtanen et al., 2020). We use a sample size of 10,000 and vary the number of features in each view from 10 to 5,000. We solve for the top-5 CCA subspace and repeat each experiment 5 times. We compare the time taken to solve the GEP using `eigh` to the time taken to train our method until the frobenius norm of the change in successive weights is less than 10^{-5} .

Observations Figure V.2 shows the results of this experiment. Up until 1,000 features, our method is slower than `eigh` but after this point, our method is significantly faster. Beyond this point, the time taken to solve the GEP using `eigh` scales quadratically with the number of features, while our method scales linearly. This is because our method scales linearly with both the number of samples and the number of features, while `eigh` scales quadratically with the number of features².

²When the number of features is greater than the number of samples as in ridge CCA and PLS, we can use the PCA or Kernel trick to scale CCA quadratically with the minimum of the number of features and samples, though this still requires a somewhat expensive PCA

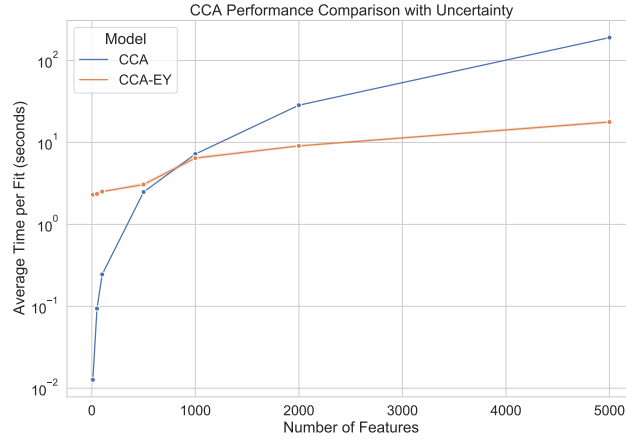


Figure V.2: Comparison of the time taken to solve CCA using `eigh` and our CCA-EY method.

4.2 Stochastic CCA

In our second experiment, we aim to demonstrate that our proposed CCA-EY method not only matches but potentially surpasses the performance of established baselines γ -EigenGame and SGHA in terms of convergence speed and robustness to hyperparameter settings. Our experimental setup largely follows the framework established by Z. Meng, Chakraborty, and Singh (2021) and I. Gemp, C. Chen, and McWilliams (2022). A key distinction in our approach, however, is the decision to not perform PCA on the data prior to applying CCA methods. This choice retains the full complexity of the datasets, providing a more rigorous evaluation of each algorithm's ability to handle high-dimensional data efficiently and accurately.

One of the central goals of this comparison is to illustrate that CCA-EY can achieve faster convergence with less hyperparameter tuning, an essential attribute for practical applications. To facilitate a fair and direct comparison with the baseline methods, we employ Stochastic Gradient Descent (SGD) as the optimization technique for all algorithms. It is worth noting that while SGD provides a baseline for performance assessment, the potential of our CCA-EY method could be further unleashed by utilizing more advanced optimization techniques such as momentum-based optimizers like Adam or Nesterov acceleration. These advanced methods are known for their ability to accelerate convergence and navigate the optimization landscape more effectively, suggesting that our method might yield even better

performance under such enhanced optimization schemes.

We train models to optimize CCA on the MediaMill and Split-CIFAR-10 datasets for a single epoch, using mini-batch sizes ranging from 5 to 100. These sizes were selected to test the scalability and efficiency of our method under varied computational loads. The Proportion of Correlation Captured (PCC) metric, defined as $PCC = (\sum_{i=1}^K \rho_k) / (\sum_{k=1}^K \rho_k^*)$, serves as our evaluation criterion. Here, ρ_k represents the correlations of the estimated representations $Z^{(i)} = X^{(i)}\hat{U}^{(i)}$ with one another on the test set, while ρ_k^* denotes the canonical correlations computed from the full batch covariance matrices. In other words, using our earlier notation, $\rho_k = MCCA_K(\hat{Z}^{(1)}, \hat{Z}^{(2)})$ and $\rho_k^* = MCCA_K(X^{(1)}, X^{(2)})$.

Despite ρ_k^* not being the ‘true’ correlations, their computation from a large sample size renders them a reliable benchmark. PCC is an efficient metric for tracking algorithmic performance over time, minimizing computational overhead(Z. Meng, Chakraborty, and Singh, 2021; I. Gemp, C. Chen, and McWilliams, 2022; Ma, Lu, and Foster, 2015; Ge, Jin, Netrapalli, et al., 2016).

Data The MediaMill dataset (Snoek et al., 2005) comprises paired features of videos and corresponding commentary, with the objective of learning joint representations that capture their correlation. This representation could potentially enable prediction of commentary from video, or vice versa. The dataset includes 25,800 test images, with 120 and 101 features respectively.

The Split-CIFAR dataset (Z. Meng, Chakraborty, and Singh, 2021) consists of 50,000 training and 10,000 test RGB images, each split in half with 32x16x3 features. The aim is to learn joint representations of the two halves that reveal correlations, expected to be high within the same class and low across different classes. These datasets are chosen for their diverse nature and complexity, providing a comprehensive test bed for our method.

Parameters For each method, we searched over the hyperparameter grid in table ?? using Biewald (2020).

Observations In machine learning, a learning curve represents a graph showing the model’s learning progress over time in terms of experience or iterations. For the MediaMill dataset, Figure V.3 compares the algorithms’ learning curves for various mini-batch sizes, showing CCA-EY’s consistent outperformance. Figure V.4 further examines the learning curves for batch sizes 5 and 100, illustrating CCA-EY’s superior performance over time.

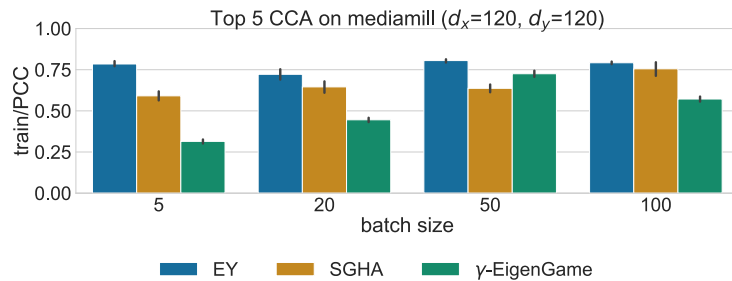


Figure V.3: Stochastic CCA on MediaMill using PCC: Performance across varying mini-batch sizes. Shaded regions signify \pm one standard deviation around the mean of 5 runs.

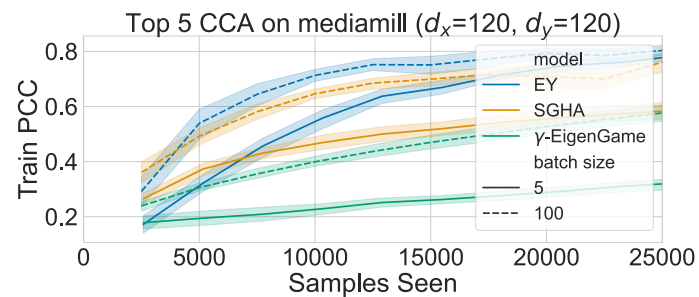


Figure V.4: Stochastic CCA on MediaMill: Training progress over a single epoch for mini-batch sizes 5, 100.

Parameter	Values
minibatch size	5,20,50,100
components	5
epochs	1
seed	1, 2, 3, 4, 5
lr	0.01, 0.001, 0.0001
γ^3	0.01,0.1,1,10

For the CIFAR dataset, Figure V.5 shows the performance comparison across batch sizes, while Figure V.6 details the learning curves, highlighting the underperformance of γ -EigenGame, especially for smaller batch sizes.

4.3 Stochastic PLS UK Biobank

In this section, we aim to demonstrate the exceptional scalability and efficiency of our Stochastic PLS method, PLS-EY, in handling extremely high-dimensional imaging genetics data. We employ imaging genetics data from the UK Biobank (Sudlow et al., 2015) as our test bed, given its comprehensive and complex nature.

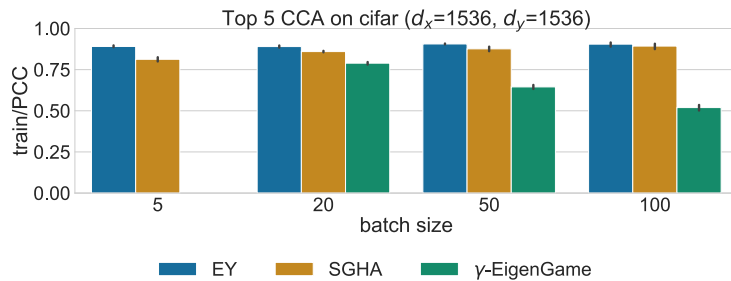


Figure V.5: Stochastic CCA on CIFAR using PCC: Performance across varying mini-batch sizes. Shaded regions signify \pm one standard deviation around the mean of 5 runs.

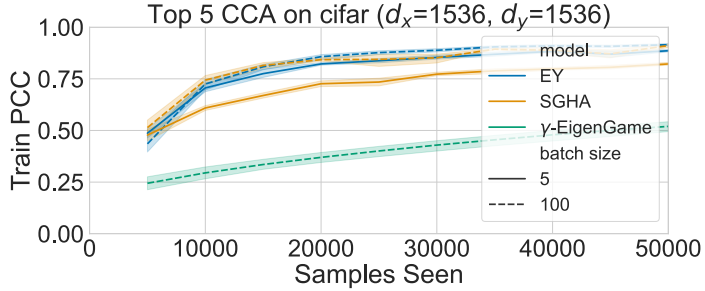


Figure V.6: Stochastic CCA on CIFAR: Training progress over a single epoch for mini-batch sizes 5, 100.

The UK Biobank dataset presents a unique challenge due to the sheer scale of its genetic data, requiring sophisticated regularization strategies.

PLS is particularly suited for imaging-genetics studies due to its capability to handle high dimensionality and reveal novel phenotypes as well as genetic mechanisms underlying diseases and brain morphometry. Historically, imaging genetics analyses have been constrained to smaller datasets due to computational limitations ([Lorenzi2018](#); Taquet et al., 2021; Le Floch et al., 2012). Moreover, the few studies that have attempted to analyze data of comparable scale to the UK Biobank have typically resorted to partitioning the data into smaller clusters, thereby limiting the scope of their analysis (Lorenzi et al., 2017; Altmann et al., 2023).

Our experiment with PLS-EY, conducted on a subset of the UK Biobank dataset consisting of brain imaging data (82 regional volumes) and genetic data (582,565 variants) for 33,333 subjects, is designed to overcome these limitations. A particular computational challenge we address is maintaining orthogonality between the weight vectors u_k in the PLS model, which is crucial for the method's effectiveness. We run PLS-EY with a mini-batch size of 500 and train the GEP-EY PLS analysis for 100 epochs using a learning rate of 0.0001. This approach allows us to not only manage the high-dimensional nature of the data but also to preserve the integrity and interpretability of the analysis. To our knowledge, this represents the largest-scale PLS analysis of biomedical data to-date, showcasing the potential of our method to facilitate discoveries in extremely large datasets.

Data The UK BioBank data consisted of real-valued continuous brain volumes and ordinal, integer genetic variants. We used pre-processed (using FreeSurfer

(Fischl, 2012)) grey-matter volumes for 66 cortical (Desikan-Killiany atlas) and 16 subcortical brain regions and 582,565 autosomal genetic variants. The affects of age, age squared, intracranial volume, sex, and the first 20 genetic principal components for population structure were removed from the brain features using linear regression to account for any confounding effects. Each brain ROI was normalized by removing the mean and dividing the standard deviation. We processed the genetics data using PLINK (Purcell et al., 2007) keeping genetic variants with a minor allele frequency of at least 1% and a maximum missingness rate of 2%. We used mean imputation to fill in missing values and centered each variant. To generate measures of genetic disease risk, we calculated polygenic risk scores using PRSice (Euesden, Lewis, and O'Reilly, 2014). We calculated scores, with a p-value threshold of 0.05, using GWAS summary statistics for the following diseases; Alzheimer's (Lambert et al., 2013), Schizophrenia (Trubetskoy et al., 2022), Bipolar (Mullins et al., 2021), ADHD (Demontis et al., 2023), ALS (Rheenen et al., 2021), Parkinson's (Nalls et al., 2019), and Epilepsy (International League Against Epilepsy Consortium on Complex Epilepsies, 2018), using the referenced GWAS studies.

Observations We observed strong validation correlations between all 10 corresponding pairs of representations $Z_k^{(1)}$ and $Z_k^{(2)}$ in the PLS model, with weak cross-correlations between $Z_k^{(1)}$ and $Z_i^{(2)}$ for $i \neq k$. This indicates that our model learned a coherent and orthogonal subspace, as shown in Figure V.7. Furthermore, the PLS representations Z were significantly associated with genetic risk measures for several disorders, suggesting that the learned PLS subspace encodes relevant information for genetic disease risk, a critical insight for biomedical research (Figure V.8). These results demonstrate the scalability of our method to extremely high-dimensional data, and its ability to learn interpretable representations.

5 Discussion

5.1 Limitations

This chapter presents a comprehensive exploration and development of novel algorithms for Canonical Correlation Analysis (CCA) and Partial Least Squares (PLS), focusing on scalability and efficiency in high-dimensional and large-scale datasets. Our approach introduces the Eckhart-Young (EY) inspired objectives for Generalized Eigenvalue Problems (GEPs) and their application in stochastic or data-streaming settings, paving the way for more efficient and scalable solutions to

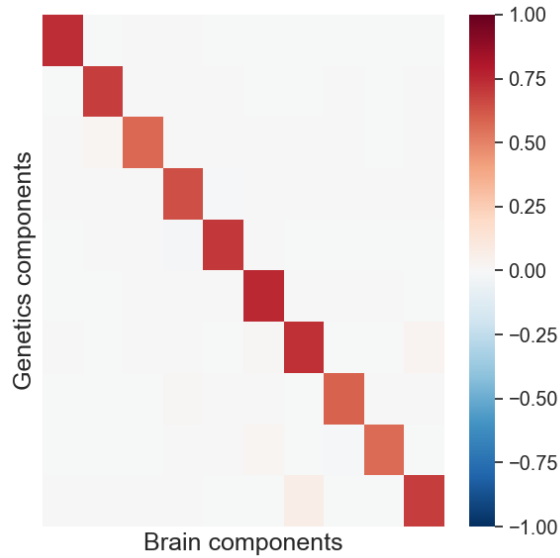


Figure V.7: Pearson correlations among PLS latent variables Z_k derived from UK Biobank data.

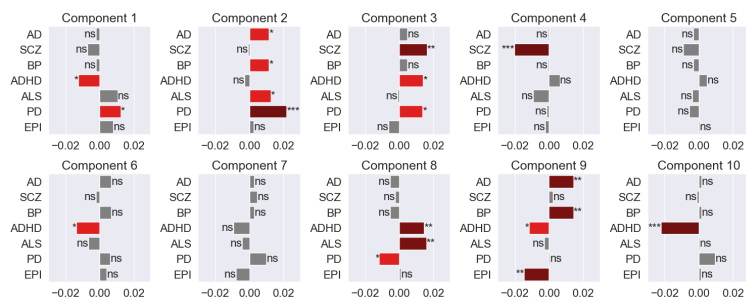


Figure V.8: Correlation between PLS brain representations Z and genetic risk scores for various disorders. AD=Alzheimer's disease, SCZ=Schizophrenia, BP=Bipolar, ADHD=Attention deficit hyperactivity disorder, ALS=Amyotrophic lateral sclerosis, PD=Parkinson's disease, EPI=Epilepsy. ns : $0.05 < p \leq 1$, * : $0.01 < p \leq 0.05$, ** : $0.001 < p \leq 0.01$, *** : $0.0001 < p \leq 0.001$.

classical subspace learning problems.

Our proposed CCA-EY and PLS-EY methods demonstrate significant advancements over traditional approaches in handling the computational complexity and scalability issues inherent in high-dimensional data. By reformulating the CCA and PLS objectives, we provide a path to efficiently analyze large datasets, which was previously infeasible due to computational limitations. The empirical evaluation on diverse datasets, including MediaMill, Split-CIFAR-10, and the UK Biobank, not only validates the effectiveness of our methods but also highlights their superiority in convergence speed and robustness to hyperparameter tuning.

The results from the MediaMill and Split-CIFAR-10 datasets underscore the potential of CCA-EY in achieving faster convergence with minimal hyperparameter tuning, a crucial factor for practical applications. This advantage is particularly pronounced when comparing our method to established baselines like γ -EigenGame and SGHA. Additionally, the application of our methods to the UK Biobank dataset represents a breakthrough in the analysis of imaging genetics data, showcasing the capability of PLS-EY to manage extraordinarily high-dimensional data while extracting meaningful and interpretable representations.

Furthermore, our methods' ability to capture relevant information for genetic disease risk, as evidenced in the UK Biobank study, opens new avenues for biomedical research. The significant associations between the PLS representations and genetic risk measures for various disorders provide valuable insights into the genetic mechanisms underlying diseases and brain morphometry.

5.2 Conclusion

In summary, this chapter contributes to the fields of machine learning and multiview data analysis by introducing scalable and efficient solutions for CCA and PLS, applicable in a variety of domains, including but not limited to neuroimaging and genetics. Our work not only addresses significant computational challenges but also lays the groundwork for future research and practical applications in analyzing large-scale, high-dimensional datasets.

Chapter VI

Deep CCA and Self-Supervised Learning: Non-Linear Functions

Contents

1	Introduction.....	126
2	Background: Deep Representation Learning	127
2.1	Deep Learning	127
2.2	DCCA and Deep Multiview CCA	127
2.3	Self-Supervised Learning and Joint Embedding.....	129
3	Methods: Novel Objectives and Algorithms	132
3.1	Applications to (multi-view) stochastic CCA and PLS, and Deep CCA	132
3.2	Application to SSL.....	132
4	Experiments and Results.....	132
4.1	Deep CCA	132
4.2	Deep Multiview CCA: Robustness Across Different Batch Sizes.....	136
4.3	Self-Supervised Learning with SSL-EY.....	137
5	Discussion.....	141

5.1	Limitations	141
5.2	Conclusion.....	142

Preface

This chapter is based on work presented in Chapman and Wells (2023) and Chapman, Wells, and Aguila (2023).

1 Introduction

Deep CCA (Andrew et al., 2013) secured a runner-up position for the test-of-time award at ICML 2023 (ICML, 2023). However, its direct application has been limited in large datasets due to biased gradients in the stochastic minibatch setting. There have since been proposals to scale-up Deep CCA in the stochastic case with adaptive whitening (W. Wang, Arora, Livescu, and Srebro, 2015) and regularization Chang, Xiang, and T. M. Hospedales, 2018, but these techniques are highly sensitive to hyperparameter tuning.

Self-Supervised Learning (SSL) methods have reached the state-of-the-art in tasks such as image classification (Balestriero, Ibrahim, et al., 2023), learning representations without labels that can be used to classify images using a linear probe in the zero-shot setting. A family of SSL methods that are closely aligned with Canonical Correlation Analysis (CCA) has garnered particular interest. This family notably includes Barlow Twins (Zbontar et al., 2021), VICReg (Bardes, Ponce, and LeCun, 2021), and W-MSE (Ermolov et al., 2021) and they aim to transform a pair of data views into similar representations, similar to the objective of CCA. Similarly, some generative approaches to SSL Sansone and Manhaeve, 2022 bear a striking resemblance to Probabilistic CCABach and Jordan, 2005. These connections have started to be explored in Balestriero and LeCun, 2022.

In this chapter, we propose a novel formulation of Deep CCA that is unbiased in the stochastic setting and scales to large datasets. We also propose a novel SSL method, SSL-EY, that is competitive with existing methods on CIFAR-10 and CIFAR-100. We highlight the connections between our work and existing SSL methods, and show that our method is more robust to hyperparameter tuning.

2 Background: Deep Representation Learning

2.1 Deep Learning

Deep learning is a subfield of machine learning that uses functions parameterised by neural networks. Deep learning has been applied to a wide range of domains, including computer vision, speech recognition, natural language processing, and bioinformatics, where they have produced state-of-the-art results on many tasks. Neural networks are usually composed of many linear layers followed by nonlinear activation functions such as the rectified linear unit (ReLU). The ReLU activation function is defined as $\text{ReLU}(x) = \max(0, x)$. The ReLU activation function is piecewise linear, and so the composition of ReLU activations with linear functions is a piecewise linear function. It has been shown that neural networks with ReLU activations can approximate any continuous function on a compact set to arbitrary accuracy (Perekrestenko et al., 2018), and so are universal function approximators. This flexibility, combined with increasingly large datasets, allows neural networks to learn complex functions from data. Owing to the size of the models and datasets, neural networks are usually trained using the backpropagation algorithm and stochastic gradient descent (SGD) (Amari, 1993).

2.2 DCCA and Deep Multiview CCA

Thus far, our focus has been on linear Canonical Correlation Analysis (CCA). However, in dealing with high-dimensional and complex data structures commonly found in modern applications, nonlinear extensions of CCA become essential. Deep CCA (DCCA) and Deep Multiview CCA (DMCCA) represent such nonlinear extensions, aiming to capture more intricate relationships between data views.

In essence, the objective of DCCA and DMCCA is to learn nonlinear representations of data that are linearly correlated across different views. We define this goal using our MCCA notation:

$$\|\text{MCCA}_K\left(Z^{(1)}, \dots, Z^{(I)}\right)\|_2 \quad (\text{VI.1})$$

where $Z^{(i)} = f^{(i)}(X^{(i)}; \theta^{(i)})$ are representations learned by neural networks for each view $i \in [I]$.

Figure VI.1 illustrates the conceptual framework of DCCA, where data from different views are transformed through neural networks to achieve correlated repre-

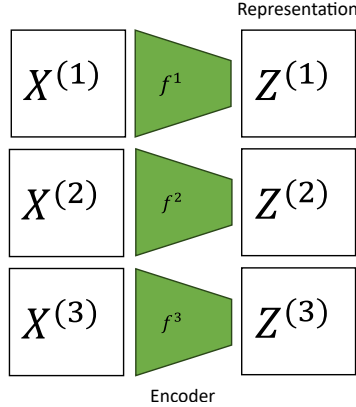


Figure VI.1: Schematic of the DCCA approach highlighting the nonlinear transformation of data into correlated views.

sentations.

The full-batch approach of DCCA, formulated by Andrew et al. (2013), seeks to maximize the correlation between these different views. The objective, operationalized as a loss function, is defined by the trace of matrix T : The full-batch approach of DCCA, formulated by Andrew et al. (2013), seeks to maximize the correlation between these different views. The objective, operationalized as a loss function, is defined by the trace of matrix T :

$$T = \left(\text{cov}(Z^{(1)}) \right)^{-\frac{1}{2}} Z^{(1)\top} Z^{(2)} \left(\text{cov}(Z^{(2)}) \right)^{-\frac{1}{2}} \quad (\text{VI.2})$$

$$\mathcal{L}_{\text{Rayleigh}} = -\text{Tr}(T) \quad (\text{VI.3})$$

This approach, while theoretically sound, faces scalability issues with large datasets. DCCA-STOL, proposed by W. Wang, Arora, Livescu, and Bilmes (2015), adapts this objective to large mini-batches but suffers from biased gradients due to the matrix inversions in equation equation VI.2. This necessitates batch sizes larger than the representation size, limiting its practical application.

Extensions such as DMCCA (Somandepalli et al., 2019) and DGCCA (Benton et al., 2017) attempt to mitigate these limitations by forming matrices A and B from mini-batch representations for the generalized eigenvalue problem in CCA. However, their loss function, given by

$$\mathcal{L}_{\text{Rayleigh}} = -\text{Tr} \left(B^{-\frac{1}{2}} A B^{-\frac{1}{2}} \right), \quad (\text{VI.4})$$

still encounters similar challenges.

Adaptive whitening methods (W. Wang, Arora, Livescu, and Srebro, 2015; Chang, Xiang, and T. M. Hospedales, 2018) offer another solution by reducing the bias in the DCCA objective. However, as noted in DCCA-NOI (W. Wang, Arora, Livescu, and Bilmes, 2015), these methods introduce a time constant that complicates analysis and requires extensive tuning.

$$\mathcal{L}_{\text{NOI}} = \|\tilde{\Sigma}_1^{-\frac{1}{2}} Z^{(1)} - \tilde{\Sigma}_2^{-\frac{1}{2}} Z^{(2)}\|_F^2 \quad (\text{VI.5})$$

Where $\tilde{\Sigma}_{11}$ and $\tilde{\Sigma}_{22}$ are estimates of the covariance matrices of $Z^{(1)}$ and $Z^{(2)}$ respectively. However, the authors of **DCCA-NOI** highlight that the associated time constant complicates analysis and requires extensive tuning. These limitations highlight the need for more scalable and efficient nonlinear CCA methods that can handle large datasets without compromising on representation quality or requiring extensive hyperparameter tuning.

2.3 Self-Supervised Learning and Joint Embedding

Self-Supervised Learning (SSL) has emerged as a crucial approach in deep learning, especially for tasks with limited labeled data. A fundamental strategy in SSL, particularly in non-contrastive SSL, involves creating joint embeddings of augmented images. This process entails generating two distinct views of the same image, denoted as X_1 and X_2 , using various augmentation techniques. The primary aim is to align their representations, $Z^{(1)}$ and $Z^{(2)}$, in a shared embedding space. This alignment leverages the inherent patterns within the data to develop feature representations absent explicit labels. A significant challenge in this methodology is averting the collapse of representations, where models produce constant features irrespective of input variability.

In SSL, augmented data generation serves to create multiple perspectives of the same underlying content, such as cropping or rotating an image. The objective is to learn representations that are invariant to these augmentations, thereby capturing the fundamental structure of the data. Canonical Correlation Analysis (CCA) emerges as a fitting tool for this task, especially given that augmentations represent redundant rather than complementary information, offering different perspectives of the same underlying data.

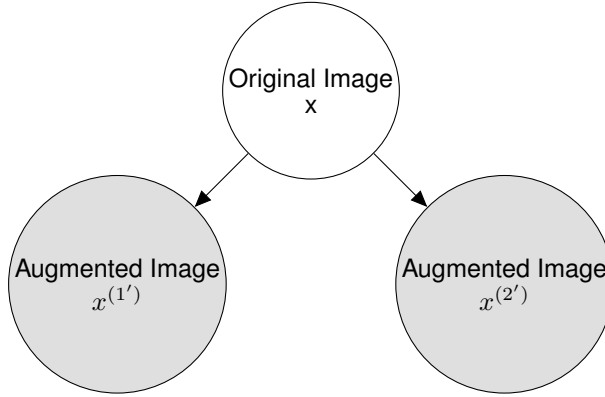


Figure VI.2: Joint Embedding Data Generation Process: The original image x is augmented to produce two views $x^{(1')}$ and $x^{(2')}$.

2.3.1 Encoder-Projector Model in SSL

SSL methods like Barlow Twins and VICReg employ an encoder-projector model, as shown in Figure VI.3. In this model, input data is transformed by an encoder g into representations, which are further processed by a projector h into higher-dimensional embeddings. These embeddings are integral to training, with the representations being critical for downstream tasks. The encoder is typically a neural network suited to the domain, while the projector is often a simpler multi-layer perceptron.

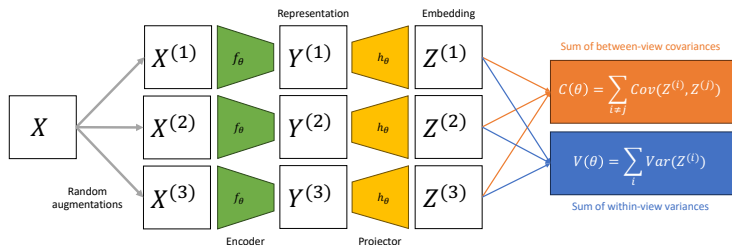


Figure VI.3: Schematic of the encoder-projector setup in SSL.

The essence of joint embedding in SSL is that similar inputs, X and its augmented version X' , should yield similar embeddings, Z and Z' . The encoder and projector are optimized to minimize the distance between Z and Z' , reflecting the similarity of the inputs.

2.3.2 CCA-based SSL Methods: Barlow Twins and VICReg

Barlow Twins and VICReg are two pivotal methods in SSL that build upon canonical correlation principles to generate robust representations from augmented views. Both methods aim to align representations of two augmented views while ensuring distinct yet correlated representations.

Barlow Twins employs a redundancy reduction objective to ensure similarity between representations of the same augmented views and to decorrelate representations within each view. Its loss function is expressed as:

$$\mathcal{L}_{\text{BT}} = \underbrace{\gamma \mathbb{E} \|Z^{(1)} - Z^{(2)}\|^2}_{\text{Invariance}} + \underbrace{\beta \sum_{\substack{k,l=1 \\ k \neq l}}^K \text{Cov}(\hat{Z}_k^{(i)}, \hat{Z}_l^{(i)})^2}_{\text{Redundancy Reduction}}, \quad (\text{VI.6})$$

where $\hat{Z}^{(i)}$ denotes the batch-normalized versions of the representations, with γ and β as hyperparameters controlling the similarity and decorrelation terms, respectively.

VICReg, in contrast, introduces a variance term and omits batch normalization, focusing on variance-invariance-covariance regularization. The VICReg loss is defined as:

$$\mathcal{L}_{\text{VR}} = \underbrace{\gamma \mathbb{E} \|Z^{(1)} - Z^{(2)}\|^2}_{\text{Invariance}} + \left[\underbrace{\sum_{i \in \{1,2\}} \alpha \sum_{k=1}^K \left(1 - \sqrt{\text{Var}(Z_k^{(i)})} \right)_+}_{\text{Variance}} + \underbrace{\beta \sum_{\substack{k,l=1 \\ k \neq l}}^K \text{Cov}(Z_k^{(i)}, Z_l^{(i)})^2}_{\text{Covariance}} \right], \quad (\text{VI.7})$$

with α , β , and γ as tuning parameters balancing the influence of variance, invariance, and covariance regularization.

These approaches, grounded in canonical correlation principles, offer foundational baselines for our experiments in SSL.

3 Methods: Novel Objectives and Algorithms

3.1 Applications to (multi-view) stochastic CCA and PLS, and Deep CCA

Lemma 3.1. [Objective recovers Deep Multi-view CCA] Assume that there is a final linear layer in each neural network $f^{(i)}$. Then at any local optimum, $\hat{\theta}$, of the population problem, we have

$$\mathcal{L}_{EY}(\hat{\theta}) = -\|\text{MCCA}_K(\hat{Z})\|_2^2$$

where $\hat{Z} = f_{\hat{\theta}}(X)$. Therefore, $\hat{\theta}$ is also a local optimum of objectives from Andrew et al., 2013; Somandepalli et al., 2019 as defined in Equation (VI.1).

Proof sketch: see Section 5 for full details. Consider treating the penultimate-layer representations as fixed, and optimising over the weights in the final layer. This is precisely equivalent to optimising the Eckhart-Young loss for linear CCA where the input variables are the penultimate-layer representations. So by Proposition 3.2, a local optimum is also a global optimum, and by Proposition 3.1 the optimal value is the negative sum of squared generalised eigenvalues. \square

3.2 Application to SSL

We can directly apply Algorithm 1 to SSL. If we wish to have the same neural network transforming each view, we can simply tie the weights $\theta^{(1)} = \theta^{(2)}$. When the paired data are generated from applying independent, identically distributed (i.i.d.) augmentations to the same original datum, it is intuitive that tying the weights is a sensible procedure, and perhaps acts as a regulariser.

4 Experiments and Results

4.1 Deep CCA

In this experiment, we aim to establish the superiority of our DCCA-EY method over existing Deep Canonical Correlation Analysis (DCCA) approaches. We specifically focus on showcasing how DCCA-EY outperforms these methods in terms of correlation capture, convergence speed, and ease of hyperparameter tuning. The

experimental setup is aligned with that of W. Wang, Arora, Livescu, and Srebro (2015), providing a direct comparison under identical conditions.

As per W. Wang, Arora, Livescu, and Srebro (2015), our architecture comprises multilayer perceptrons with two hidden layers of size 800 and an output layer of 50 with ReLU activations. We train these networks for 20 epochs. However, our primary goal is to learn $K = 50$ dimensional representations over a range of mini-batch sizes (from 20 to 100) across 50 epochs, demonstrating the robustness and scalability of DCCA-EY even in varying batch conditions.

In this chapter, we employ the Total Correlation Captured (TCC) metric for evaluation. While similar to the PCC metric described in the previous chapter, TCC does not rely on a ground truth for its computation. Instead, it is defined as $TCC = \sum_{k=1}^K \rho_k$, where ρ_k are the empirical correlations between the neural network-based representations $Z^{(i)} = f^{(i)}(X^{(i)})$ on a validation set, rather than on the training set as was the case with PCC. This distinction is crucial as TCC evaluates the model's performance in capturing correlations in an unseen dataset, offering a more robust measure of its generalization capability.

Data The Split MNIST dataset is a modified version of the original MNIST dataset, where each 28x28 pixel grayscale image of handwritten digits (0-9) is divided into left and right halves, creating two distinct views. This split challenges models to learn from partial information, as each view contains only half of the digit, either the left or the right side. The dataset comprises 50,000 training and 10,000 test images. The X-Ray Microbeam Speech Production Database (XRMB) is a multi-view dataset used for studying articulatory speech data. It comprises around 40,000 spoken utterances from 47 American English speakers. The dataset provides two views: acoustic features and articulatory measurements. The acoustic features consist of 273-dimensional vectors representing spectral characteristics, while the articulatory measurements include 112-dimensional vectors capturing the position and movement of speech articulators (like the tongue and lips). The XRMB dataset is notable for its complexity and high dimensionality, making it a challenging testbed for multiview learning algorithms.

Parameters For each method, we searched over a hyperparameter grid using Biewald (2020).

Observations on SplitMNIST For the SplitMNIST dataset, Figure VI.4 shows the comparison of methods across different batch sizes. We observe that DCCA-STOL

Parameter	Values
minibatch size	100, 50, 20
lr	1e-3, 1e-4, 1e-5
ρ^1	0.6, 0.8, 0.9
epochs	50

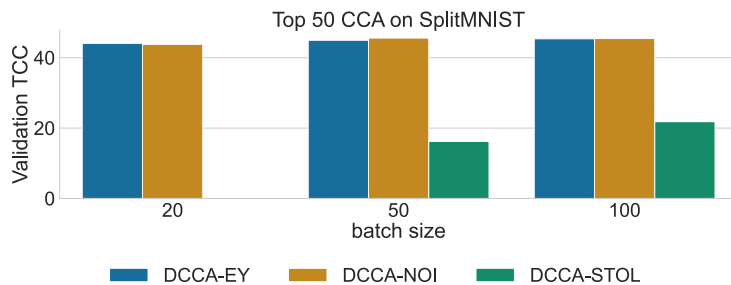


Figure VI.4: Deep CCA on SplitMNIST: Comparison of methods across varying batch sizes.

captures significantly less correlation than the other methods and breaks down when the mini-batch size is smaller than the dimension $K = 50$. Figure VI.5 illustrates the learning progress over 50 epochs, where DCCA-NOI, despite performing similarly to DCCA-EY, requires more careful hyperparameter tuning and demonstrates a slower convergence speed.

Observations on XRMB On the XRMB dataset, as seen in Figure VI.6, similar trends are evident. DCCA-STOL struggles with smaller mini-batch sizes, while DCCA-NOI, though comparable to DCCA-EY in performance, lags in convergence speed, as shown in Figure VI.7.

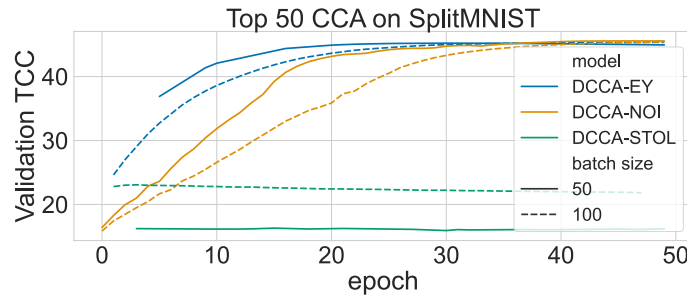


Figure VI.5: Deep CCA on SplitMNIST: Learning progress over 50 epochs.

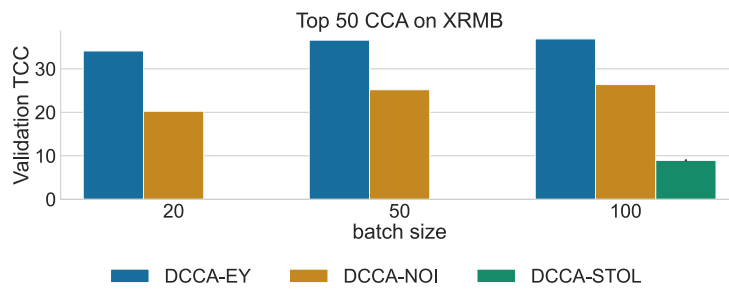


Figure VI.6: Deep CCA on XRMB: Comparison of methods across varying batch sizes.

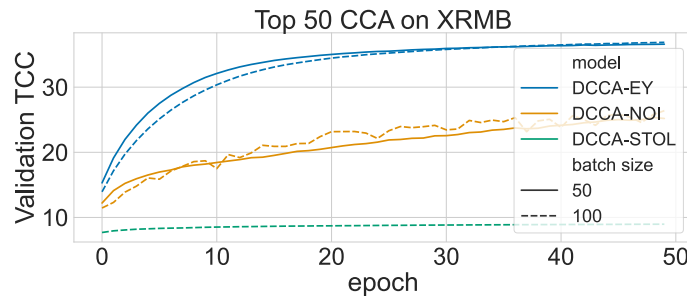


Figure VI.7: Deep CCA on XRMB: Learning progress over 50 epochs.

4.2 Deep Multiview CCA: Robustness Across Different Batch Sizes

In our second experiment, our objective is to showcase the adaptability and effectiveness of the DCCA-EY method in the multiview context, particularly in comparison to existing methods such as DMCCA and DGCCA. We again learn $K = 50$ dimensional representations, but now train for 100 epochs. We employ a multiview extension of the Total Correlation Captured (TCC) metric, termed Total Multiview Correlation Captured (TMCC). TMCC averages the correlation across views and is defined using the consistent notation from Section 2 as:

$$\text{TMCC} = \sum_{k=1}^K \frac{1}{I(I-1)} \sum_{\substack{i,j \leq I \\ i \neq j}} \text{corr}(Z_k^{(i)}, Z_k^{(j)}),$$

where $Z_k^{(i)}$ represents the k -th dimension of the i -th view's representation. This metric effectively measures the extent to which our method captures correlations between different views in a multidimensional representation space.

Data We choose the mfeat dataset for this purpose, which comprises 2,000 handwritten numeral patterns represented through six distinct feature sets, including Fourier coefficients, profile correlations, Karhunen-Love coefficients, pixel averages in 2×3 windows, Zernike moments, and morphological features. These diverse features present an ideal testbed for evaluating the performance of multiview learning methods.

Parameters For each method, we searched over a hyperparameter grid using Biewald (2020).

Observations Figure VI.8 illustrates the comparison of DCCA-EY with DGCCA and DMCCA across different mini-batch sizes, using the validation TMCC metric. DCCA-EY consistently outperforms both DGCCA and DMCCA, showcasing its superior ability to capture validation TMCC. Notably, DMCCA encounters issues when the batch size is smaller than $K = 50$, likely due to singular empirical covariances. DGCCA, while not breaking down, significantly underperforms with smaller batch sizes, highlighting limitations in scalability and efficiency for large-scale data applications.

Parameter	Values
minibatch size	5,10,20,50,100,200
components	50
epochs	100
lr	0.01, 0.001, 0.0001, 0.00001

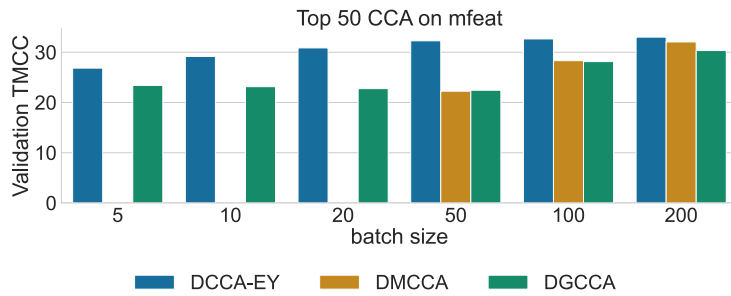


Figure VI.8: Deep Multi-view CCA on mfeat: Comparison across various mini-batch sizes using the Validation TMCC metric.

In Figure VI.9, we observe the learning curves for batch sizes 50 and 100. Both DMCCA and DGCCA demonstrate rapid initial learning of significant correlations but reach a plateau relatively quickly. In contrast, DCCA-EY exhibits a consistent improvement over time and notably outperforms the other methods by the end of the training period. This behavior underscores the enhanced learning capability and efficiency of DCCA-EY, especially in the context of large-scale, high-dimensional data.

4.3 Self-Supervised Learning with SSL-EY

Finally, we benchmark our self-supervised learning algorithm, SSL-EY, with Barlow Twins and VICReg on standard SSL benchmarks. We follow a standard experimental design (Tong et al., 2023). Indeed, we use the solelearn library (Da Costa et al., 2022), which offers optimized setups particularly tailored for VICReg and Barlow Twins. All methods use a ResNet-18 encoder coupled with a bi-layer projector

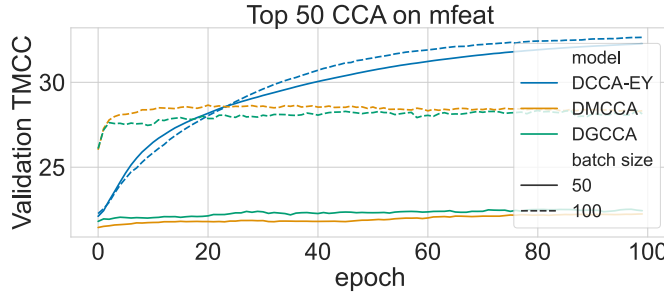


Figure VI.9: Deep Multi-view CCA on mfeat: Learning progress over 100 epochs for batch sizes 50 and 100.

network. Training spans 1,000 epochs with batches of 256 images. For SSL-EY, we use the hyperparameters optimized for Barlow Twins, aiming not to outperform but to showcase the robustness of our method. We predict labels via a linear probe on the learnt representations and evaluate performance with Top-1 and Top-5 accuracies on the validation set.

Data We use the CIFAR-10 and CIFAR-100 datasets, which comprise 60,000 labelled images of size 32x32. CIFAR-10 contains 10 classes, while CIFAR-100 contains 100 classes.

Observations As Table 4.1 demonstrates, SSL-EY rivals Barlow Twins and VICReg, despite employing general hyperparameters as opposed to the latter’s specifically optimized ones.

Method	CIFAR-10 Top-1	CIFAR-10 Top-5	CIFAR-100 Top-1	CIFAR-100 Top-5
Barlow Twins	92.1	99.73	71.38	92.32
VICReg	91.68	99.66	68.56	90.76
SSL-EY	91.43	99.75	67.52	90.17

Table 4.1: Comparing the performance of SSL methods on CIFAR-10 and CIFAR-100.

Model Convergence In deep learning, a learning curve usually represents a graph showing the model's learning progress against number of epochs. Figure VI.10 illustrates that the performance variations at 1,000 epochs, shown in Table 4.1, primarily stem from optimization noise, with convergence speeds being comparable among methods.

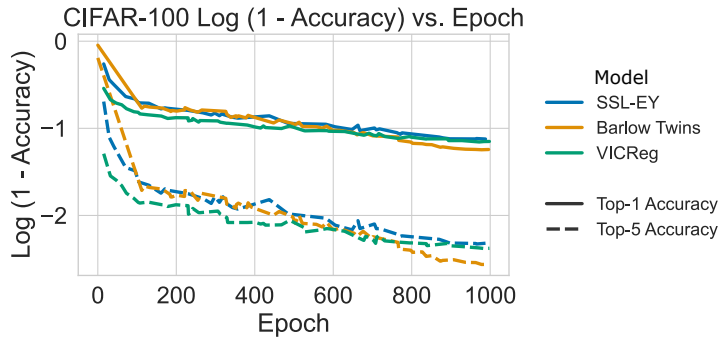


Figure VI.10: Learning curves for SSL-EY, Barlow Twins, and VICReg on CIFAR-100, depicting 1,000-epoch performance.

Projector Size Variation We hypothesized that SSL-EY's robustness to projector size might allow for efficient performance even with smaller projectors or without one. This hypothesis led us to experiment with varying projector output dimensions and completely removing the projector while maintaining the encoder size. Figure VI.11a shows SSL-EY's sustained performance with reduced projector size, indicating more efficient representations compared to Barlow Twins and VICReg. Furthermore, as Table 4.1 and Figure VI.11b suggest, SSL-EY performs consistently well even without a projector, underlining its reduced reliance on this architectural component.

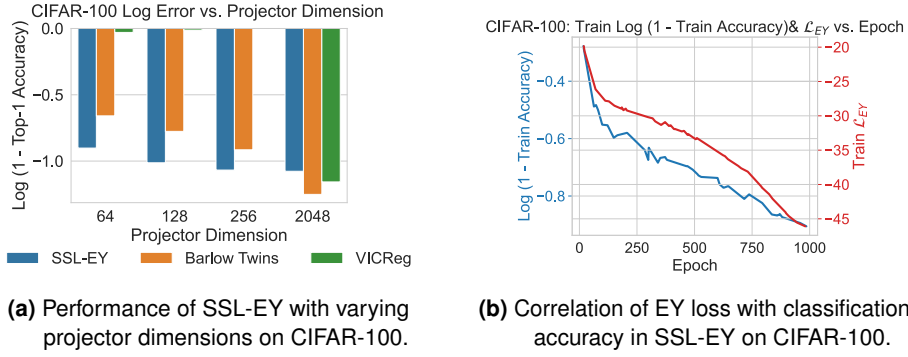


Figure VI.11: CIFAR 100 Projector Analysis: (a) Examining the impact of projector size on SSL-EY's performance. (b) Investigating the relationship between EY loss and classification accuracy.

\mathcal{L}_{EY} as an Informative Metric Figure VI.11b offers two insights. First, it evidences the close relationship between EY loss and classification accuracy, highlighting the potential of maximizing canonical correlation as a pretext task in SSL. Second, it reveals that even a reduced projector dimensionality does not reach full capacity within 1,000 epochs, implying untapped potential in SSL-EY's representation capacity. The evolution of the correlation, measured by \mathcal{L}_{EY} , suggests a new avenue for monitoring model training, potentially eliminating the need for a separate validation task.

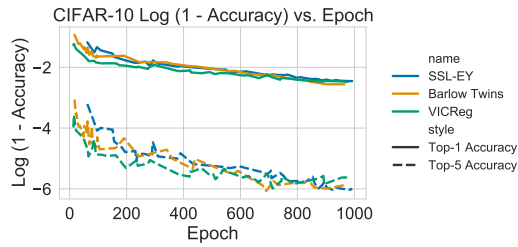


Figure VI.12: Learning curves for SSL-EY, Barlow Twins, and VICReg on CIFAR-10, depicting 1,000-epoch performance.

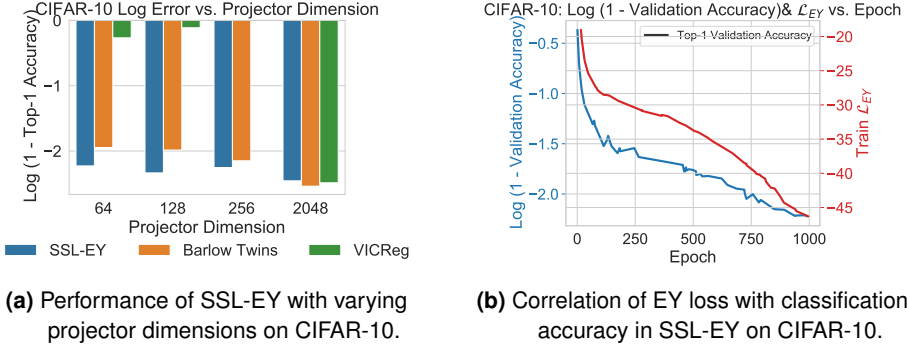


Figure VI.13: CIFAR 10 Projector Analysis: (a) Examining the impact of projector size on SSL-EY's performance. (b) Investigating the relationship between EY loss and classification accuracy.

5 Discussion

5.1 Limitations

Our innovative formulation of DCCA-EY successfully addresses the limitations of traditional DCCA methods, particularly in stochastic settings. The experimental results on Split MNIST and XRMB datasets demonstrate DCCA-EY's superior capability in capturing correlations efficiently across a range of mini-batch sizes, thereby validating its scalability and robustness. Furthermore, our method shows notable improvements in convergence speed and reduced sensitivity to hyperparameter tuning, aspects critically important for practical applications.

In SSL, SSL-EY stands out as a competitive and robust approach. Our experiments on CIFAR-10 and CIFAR-100 highlight SSL-EY's ability to achieve comparable performance with state-of-the-art methods like Barlow Twins and VICReg, even while using general hyperparameters. This is important given the time it takes to run experiments with SSL methods which, as here, can be up to 1,000 epochs. This underscores SSL-EY's adaptability and robustness in different settings. Particularly noteworthy is its performance with reduced or absent projectors, indicating its efficiency and potential for broader applications in SSL. Moreover, the insights gleaned from the correlation of EY loss with classification accuracy in SSL-EY open new avenues for understanding and leveraging canonical correlations in SSL. The observed relationships provide a promising direction for future research in developing more effective and efficient SSL methods.

5.2 Conclusion

Our work bridges significant gaps in the literature and establishes a strong foundation for future explorations in both DCCA and SSL. The proposed methods not only enhance our understanding of these domains but also pave the way for practical applications where scalability, efficiency, and robustness are paramount. In summary, this chapter contributes to the advancement of DCCA and SSL by introducing novel approaches that are not only theoretically sound but also practically viable, offering valuable tools for researchers and practitioners alike in the ever-evolving landscape of machine learning.

Chapter VII

CCA-Zoo: A collection of Regularized, Deep Learning-based, Kernel, and Probabilistic methods in a scikit-learn style framework

Preface

This work was published in the Journal of Open Source Software (Chapman and H.-T. Wang, 2021). I have been the lead developer of the CCA-Zoo package since its inception in 2020. All of the methods we have described in this thesis are implemented in CCA-Zoo and are immediately available for use by the research community.

1 Introduction

The Python programming language has seen a surge in popularity in the machine learning community due to its versatility and extensive libraries. However, when it comes to the domain of multiview learning, there is a noticeable void in the Python

ecosystem. Existing libraries, such as `scikit-learn`^{Pedregosa et al., 2011}, offer basic implementations for CCA and PLS, yet fall short of providing a comprehensive toolkit for multiview learning techniques. This is particularly striking given the widespread recognition that the availability of quality software implementations often acts as a catalyst for the adoption of novel methodologies in the statistical learning community.

One glaring example of this trend is Sparse PLS. Despite its known limitations, Sparse PLS has effectively become the go-to method for sparse CCA applications, primarily due to its robust implementation in the R programming language. The discrepancy between the availability of multiview learning tools in R and Python has not only hindered the diversification of methodologies but also impeded the community from leveraging the more recent advances in the field.

2 Background

The research community continues to show a heightened interest in multiview learning. Traditionally, this field has been dominated by contributions from statistical learning researchers who predominantly used R and MATLAB for their work. These platforms have been the birthplace of many state-of-the-art algorithms and methodologies, including Sparse PLS.

However, this posed a challenge for Python-oriented researchers and practitioners, leaving them with two less-than-ideal options: either port existing R or MATLAB code into Python, often a non-trivial task requiring domain expertise, or resort to using the limited set of methods available in native Python libraries like `scikit-learn`. This fragmentation has, in effect, created barriers to entry and possibly slowed down the progress in applying multiview learning techniques in Python-based projects.

The CCA-Zoo package aims to bridge this divide by offering a broad range of multiview learning algorithms, creating a unified platform that fosters both academic research and practical applications in Python.

3 Methods

In this section, we describe the implementation of CCA-Zoo as depicted in Figure VII.1 and the design decisions that were made during its development. We highlight the package's optimization for use with high-dimensional biomedical data and elaborate on its compatibility with standard machine learning packages.

3.1 API

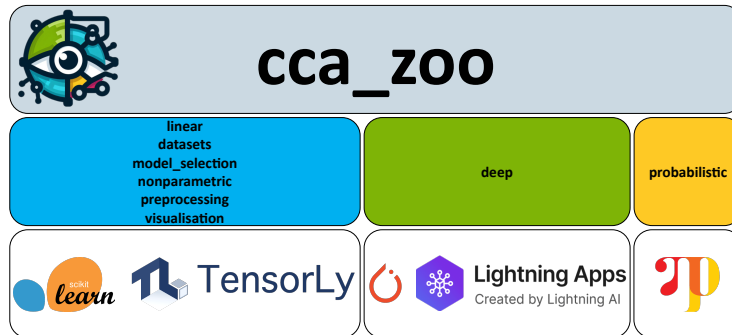


Figure VII.1: The CCA-Zoo compatibility map showcases integration with various machine learning packages. The deep learning module is built upon PyTorch and Lightning, reflecting their status as industry standards for neural network implementations. The probabilistic module employs NumPyro for its Bayesian inference capabilities, enhancing the application of probabilistic approaches in CCA.

The `scikit-learn` API is familiar to many machine learning practitioners and researchers, and is the de facto standard for machine learning in Python. CCA-Zoo has been designed to be consistent with the `scikit-learn` API, inheriting its user-friendly characteristics and ensuring compatibility with the `scikit-learn` ecosystem. Furthermore, the deep module within CCA-Zoo integrates PyTorch and Lightning, harnessing their powerful features for deep learning research and applications. The probabilistic module takes advantage of NumPyro, which offers advanced features for probabilistic programming and Bayesian methods, further extending the versatility and functionality of CCA-Zoo.

3.2 Usage

The CCA-Zoo package is a comprehensive toolkit that includes modules for datasets, preprocessing, model selection, various models (linear, deep, nonparametric, probabilistic), and visualization. It is designed to plug seamlessly into `scikit-learn` pipelines, allowing users to select and utilize components as needed. This design enhances the flexibility and applicability of multiview learning methods.

In this section, we will walk through the complete CCA-Zoo workflow, from data generation to model selection and evaluation. We will highlight the package's design choices and its integration capabilities. Figure VII.2 illustrates the overall

structure and flow of the CCA-Zoo pipeline, demonstrating its compatibility with the scikit-learn API and how it facilitates integration with existing machine learning workflows.

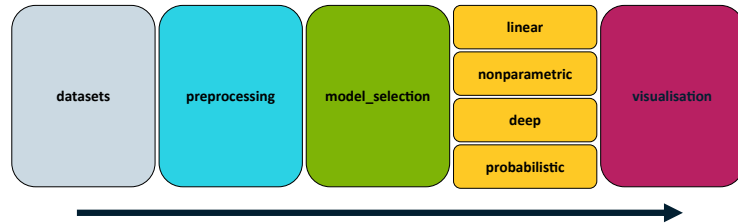


Figure VII.2: The CCA-Zoo pipeline. Designed for compatibility with the scikit-learn API, it facilitates integration with existing machine learning workflows.

The complete pipeline for CCA-Zoo is straightforward and user-friendly. The following example demonstrates the implementation of a regularized CCA model with a ridge penalty, showcasing the practical application of the pipeline:

```

# Import required libraries
import numpy as np
from cca_zoo.datasets import LatentVariableData
from cca_zoo.preprocessing import
from cca_zoo.linear import rCCA
from cca_zoo.model_selection import GridSearchCV
from cca_zoo.visualisation import Di

# Generate synthetic multiview data
data = LatentVariableData(view_features=[10,10],latent_dims: int = 2)
(X,Y) = data.sample(n_samples=100)

# Define grid of potential regularization parameters
c1 = [0.1, 0.3, 0.7, 0.9]
c2 = [0.1, 0.3, 0.7, 0.9]
param_grid = {'c': [c1, c2]}

cv = 5 # Number of folds in cross-validation

# Conduct grid search

```

```

ridge = GridSearchCV(rCCA(latent_dimensions=2), param_grid=param_grid,
                     cv=cv, verbose=True, scoring=scorer).fit((train_view_1, train_view_2))

# Get best model
best_model = ridge.best_estimator_

# Visualize

```

3.3 Datasets

CCA-Zoo provides a range of datasets for testing and benchmarking, which are outlined in Table 3.1. These datasets are designed to be compatible with the scikit-learn API, allowing users to easily integrate them into their workflows. In particular, this module includes the LatentVariableData class which implements the explicit latent variable model and JointData which implements the implicit latent variable model described in Chapter IV. Additionally, CCA-Zoo includes a variety of real-world datasets, including the MNIST, CIFAR10, and Mfeat datasets, as well as the Breast Cancer dataset from the UCI repository which has been used extensively in the literatureD. M. Witten, Robert Tibshirani, and Hastie, 2009.

Class Name	Method Name
LatentVariableData	Latent Variable Data
JointData	Joint Data
load_breast_data	Breast Cancer Data
load_split_cifar10_data	CIFAR10 Data
load_split_mnist_data	MNIST Data
load_mfeat_data	Mfeat Data

Table 3.1: Class Names and Method Names

3.4 Model Selection Utilities

For model selection and evaluation, CCA-Zoo includes various utilities as shown in Table 3.2. The existing `scikit-learn` API contains a number of methods for model selection, including `GridSearchCV` and `RandomizedSearchCV` as well as permutation tests and learning curves. Unfortunately, these methods are not compatible with multiview learning methods, which have separate parameters for each view. To address this issue, CCA-Zoo puts a thin wrapper around these methods, combining multiview parameter combinations so that they appear as single view models to `scikit-learn`, but splitting them back into their constituent views when fitting the model. This means that CCA-Zoo benefits from the multiprocessor capabilities of `scikit-learn` as well as a standardized outputs including the `best_estimator_` attribute, model fit times, and a dictionary summarizing the results of the cross-validation.

Class Name	Method Name
<code>GridSearchCV</code>	Grid Search Cross Validation
<code>RandomizedSearchCV</code>	Randomized Search Cross Validation
<code>cross_validate</code>	Cross Validation
<code>learning_curve</code>	Learning Curve
<code>permutation_test_score</code>	Permutation Test Score

Table 3.2: Class Names and Method Names

3.5 Linear

In this section, we explore a variety of linear multiview learning methods available in CCA-Zoo, as detailed in Table 3.3.

3.6 Deep

Table 3.4 lists the deep learning methods implemented in CCA-Zoo, offering advanced capabilities for deep canonical correlation analysis and related techniques.

3.7 Probabilistic

The probabilistic methods in CCA-Zoo, including variations of probabilistic CCA and PLS, are summarized in Table 3.5. While we have not explored these methods in detail in this thesis, they are included in CCA-Zoo for completeness and to facilitate future research. Probabilistic methods for multiview learning are an active area of research, that is notably limited by computational constraints. Existing publicly available implementations use the Expectation-Maximization algorithm, which is efficient for simple models but can be slow to converge. By leveraging a GPU-enabled probabilistic programming language, CCA-Zoo can use stochastic variational inference to speed up the training process, or MCMC sampling to obtain more accurate estimates of the posterior distribution.

3.8 Nonparametric

Table 3.6 presents the nonparametric methods in CCA-Zoo, focusing on kernel-based techniques for multiview learning.

3.9 Visualization

CCA-Zoo also provides a range of visualization tools for multiview learning, which are outlined in Table 3.7.

3.10 Code Availability

The code for CCA-Zoo is available at.

CCA-Zoo has received 155 stars and 30 forks on GitHub, and has nearly 500 downloads per month on PyPI¹.

Documentation for CCA-Zoo is available at². The documentation includes a user guide, API reference, and examples.

The package can be installed using `pip install cca-zoo` or `poetry add cca-zoo`.

¹<https://pypistats.org/packages/cca-zoo>

²<https://cca-zoo.readthedocs.io/en/latest/>

4 Benchmarking

In this section, we compare the performance of CCA-Zoo against `scikit-learn`, focusing on the efficiency of the basic CCA and PLS methods. We conducted experiments on synthetic datasets with varying dimensions to evaluate their average execution time. The datasets consisted of random matrices with a varying number of dimensions: 50, 100, 200, 400, and 800. Each matrix had 100 samples. We set the latent dimensions for both CCA and PLS to 10. For each dimension, the experiment was repeated 10 times to obtain reliable performance metrics.

Libraries Used:

- CCA-Zoo (version: 2.4.0)
- Scikit-learn (version: 1.3.0)

4.1 Canonical Correlation Analysis:

Figure VII.3 presents the comparison between CCA-Zoo and `scikit-learn` for Canonical Correlation Analysis. We observe that CCA-Zoo exhibits a competitive runtime profile when compared to `scikit-learn` across all dimensions. This is because CCA-Zoo computes CCA in the principal component space, which is more efficient than the standard approach of computing the covariance matrices directly for high dimensional data.

4.2 Partial Least Squares:

The comparison for Partial Least Squares is shown in Figure VII.4. Like the CCA experiment, CCA-Zoo maintains a robust performance profile that is competitive with `scikit-learn`.

The results indicate that CCA-Zoo is an efficient Python package for both CCA and PLS methods, holding its own against the widely-used `scikit-learn` library. These experiments underscore the capability of CCA-Zoo to handle high-dimensional data efficiently, making it a suitable choice for applications in bioinformatics, natural language processing, and other high-dimensional data domains.

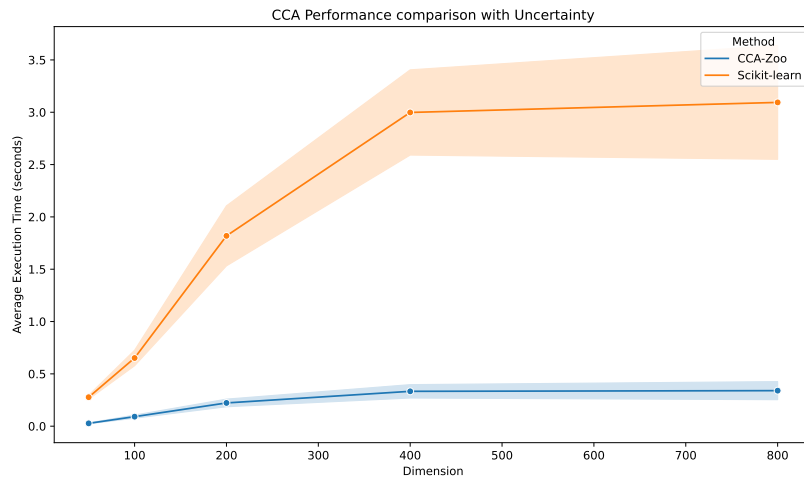


Figure VII.3: Performance comparison for CCA methods

5 Discussion

5.1 Limitations

CCA-Zoo fills a big gap in Python's tools for multiview learning. It makes many multiview learning methods easy to use for Python users. This package works well with known Python libraries like `scikit-learn`, PyTorch, and others, making it user-friendly.

CCA-Zoo is as good as `scikit-learn` in speed, especially for big data tasks in CCA and PLS. This is important for fields like bioinformatics where data is often large.

The package offers various methods, like linear, deep, and probabilistic models, and includes many datasets and tools for picking models and showing results. This makes CCA-Zoo flexible and useful for different tasks.

A key goal of this thesis was to create practical tools for researchers, and CCA-Zoo achieves this. It includes most methods from the thesis, ready for use. This should help more people use and develop multiview learning methods.

5.2 Conclusion

In conclusion, CCA-Zoo is a valuable addition to Python's machine learning tools. It offers a wide range of multiview learning methods in an efficient, easy-to-use

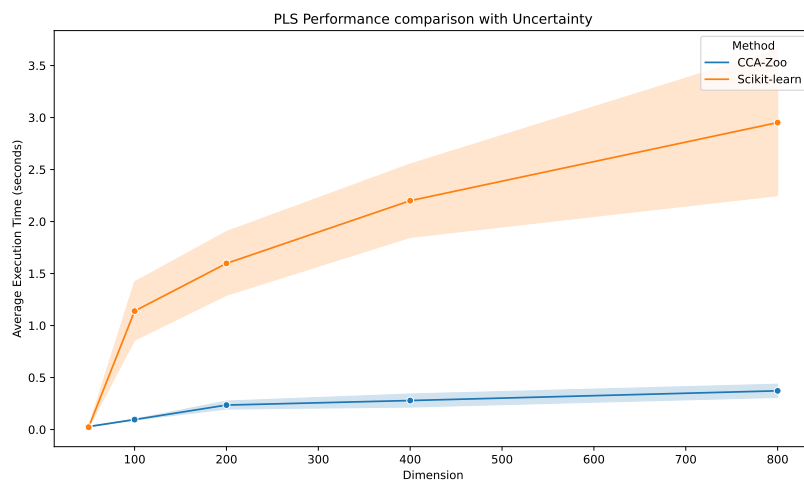


Figure VII.4: Performance comparison for PLS methods

package.

Class Name	Method Name
MCCA	Multiview (Ridge) CCA(Rupnik and Shawe-Taylor, 2010)
CCA	Canonical Correlation Analysis(Hotelling, 1992)
rCCA	Ridge CCA(Vinod, 1976)
PLS	Partial Least SquaresWold, 1975
MPLS	Multiview Partial Least Squares
GCCA	Generalized (Ridge) CCA(Carroll, 1968; A. Tenenhaus and M. Tenenhaus, 2011)
GRCCA	Group Ridge Regularized CCA(Tuzhilina, Tozzi, and Hastie, 2023)
PartialCCA	Partial CCA(Rotman, Vulić, and Reichart, 2018)
PRCCA	(Tuzhilina, Tozzi, and Hastie, 2023)
TCCA	Tensor CCA(Kim, Wong, and Cipolla, 2007)
PCACCA	PCA-CCA(mihali)
SCCA_IPLS	Sparse CCA using Iterative Lasso
ElasticCCA	Elastic CCA using FRALS
PLS_ALS	PLS using Alternating Least Squares
SPLS	Sparse PLS
SCCA_Parkhomenko	Penalized CCA
SCCA_Span	Sparse CCA using Span Bound
CCA_EY	CCA by Eckart-Young
PLS_EY	PLS by Eckart-Young
CCA_GHA	CCA using Generalized Hebbian Algorithm
CCA_SVD	CCA using SVD

Class Name	Method Name
DCCA	Deep CCA
DCCA_GHA	Deep CCA by Generalized Hebbian Algorithm
DCCA_SVD	Deep CCA by SVD
DMCCA	Deep Multiview CCA
DGCCA	Geep Generalised CCA
DCCAE	Deep Canonically Correlated Autoencoders
DCCA NOI	Deep CCA by nonlinear orthogonal iterations
DCCA SDL	Deep CCA by stochastic decorrelation loss
DVCCA	Deep Variational CCA
BarlowTwins	Barlow Twins
VICReg	VICReg
DTCCA	Deep Tensor CCA
DCCA_EY	Deep CCA by Eckart-Young
architectures	

Table 3.4: Class Names and Method Names

Class Name	Method Name
PCCA	Probabilistic CCA
PPLS	Probabilistic PLS

Table 3.5: Class Names and Method Names

Class Name	Method Name
KCCA	Kernel CCA
KPLS	Kernel PLS

Table 3.6: Class Names and Method Names

Class Name	Method Name
ExplainedVarianceDisplay	Explained Variance Display
RepresentationScatterDisplay	Representation Scatter Display
JointRepresentationScatterDisplay	Joint Representation Scatter Display
SeparateRepresentationScatterDisplay	Separate Representation Scatter Display
SeparateJointRepresentationDisplay	Separate Joint Representation Display
PairRepresentationScatterDisplay	Pair Representation Scatter Display
ExplainedCovarianceDisplay	Explained Covariance Display
WeightHeatmapDisplay	Weight Heatmap Display
CorrelationHeatmapDisplay	Correlation Heatmap Display
CovarianceHeatmapDisplay	Covariance Heatmap Display

Table 3.7: Class Names and Method Names for Visualization in CCA-Zoo

Chapter VIII

Thoughts and Implications

This chapter summarizes the main findings of this thesis and discusses their implications. It also discusses the limitations of the work and suggests directions for future research.

1 Summary of findings

2 Implications

Chapter IV has important consequences for the interpretation of CCA models as well as the motivation behind variants of regularized CCA including our own contribution in chapter III. In the context of Linear Regression and Lasso regularization, we can interpret the Lasso as a Bayesian prior on the regression coefficients. In the context of CCA,

3 Future work

3.1 Applications

One of the disappointing aspects of this thesis is that, with the exception of the UK Biobank application in chapter VI, we have not discovered new associations within the limited datasets we have worked with. This is perhaps not surprising given the great popularity of the HCP and ADNI datasets we presented in chapter III. Nonetheless, the scalable methods we have developed in chapters V and VI

are well-suited to the analysis of larger datasets including the UK Biobank and Adolescent Brain Cognitive Development (ABCD) datasets. We worked briefly with the ABCD dataset to explore the possibility of regularisation by proximal gradient descent on regularised versions of the family of objectives we defined in chapter V. These results showed early promise but were too immature to include in this thesis. We expect that the UKBB dataset will be a fruitful source of new associations for the foreseeable future and we believe that the methods we have developed in this thesis will be well-suited to this task. We also hope that by linking CCA to gradient descent, we have opened the door to the application of deep learning methods to CCA. With the great success of deep learning in imaging, text, and other domains, we believe that this is a promising direction for future research. In particular it opens up the possibility of using CCA methods to combine other non-imaging modalities such as Electronic Health Records or audio transcripts with imaging data given the success of the transformer architecture in natural language processing (Vaswani et al., 2017).

3.2 Methods

4 Closing Remarks

Reflecting on my undergraduate years in Engineering Science, I remember struggling to grasp the concepts of Eigenvalues and Eigenvectors.

This now seems like a distant memory as I conclude my doctoral research, immersed in the nuances of a specific class of Eigenvalue problems, and most of all, Canonical Correlation Analysis.

Far from being a narrow topic, understanding this problem has led me to explore a wide variety of topics including optimization, Bayesian statistics, deep learning, and Software Engineering.

With a history stretching back to the 1930s, CCA has been used to discover new associations in a wide variety of domains. We hope that this thesis has illustrated and contributed to the continued relevance of CCA in the modern era of large datasets and deep learning.

Thank you for reading.

Appendices

1 HCP and ADNI Loadings

1.1 Human Connectome Project (HCP) Data

1.1.1 Brain Connectivity Weights and Loadings

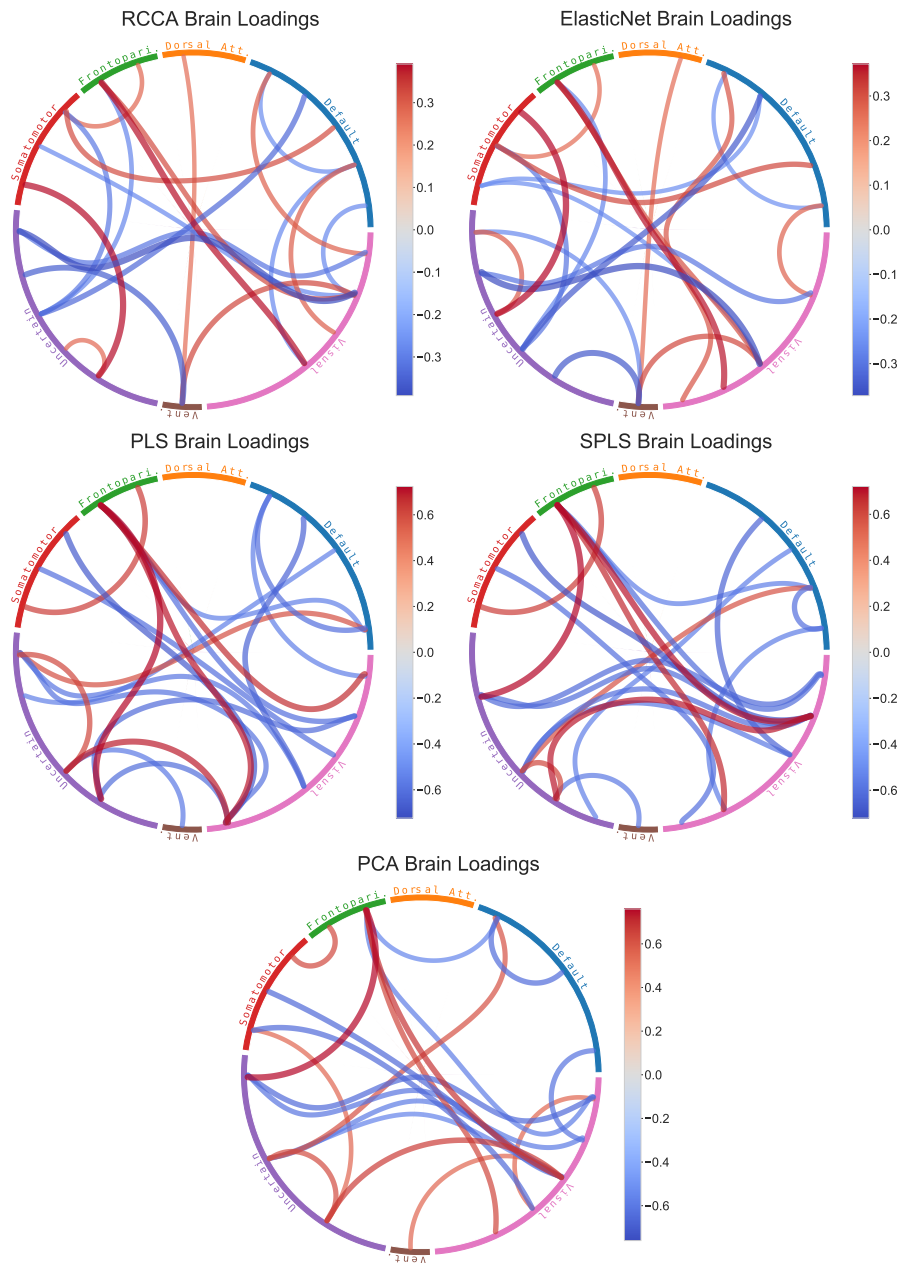
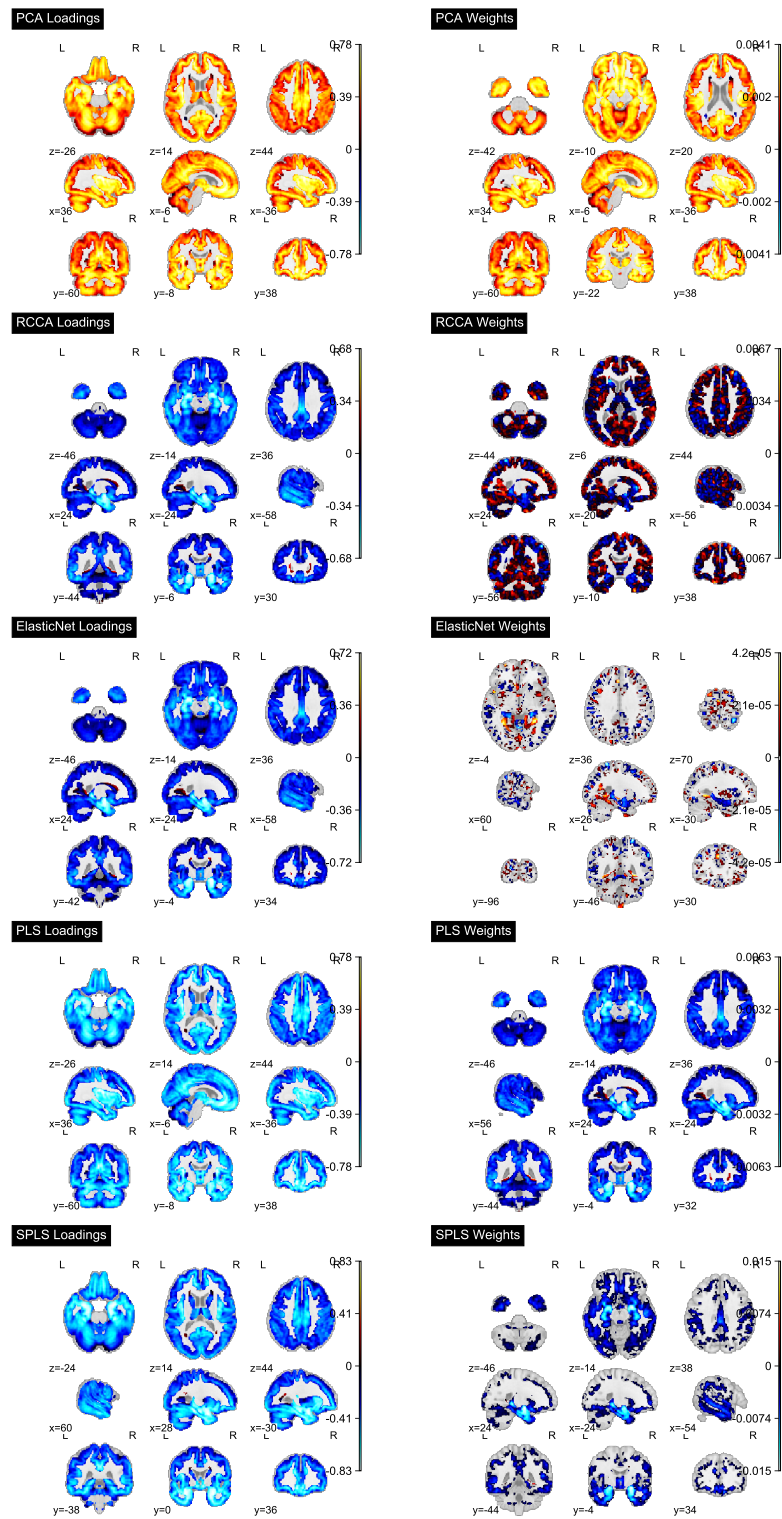


Figure .1: Chord diagrams of the top 8 positive and negative brain loadings for each model.

1.2 Alzheimer's Disease Neuroimaging Initiative (ADNI) Data

1.2.1 Brain Structure Weights and Loadings



2 Eckhart-Young characterization of GEP subspace

2.1 Formal definitions

There are various different notations and conventions for GEPs and SVDs. We largely follow the standard texts on Matrix Analysis (Stewart and J.-G. Sun, 1990; R. Bhatia, 1997) but seek a more careful handling of the equality cases of certain results. To help, we use the following non-standard definitions, largely inspired by Carlsson (2021).

Definition 2.1 (Top- K subspace). *Let the GEP (A, B) on \mathbb{R}^d have eigenvalues $\lambda_1 \geq \dots \geq \lambda_d$. Then a top- K subspace is that spanned by some w_1, \dots, w_K , where w_k is a λ_i -eigenvector of (A, B) for $k = 1, \dots, K$.*

Definition 2.2 (B -orthonormality). *Let $B \in \mathbb{R}^{d \times d}$ be strictly positive definite. Then we say a collection $w_1, \dots, w_K \in \mathbb{R}^d$ of vectors is B -orthonormal if $w_k^T B w_l = \delta_{kl}$ for each $k, l \in \{1, \dots, K\}$.*

Definition 2.3 (Top- K matrix). *We say $W \in \mathbb{R}^{d \times K}$ is a top- K matrix for a GEP (A, B) if the k^{th} column w_i of W is a λ_k -eigenvector for each k and the columns are B -orthonormal.*

2.2 Standard Eckhart–Young inequality

Theorem 2.1 (Eckhart–Young). *Let $M \in \mathbb{R}^{p \times q}$. Then \hat{M} minimises $\|M - \tilde{M}\|_F$ over matrices \tilde{M} of rank at most K if and only if $\hat{M} = A_K R_K B_K^\top$ where (A_K, R_K, B_K) is some top- K SVD of the target M .*

Proof. Let M, \tilde{M} have singular values $\sigma_k, \tilde{\sigma}_k$ respectively. Since \tilde{M} has rank at most K we must have $\tilde{\sigma}_k = 0$ for $k > K$.

Then by von Neumann's trace inequality (Carlsson, 2021),

$$\langle M, \tilde{M} \rangle_F \leq \sum_{k=1}^K \sigma_k \tilde{\sigma}_k$$

with equality if and only if M, \tilde{M} ‘share singular vectors’; the notion of sharing singular vectors is defined as in Carlsson (2021) and in this case means that $\tilde{M} = A_K \tilde{R}_K B_K$ where (A_K, R_K, B_K) is some top- K SVD of M and \tilde{R}_K is a diagonal matrix with decreasing diagonal elements $\tilde{\sigma}_1 \geq \dots \geq \tilde{\sigma}_K$.

Expanding out the objective and applying this inequality gives

$$\begin{aligned}\|\tilde{M} - M\|_F^2 &\geq \sum_{k=1}^d \sigma_k^2 - 2 \sum_{k=1}^K \sigma_k \tilde{\sigma}_k + \sum_{k=1}^K \tilde{\sigma}_k^2 \\ &= \sum_{k=K+1}^d \sigma_k^2 + \sum_{k=1}^K (\sigma_k - \tilde{\sigma}_k)^2 \\ &\geq \sum_{k=K+1}^d \sigma_k^2\end{aligned}$$

so indeed to have equality in both cases requires $\sigma_k = \tilde{\sigma}_k$ for each $k \leq K$ so indeed $\tilde{R}_K = R_K$ and so \hat{M} , as defined in the statement of the theorem, minimises $\|M - \tilde{M}\|_F$ over matrices \tilde{M} of rank at most K . \square

2.3 Supporting Results

Lemma 2.1 (Matrix square root lemma). *Suppose we have two full rank matrices $E, F \in \mathbb{R}^{d \times K}$ where $K \leq d$ and such that $EE^T = FF^T$; then there exists an orthogonal matrix $O \in \mathbb{R}^{K \times K}$ with $E = FO$.*

Proof. Post multiplying the defining condition gives $EE^T E = FF^T E$. Then right multiplying by $(E^T E)^{-1}$ gives

$$E = FF^T E(E^T E)^{-1} =: FO$$

to check that O as defined above is orthogonal we again use the defining condition to compute

$$O^T O = (E^T E)^{-1} E^T F F^T E (E^T E)^{-1} = (E^T E)^{-1} E^T E E^T E (E^T E)^{-1} = I_K$$

\square

Corollary 2.1 (PSD Eckhart–Young for square root matrix). *Let $M \in \mathbb{R}^{d \times d}$ be symmetric positive semidefinite. Then*

$$\arg \min_{\tilde{Z} \in \mathbb{R}^{d \times K}} \|M - \tilde{Z} \tilde{Z}^T\|_F^2$$

is precisely the set of \tilde{Z} of the form $\tilde{Z} = Z_K \Lambda_K^{1/2} O_K$ for some top- K eigenvector-matrix Z_K of the GEP (M, I) and some orthogonal $O_K \in \mathcal{O}(K)$, and where Λ_K is

a diagonal matrix of the top- K eigenvalues.

Proof. First note that when M is positive semi-definite the SVD coincides with the eigendecomposition.

Second note that taking $\tilde{Z} = Z_K \Lambda_K^{1/2} O_K$ attains the minimal value by the Eckhart–Young inequality, Theorem 2.1.

Next note that if \tilde{Z} attains the minimal value then it must have $\tilde{Z}\tilde{Z}^T = Z_K \Lambda_K Z_K^T$ by the equality case of Eckhart–Young. Then by matrix square root Lemma 2.1 we must indeed have $\tilde{Z} = Z_K \Lambda_K^{1/2} O_K$ for some orthogonal O_K . \square

Corollary 2.2 (Symmetric Eckhart–Young for square root matrix). *Let $M \in \mathbb{R}^{d \times d}$ be symmetric with eigenvalues $\lambda_1 \geq \dots \geq \lambda_d$ such that $\lambda_K > 0$. Then*

$$\arg \min_{\tilde{Z} \in \mathbb{R}^{d \times K}} \|M - \tilde{Z}\tilde{Z}^T\|_F^2$$

is precisely the set of \tilde{Z} of the form $\tilde{Z} = Z_K \Lambda_K^{1/2} O_K$ for some top- K eigenvector-matrix Z_K of the GEP (M, I) and some orthogonal $O_K \in \mathcal{O}(K)$, and where Λ_K is a diagonal matrix of the top- K eigenvalues.

Proof. Let $\tilde{Z} \in \mathbb{R}^{d \times K}$. Because M is symmetric it has some eigen-decomposition; separate this into strictly positive and non-positive eigenvalues $M = M_+ + M_- = Z_+ \Lambda_+ Z_+^T + Z_- \Lambda_- Z_-^T$, with rank d_+, d_- respectively. Let the corresponding projections be $P_+ = Z_+ Z_+^T, P_- = Z_- Z_-^T$.

Now define $\tilde{Z}_+ = P_+ \tilde{Z}, \tilde{Z}_- = P_- \tilde{Z}$. Then note by orthogonality of the projections we have for any matrix A that

$$\|A\|^2 = \|(P_+ + P_-)A(P_+ + P_-)\|^2 = \|P_+ A P_+\|^2 + \|P_+ A P_-\|^2 + \|P_- A P_+\|^2 + \|P_- A P_-\|^2$$

So we can expand out

$$\begin{aligned} \|M - \tilde{Z}\tilde{Z}^T\|^2 &= \|(P_+ + P_-)(M - \tilde{Z}\tilde{Z}^T)(P_+ + P_-)\|^2 \\ &= \underbrace{\|M_+ - \tilde{Z}_+ \tilde{Z}_+^T\|^2}_{\geq \sum_{k=K+1}^{d_+} \lambda_k^2} + \underbrace{\|M_- - \tilde{Z}_- \tilde{Z}_-^T\|^2}_{\geq \|M_-\|^2} + \underbrace{\|\tilde{Z}_+ \tilde{Z}_-^T\|^2}_{\geq 0} + \underbrace{\|\tilde{Z}_- \tilde{Z}_+^T\|^2}_{\geq 0} \geq \sum_{k=K+1}^d \lambda_k^2 \end{aligned} \tag{1}$$

where the first inequality follows from the previous Corollary 2.1 and the second

inequality is just from

$$\|M_- - \tilde{Z}_-\tilde{Z}_-^T\|^2 - \|M_-\|^2 = -2 \operatorname{trace}(\tilde{Z}_-^T M_- \tilde{Z}_-) + \|\tilde{Z}_-\tilde{Z}_-^T\|^2 \geq 0$$

because M_- has negative eigenvalues.

Moreover equality in (1) requires the equality case of all the component inequalities; the first gives $\tilde{Z}_+ = Z_K \Lambda_K^{1/2} O_K$ for some Z_K, O_K as in the statement of Corollary 2.1, and the second that $\tilde{Z}_- = 0$; so indeed combining $\tilde{Z} = \tilde{Z}_+ + \tilde{Z}_-$ gives the result. \square

2.4 GEP-EY Objective

Proposition 2.1 (GEP-EY-Objective). *Consider the GEP (A, B) with A symmetric and B positive definite; suppose there are at least K strictly positive (generalized) eigenvalues. Then:*

$$\tilde{W} \in \arg \max_{\tilde{W} \in \mathbb{R}^{d \times k}} \operatorname{trace} \left\{ 2 \left(\tilde{W}^T A \tilde{W} \right) - \left(\tilde{W}^T B \tilde{W} \right) \left(\tilde{W}^T B \tilde{W} \right) \right\}$$

if and only if $\tilde{W} = W_K \Lambda_K^{1/2} O_K$ for some top- K matrix W_K of the GEP and some orthogonal $O_K \in \mathcal{O}(k)$, where Λ_K is a diagonal matrix of the top- K eigenvalues.

Moreover, the maximum value is precisely $\sum_{k=1}^K \lambda_k^2$.

Proof. First recall that there is a bijection between eigenvectors w for the GEP (A, B) and eigenvectors $z = B^{1/2}w$ for the GEP (M, I) where $M := B^{-1/2}AB^{-1/2}$ (e.g. see Chapman, Aguila, and Wells (2022)).

Now consider how the Eckhart–Young objective from Corollary 2.2 transforms under the bijection $Z = B^{1/2}W$.

We get

$$\begin{aligned} \|M - \tilde{Z}\tilde{Z}^T\|_F^2 &= \|B^{-1/2}AB^{-1/2} - B^{1/2}\tilde{W}\tilde{W}^T B^{1/2}\|_F^2 \\ &= \|B^{-1/2}AB^{-1/2}\|_F^2 - 2 \operatorname{trace} \left(B^{-1/2}AB^{-1/2}B^{1/2}\tilde{W}\tilde{W}^T B^{1/2} \right) \\ &\quad + \operatorname{trace} \left(B^{1/2}\tilde{W}\tilde{W}^T B^{1/2} B^{1/2}\tilde{W}\tilde{W}^T B^{1/2} \right) \\ &= \|B^{-1/2}AB^{-1/2}\|_F^2 - \operatorname{trace} \left\{ 2 \left(\tilde{W}^T A \tilde{W} \right) - \left(\tilde{W}^T B \tilde{W} \right) \left(\tilde{W}^T B \tilde{W} \right) \right\}, \end{aligned}$$

where the first term is independent of \tilde{W} , so we can conclude by Corollary 2.2. The moreover conclusion can follow from computing the objective at any max-

imiser of the form above. We note that

$$\begin{aligned}\tilde{W}^T A \tilde{W} &= O_K^T \Lambda_K^{1/2} W_K^T A W_K \Lambda_K O_K = O_K^T \Lambda_K^2 O_K \\ \tilde{W}^T B \tilde{W} &= O_K^T \Lambda_K^{1/2} W_K^T B W_K \Lambda_K O_K = O_K^T \Lambda_K O_K\end{aligned}$$

plugging into the objective gives

$$\text{trace} \left(2 (\tilde{W}^T A \tilde{W}) - (\tilde{W}^T B \tilde{W})^2 \right) = \text{trace} \left(2 O_K^T \Lambda_K^2 O_K - O_K^T \Lambda_K^2 O_K \right) = \sum_{k=1}^K \lambda_k^2$$

because the trace of a symmetric matrix is equal to the sum of its eigenvalues. \square

3 Tractable Optimization - no spurious local minima

First in Section 3.1 we prove that for general A, B our loss $\mathcal{L}_{\text{EY}}(U)$ has no spurious local minima. Then in Section 3.2 we apply a result from Ge, Jin, and Zheng (2017). This application is somewhat crude, and we expect that a quantitative result with tighter constants could be obtained by adapting the argument of Section 3.1; we leave such analysis to future work.

3.1 Qualitative results

First we prove an auxillary result.

Lemma 3.1. *Let $M \in \mathbb{R}^{D \times D}$ be a symmetric matrix and let $U \in \mathbb{R}^{D \times K}$. Let*

$$\hat{\Gamma} := \arg \min_{\Gamma \in \mathbb{R}^{K \times K}} \|M - U\Gamma U^T\|_F^2$$

Then $U\hat{\Gamma}U^T = \mathcal{P}_U M \mathcal{P}_U$ and the minimum value is precisely

$$\|M\|_F^2 - \|\mathcal{P}_U M \mathcal{P}_U\|_F^2 \tag{2}$$

Moreover, if U has orthonormal columns then $\hat{\Gamma} = U^T M U$, and $\|\mathcal{P}_U M \mathcal{P}_U\|_F^2 = \|\hat{\Gamma}\|_F^2$

Proof. Simply complete the square to give

$$\begin{aligned}\|M - U\Gamma U^T\|_F^2 &= \text{trace}(U^T U)\Gamma^T(U^T U)\Gamma - 2 \text{trace } D(U^T M U) + \|M\|_F^2 \\ &= \|(U^T U)^{1/2}\Gamma(U^T U)^{1/2} - (U^T U)^{-1/2}(U^T M U)(U^T U)^{-1/2}\|_F^2 + \|M\|_F^2 - \|\mathcal{P}_U M \mathcal{P}_U\|_F^2\end{aligned}$$

from which we can read off that the minimum is attained precisely when

$$\Gamma = (U^T U)^{-1} (U^T M U) (U^T U)^{-1}$$

and that the optimal value is precisely the value of Equation (2) as claimed. Finally, if U has orthonormal columns, $U^T U = I_K$ so Γ^* is of the form claimed, and the final equality comes from expanding out the trace form of the Frobenius norm. \square

Lemma 3.2. *Let $M \in \mathbb{R}^{D \times D}$ be a symmetric matrix and \mathcal{U} a subspace of \mathbb{R}^D of dimension L . Then there exists an orthonormal basis u_1, \dots, u_L for \mathcal{U} such that*

$$u_L \perp M u_l \text{ for } l \in \{1, \dots, L-1\}$$

Proof. Consider the action of $\tilde{M} := \mathcal{P}_{\mathcal{U}} M \mathcal{P}_{\mathcal{U}}$ on \mathcal{U} . Then \tilde{M} is symmetric matrix whose range is a subspace of \mathcal{U} and so there exists an orthonormal set of eigenvectors u_1, \dots, u_L that give a basis for \mathcal{U} with corresponding eigenvalues $\tilde{\lambda}_1 \geq \dots \geq \tilde{\lambda}_L$. Then we can read off

$$\langle u_L, M u_l \rangle = \langle u_L, \tilde{M} u_l \rangle = \tilde{\lambda}_l \langle u_L, u_l \rangle = 0$$

as required. \square

Proposition 3.1 (No spurious local minima). *The (population) objective \mathcal{L}^{EY} has no spurious local minima. That is, any matrix \bar{W} that is a local minimum of \mathcal{L}^{EY} must in fact be a global minimum of the form described in Proposition 3.1.*

Proof. We shall show that for any matrix W that is not a global optimum, there is a (continuous) path of solutions W_t with:

$$W_0 = W, \quad W_1 = \hat{W}, \quad W_t \rightarrow W \text{ as } t \rightarrow 0, \quad \text{and} \quad \mathcal{L}^{EY}(W_t) < \mathcal{L}^{EY}(W) \forall t > 0$$

As in the proof of Proposition 3.1 we first reduce to the $B = I$ setting by defining $Z := B^{-1/2}W$ and $M = B^{-1/2}AB^{-1/2}$. Let the eigendecomposition of M be $M = V^* D^* V^{*\top}$. Define the loss

$$l(Z) := \|M - ZZ^\top\|_F^2$$

It is now sufficient to show that: for any matrix $Z \in \mathbb{R}^{D \times K}$ that is not of the form $V_K^* D_K^* O_K$ where V_K^* is a matrix whose columns are a set of top- K eigenvectors

for M , and $O_K \in \mathbb{R}^{K \times K}$ is some arbitrary orthogonal matrix cannot be a local minimum.

For notational simplicity we will assume that the $\lambda_K(M) > \lambda_{K+1}(M)$ from now on, such that V_K^* can be made well-defined¹.

Now, take such a Z and suppose, for contradiction that it is a local minimum. We will construct a continuous path of matrices $Z(t) : t \in [0, 1]$ with $Z(0) = Z$ and $l(Z(t)) < l(Z) \forall t > 0$.

Then by our assumption on the form of Z , we have

$$\mathcal{V}_K := \text{span}\{Z\} \neq \text{span}\{V_K^*\} =: \mathcal{V}_K^*$$

Now comes the clever part of the proof. Define $\kappa_{\cap} = \dim \text{span}\{\mathcal{V}_K \cap \mathcal{V}_K^*\}$. Then pick orthonormal bases

- $u_1, \dots, u_{\kappa_{\cap}}$ for $\mathcal{V}_K \cap \mathcal{V}_K^*$
- $u_{\kappa_{\cap}+1}, \dots, u_K$ for $\mathcal{V}_K \cap \mathcal{V}_K^*$ such that $u_k \perp Mu_k$ for all $k = \kappa_{\cap}+1, \dots, K-1$
by Lemma 3.2
- $u_{\kappa_{\cap}+1}^*, \dots, u_K^*$ for $\mathcal{V}_K^* \cap \mathcal{V}_K$

Let $U_K = \begin{pmatrix} & & \\ u_1 & \dots & u_K \end{pmatrix}$. Then by Lemma 3.1, for Z to be a local minimum we must have

$$ZZ^T = U_K(U_K^T M U_K)U_K^T$$

Moreover the objective value must therefore be

$$l(Z) = \|M\|_F^2 - \|U_K^T M U_K\|_F^2 \tag{3}$$

We now make the observation that the second term is the ‘signal of M captured by the subspace of U_K ’. So aligning U_K with higher-eigenvalue subspaces of M should increase this amount of signal captured and decrease this loss.

We now construct a path $U_K(t)$ which captures this intuition.

Let $u_K(t) = \cos(t)u_K + \sin(t)u_K^*$. Then let $U_K(t)$ have columns $u_1, \dots, u_{K-1}, u_K(t)$. By construction this is still an orthonormal set of basis vectors, so $U_K(t)^T U_K = I_K$. Let $\Gamma(t) = U_K(t)^T M U_K(t)$.

¹with symmetry breaking for earlier repeated eigenvalues if required.

We are finally ready to construct the path $Z(t)$. Because U_K is a basis for the column space of Z , and Z is assumed to be a local optimum, we must have

$$ZZ^T = U_K \Gamma(0) U_K^T$$

by Lemma 3.1. So $Z = U_K \Gamma^{1/2} O_K$ for some orthogonal matrix $O_K \in \mathbb{R}^{K \times K}$ where $\Gamma^{1/2}$ is the unique positive semi-definite square root of Γ . So define

$$Z(t) = U_K(t) \Gamma(t)^{1/2} O_K$$

where again $\Gamma(t)^{1/2}$ is the unique positive semi-definite square root and therefore both $U_K(t)$ and $\Gamma(t)^{1/2}$ are continuous functions of t and therefore so is Z .

Then

$$l(Z(t)) = \|M\|_F^2 - \|U_K(t)^T M U_K(t)\|_F^2 \quad (4)$$

So it is sufficient to show that $\|U_K(t)^T M U_K(t)\|_F^2 > \|U_K^T M U_K\|_F^2$ for $t \in [0, \pi/2]$. Indeed, we can compute

$$\begin{aligned} \|U_K(t)^T M U_K(t)\|_F^2 - \|U_K^T M U_K\|_F^2 &= (u_K(t)^T M u_K(t))^2 - (u_K^T M u_K)^2 \\ &\quad + 2 \sum_{k=1}^{K-1} \left\{ (u_K(t)^T M u_k)^2 - (u_K^T M u_k)^2 \right\} \\ &\geq (u_K(t)^T M u_K(t))^2 - (u_K^T M u_K)^2 \end{aligned}$$

because $u_K^T M u_k = 0$ for $k = 1, \dots, K-1$ by construction. Finally we have

$$\begin{aligned} u_K(t)^T M u_K(t) &= \sin^2(t) \langle u_K^*, M u_K^* \rangle + 2 \sin(t) \cos(t) \langle u_K, M u_K^* \rangle + \cos^2(t) \langle u_K, M u_K \rangle \\ &= \sin^2(t) \langle u_K^*, M u_K^* \rangle + \cos^2(t) \langle u_K, M u_K \rangle \\ &> u_K^T M u_K \end{aligned}$$

Here we used that $\langle u_K^*, M u_K^* \rangle \geq \lambda_K > \langle u_K, M u_K \rangle$ and that the middle term vanishes because $M u_K^* \in \mathcal{U}_K^*$ and is therefore orthogonal to u_K .

□

3.2 Quantitative results

To use the results from Ge, Jin, and Zheng (2017) we need to introduce their definition of a (θ, γ, ζ) -strict saddle.

Definition 3.1. We say function $l(\cdot)$ is a (θ, γ, ζ) -**strict saddle** if for any x , at least one of the following holds:

1. $\|\nabla l(x)\| \geq \theta$
2. $\lambda_{\min}(\nabla^2 l(x)) \leq -\gamma$
3. x is ζ -close to \mathcal{X}^* - the set of local minima.

We can now state restate Lemma 13 from Ge, Jin, and Zheng (2017) in our notation; this was used in their analysis of robust PCA, and directly applies to our PCA-type formulation.

Lemma 3.3 (Strict saddle for PCA). Let $M \in \mathbb{R}^{D \times D}$ be a symmetric PSD matrix, and define the matrix factorization objective over $Z \in \mathbb{R}^{D \times K}$

$$l(Z) = \|M - ZZ^\top\|^2$$

Assume that $\lambda_K^* := \lambda_K(M) \geq 15\lambda_{K+1}(M)$. Then

1. all local minima satisfy $ZZ^\top = \mathcal{P}_K(M)$ - the best rank- K approximation to M
2. the objective $l(Z)$ is $(\epsilon, \Omega(\lambda_K^*), \mathcal{O}(\epsilon/\lambda_K^*))$ -strict saddle.

However, we do not want to show a strict saddle of l but of $\mathcal{L}_{\text{EY}} : U \mapsto l(B^{1/2}U)$. Provided that B has strictly positive minimum and bounded maximum eigenvalues this implies that \mathcal{L}_{EY} is also strict saddle, as we now make precise.

Lemma 3.4 (Change of variables for strict saddle conditions). Suppose that l is (θ, γ, ζ) -strict saddle and let $L : U \mapsto l(B^{1/2}U)$ for B with minimal and maximal eigenvalues $\sigma_{\min}, \sigma_{\max}$ respectively.

Then L is $(\sigma_{\max}^{1/2}\theta, \sigma_{\min}\gamma, \sigma_{\max}^{1/2}\zeta)$ -strict saddle.

Proof. Write $g(U) = B^{1/2}U$. Then $L = l \circ g$, so by the chain rule:

$$D_U L = D_{B^{1/2}U} l \circ D_U g : \delta U \mapsto \langle \nabla l(B^{1/2}U), B^{1/2}\delta U \rangle = \langle B^{1/2}\nabla l(B^{1/2}U), \delta U \rangle$$

Therefore

$$\|\nabla L(U)\| = \|B^{1/2}\nabla l(B^{1/2}U)\| \geq \sigma_{\min}^{1/2}\|l(B^{1/2}U)\|$$

By a further application of the chain rule we have

$$D_U^2 L : \delta U, \delta U \mapsto D_{B^{1/2}U}^2 l(B^{1/2}\delta U, B^{1/2}\delta U)$$

Suppose $\lambda_{\min}(\nabla^2 l(Z)) \leq -\gamma$ then by the variational characterization of eigenvalues, there exists some δZ such that $\langle \delta Z, \nabla^2 l(Z)\delta Z \rangle \leq -\gamma \|\delta Z\|^2$. Then taking $\delta U = B^{-1/2}\delta Z$ gives

$$\begin{aligned} \langle \delta U, \nabla^2 L(U)\delta U \rangle &= \langle B^{1/2}\delta U, \nabla^2 l(B^{1/2}U)B^{1/2}\delta U \rangle \\ &= \langle \delta Z, \nabla^2 l(Z)\delta Z \rangle \\ &\leq -\gamma \|\delta Z\|^2 \\ &\leq -\gamma \sigma_{\min} \|\delta U\|^2 \end{aligned}$$

Thirdly, suppose that $\|B^{1/2}U - Z^*\| \leq \zeta$ for some local optimum Z^* of l . Then since B is invertible, $U^* := B^{-1/2}Z^*$ is a local optimum of L . In addition:

$$\|U - U^*\| = \|B^{1/2}(U - U^*)\| \leq \sigma_{\max}^{1/2} \|B^{1/2}U - Z^*\| \leq \zeta$$

Finally, consider some arbitrary point U_0 . Let $Z_0 = B^{1/2}U_0$. Then by the strict saddle property for l one of the following must hold:

1. $\|\nabla l(Z_0)\| \geq \theta \implies \|\nabla L(U_0)\| \geq \sigma_{\min}^{1/2}\theta$
2. $\lambda_{\min}(\nabla^2 l(Z_0)) \leq -\gamma \implies \lambda_{\min}(\nabla^2 L(U_0)) \leq -\sigma_{\min}\gamma$
3. Z_0 is ζ -close to a local-minimum Z^* , which implies that U_0 is $(\sigma_{\max}^{1/2}\zeta)$ -close to a local minimum $B^{-1/2}Z^*$ of L .

□

By combining Lemma 3.3 with Lemma 3.4, we can conclude that our objective does indeed satisfy a (quantitative) strict saddle property. This is sufficient to show that certain local search algorithms will converge in polynomial time Ge, Jin, and Zheng, 2017.

4 Fast updates for (Multi-view) Stochastic CCA (and PLS)

4.1 Back-propagation for empirical covariances

To help us analyse the full details of back-propagation in the linear case, we first prove a lemma regarding the gradients of the empirical covariance operator.

Lemma 4.1 (Back-prop for empirical covariance). *Let $e \in \mathbb{R}^M, f \in \mathbb{R}^M$. Then $\widehat{\text{Cov}}(e, f)$ and*

$$\frac{\partial \widehat{\text{Cov}}(e, f)}{\partial e}$$

can both be computed in $\mathcal{O}(M)$ time.

Proof. Let $1_M \in \mathbb{R}^M$ be a vector of ones and $\mathcal{P}_{1_M}^\perp = I_M - \frac{1}{M}1_M^T1_M$ be the projection away from this vector, then we can write $\bar{e} = \mathcal{P}_{1_M}^\perp e, \bar{f} = \mathcal{P}_{1_M}^\perp f$. Moreover, exploiting the identity-plus-low-rank structure of $\mathcal{P}_{1_M}^\perp$ allows us to compute these quantities in $\mathcal{O}(M)$ time.

Then by definition

$$\widehat{\text{Cov}}(e, f) = \frac{1}{M-1}\bar{e}^T\bar{f}$$

which is again computable in $\mathcal{O}(M)$ time.

For the backward pass, first note that

$$\frac{\partial \bar{e}}{\partial e} : \delta e \mapsto \mathcal{P}_{1_M}^\perp \delta e$$

So the derivative with respect to e is

$$\frac{\partial \widehat{\text{Cov}}(e, f)}{\partial e} = \frac{1}{M-1} \frac{\partial \bar{e}^T \bar{f}}{\partial e} = \frac{1}{M-1} \left(\frac{\partial \bar{e}}{\partial e} \bar{f} \right) = \frac{1}{M-1} \mathcal{P}_{1_M}^\perp \bar{f} = \frac{1}{M-1} \bar{f}$$

because \bar{f} is independent of e , and already mean-centred. So all that remains is element-wise division, which again costs $\mathcal{O}(M)$ time. \square

Forward Pass

1. **Compute the transformed variables \mathbf{Z} :**

$$\mathbf{Z}^{(i)} = U^{(i)} \mathbf{X}^{(i)}, \quad (5)$$

with a complexity of $\mathcal{O}(MKD)$.

2. **Compute** $\text{trace } \hat{C}(\theta)[\mathbf{Z}]$: the diagonal elements of \hat{C} are simply

$$\hat{C}_{kk} = \sum_{i \neq j} \widehat{\text{Cov}}(\mathbf{Z}_k^{(i)}, \mathbf{Z}_k^{(j)})$$

which each summand can be computed in $\mathcal{O}(M)$ time, so summing over i, j, k gives total complexity of $\mathcal{O}(I^2KM)$.

3. **Compute** $\hat{V}(\theta)[\mathbf{Z}]$: For $\hat{V}_\alpha[\mathbf{Z}]$:

$$\hat{V}_\alpha(\theta)[\mathbf{Z}] = \sum_i \alpha_i U^{(i)T} U^{(i)} + (1 - \alpha_i) \widehat{\text{Var}}(\mathbf{Z}^{(i)}),$$

each $U^{(i)T} U^{(i)}$ can be computed with a complexity of $\mathcal{O}(D_i K^2)$ and the total cost of evaluating all of these is $\mathcal{O}(K^2 D)$. Each summand in the second term costs $\mathcal{O}(MK^2)$ by Lemma 4.1 so evaluating the full second term costs $\mathcal{O}(IMK^2)$.

4. **Evaluate** $\hat{\mathcal{L}}_{\text{EY}}[\mathbf{Z}, \mathbf{Z}']$:

$$\hat{\mathcal{L}}_{\text{EY}}[\mathbf{Z}, \mathbf{Z}'] = -2 \text{trace } \hat{C}[\mathbf{Z}] + \langle \hat{V}_\alpha[\mathbf{Z}], \hat{V}_\alpha[\mathbf{Z}'] \rangle_F. \quad (6)$$

The dominant complexity here is the $\mathcal{O}(K^2)$ cost of computing the Frobenius inner product.

Backward Pass

1. **Gradient with respect to $\mathbf{Z}^{(i)}$:** Using the chain rule, the gradient will flow back from the final computed value, $\hat{\mathcal{L}}_{\text{EY}}[\mathbf{Z}, \mathbf{Z}']$, through the operations that produced it.

2. **Gradient of trace $\hat{C}(\theta)[\mathbf{Z}]$ with respect to $\mathbf{Z}_k^{(i)}$:** Is precisely

$$\frac{\partial \hat{C}_{kk}}{\partial \mathbf{Z}_k^{(i)}} = \frac{2}{M-1} \sum_{j \neq i} \bar{\mathbf{Z}}_k^{(j)},$$

where $\bar{\mathbf{Z}}_k^{(j)} = \mathcal{P}_{1_M}^\perp \bar{\mathbf{Z}}_k^{(j)}$, from Lemma 4.1 and so can be computed in $\mathcal{O}(IM)$ time.

3. **Gradients of $\langle \hat{V}_\alpha[\mathbf{Z}], \hat{V}_\alpha[\mathbf{Z}'] \rangle_F$ with respect to $\mathbf{Z}_k^{(i)}$:** By applying Lemma 4.1, the gradient of the empirical variance term is

$$\frac{\partial \widehat{\text{Var}}(\mathbf{Z}^{(i)})_{l,l'}}{\partial \mathbf{Z}_k^{(i)}} = \begin{cases} \frac{2}{M-1} \mathbf{Z}_k^{(i)} & \text{if } l = l' = k \\ \frac{1}{M-1} \mathbf{Z}_l^{(i)} & \text{if } l \neq l' = k \\ 0 & \text{otherwise.} \end{cases}$$

and so

$$\begin{aligned} \frac{\partial \langle \hat{V}_\alpha[\mathbf{Z}], \hat{V}_\alpha[\mathbf{Z}'] \rangle_F}{\partial \mathbf{Z}_k^{(i)}} &= \frac{(1 - \alpha_i)}{M-1} \left(2\hat{V}_\alpha[\mathbf{Z}']_{kk} \mathbf{Z}_k^{(i)} + \sum_l (\hat{V}_\alpha[\mathbf{Z}']_{lk} \mathbf{Z}_l^{(i)} + \hat{V}_\alpha[\mathbf{Z}']_{kl} \mathbf{Z}_k^{(i)}) \right) \\ &= \frac{2(1 - \alpha_i)}{M-1} \sum_{l=1}^K \hat{V}_\alpha[\mathbf{Z}']_{lk} \mathbf{Z}_l^{(i)} \end{aligned}$$

this can be computed in $\mathcal{O}(MK)$ time.

4. **Gradients of $\hat{\mathcal{L}}_{\text{EY}}[\mathbf{Z}, \mathbf{Z}']$ with respect to $\mathbf{Z}_k^{(i)}$:** can therefore be computed for a given $\mathbf{Z}_k^{(i)}$ in $\mathcal{O}(M(K+I))$ time and so, adding up over all i, k gives total $\mathcal{O}(IM(K+I))$ time.

5. **Gradients of $\langle \hat{V}_\alpha[\mathbf{Z}], \hat{V}_\alpha[\mathbf{Z}'] \rangle_F$ with respect to $U_k^{(i)}$:** is similarly

$$\frac{2\alpha_i}{M-1} \sum_{l=1}^K (\hat{V}_\alpha[\mathbf{Z}]_{lk} + \hat{V}_\alpha[\mathbf{Z}']_{lk}) U_l^{(i)}$$

so can be computed in $\mathcal{O}(D_i K)$ time.

6. **Finally compute gradients with respect to $U_k^{(i)}$:** simply have $Z_k^{(i)} =$

$U_k^{(i)^\top} \mathbf{X}^{(i)}$ so the final gradients are

$$\frac{\partial \hat{\mathcal{L}}_{\text{EY}}}{\partial U_k^{(i)}} = \left(\frac{\partial \hat{\mathcal{L}}_{\text{EY}}}{\partial \mathbf{Z}_k^{(i)}} \right)^\top \mathbf{X}^{(i)} + \frac{\partial \langle \hat{V}_\alpha[\mathbf{Z}], \hat{V}_\alpha[\mathbf{Z}'] \rangle_F}{\partial U_k^{(i)}} \quad (7)$$

so the dominant cost is the $\mathcal{O}(MD_i)$ multiplication.

Since $D \gg K, M$, the dominant cost each final gradient is $\mathcal{O}(MD_i)$. Summing up over i, k gives total cost $\mathcal{O}(KM \sum D_i) = \mathcal{O}(KMD)$, as claimed.

5 Eckhart-Young loss recovers Deep CCA

Lemma 3.1. [Objective recovers Deep Multi-view CCA] Assume that there is a final linear layer in each neural network $f^{(i)}$. Then at any local optimum, $\hat{\theta}$, of the population problem, we have

$$\mathcal{L}_{\text{EY}}(\hat{\theta}) = -\|\text{MCCA}_K(\hat{Z})\|_2^2$$

where $\hat{Z} = f_{\hat{\theta}}(X)$. Therefore, $\hat{\theta}$ is also a local optimum of objectives from Andrew et al., 2013; Somandepalli et al., 2019 as defined in Equation (VI.1).

Proof. Write $f^{(i)}(X^{(i)}; \theta^{(i)}) = U^{(i)T} g^{(i)}(X^{(i)}; \phi^{(i)})$ where the $U^{(i)}$ are matrices parameterising the final layer and $g^{(i)}$ defines the representations in the penultimate layer.

Because $\hat{\theta}$ is a local minimum of $\mathcal{L}_{\text{EY}}(\theta)$ we must have \hat{U} a local minimum of the map $l : U \mapsto \mathcal{L}_{\text{EY}}((U, \hat{\phi}))$. Writing $\hat{Y} = g(X; \hat{\phi})$ for the corresponding penultimate-layer representations we get

$$\begin{aligned} l(U) := \mathcal{L}_{\text{EY}}((U, \hat{\phi})) &= -2 \operatorname{trace} \left(\sum_{i \neq j} \operatorname{Cov}(U^{(i)T} \hat{Y}^{(i)}, U^{(j)T} \hat{Y}^{(j)}) \right) + \left\| \sum_i \operatorname{Var}(U^{(i)T} \hat{Y}^{(i)}) \right\|_F^2 \\ &= -2 \operatorname{trace} \left(U^T A(\hat{Y}) U \right) + \|U^T B(\hat{Y}) U\|_F^2 \end{aligned}$$

where $A(\hat{Y}), B(\hat{Y})$ are as in Equation (II.31) with X replaced by \hat{Y} . This is precisely our Eckhart-Young loss for linear CCA on the \hat{Y} . So by Proposition 3.2, \hat{U} must also be a global minimum of $l(U)$ and then by Proposition 3.1 the optimal value is precisely $-\|\text{MCCA}_K(\hat{Y})\|_2^2$.

This in turn is equal to $-\|\text{MCCA}_K(\hat{Z})\|_2^2$ by a simple sandwiching argument. Indeed, by Proposition 3.1 $\min_V \mathcal{L}_{\text{EY}}((V^{(i)T} X^{(i)})_i) = -\|\text{MCCA}_K(\hat{Z})\|_2^2$. Then we can chain inequalities

$$\begin{aligned} -\|\text{MCCA}_K(\hat{Y})\|_2^2 &= \mathcal{L}_{\text{EY}}(\hat{Z}) \geq \min_V \mathcal{L}_{\text{EY}}((V^{(i)T} X^{(i)})_i) \\ &\geq \min_U \mathcal{L}_{\text{EY}}((U^{(i)T} \hat{Y}^{(i)})_i) = -\|\text{MCCA}_K(\hat{Y})\|_2^2 \end{aligned}$$

to conclude. \square

5.1 Interlacing results

First we state a standard result from matrix analysis. This is simply Theorem 2.1 from Haemers (1995), but with notation changed to match our context. We therefore omit the (straightforward) proof.

Lemma 5.1. *Let $Z \in \mathbb{R}^{D \times K}$ such that $Z^T Z = I_K$ and let $M \in \mathbb{R}^{D \times D}$ be symmetric with an orthonormal set of eigenvectors v_1, \dots, v_D with eigenvalues $\lambda_1 \geq \dots \geq \lambda_D$. Define $C = Z^T M Z$, and let C have eigenvalues $\mu_1 \geq \dots \geq \mu_K$ with respective eigenvectors $y_1 \dots y_K$.*

Then

- $\mu_k \leq \lambda_k$ for $k = 1, \dots, K$.
- if $\mu_k = \lambda_k$ for some k then C has a μ_k -eigenvector y such that Zy is a μ_k -eigenvector of M .
- if $\mu_k = \lambda_k$ for $k = 1, \dots, K$ then Zy_k is a μ_k -eigenvector of M for $k = 1, \dots, K$.

This immediately gives us a related result for generalized eigenvalues.

Corollary 5.1 (Generalized Eigenvalue Interlacing). *Consider the GEP (A, B) where $A \in \mathbb{R}^{D \times D}$ is symmetric and $B \in \mathbb{R}^{D \times D}$ symmetric positive definite; let these have B -orthonormal generalized eigenvectors u_1, \dots, u_D with eigenvalues $\lambda_1, \dots, \lambda_D$.*

Let $U \in \mathbb{R}^{D \times K}$ such that $U^T B U = I_K$, define $C = U^T A U$, and let C have eigenvalues $\mu_1 \geq \dots \geq \mu_K$ with respective eigenvectors $y_1 \dots y_K$.

Then

- $\mu_k \leq \lambda_k$ for $k = 1, \dots, K$.
- if $\mu_k = \lambda_k$ for some k then (C, V) has a μ_k -generalised-eigenvector y such that Uy is a μ_k -generalised-eigenvector of (A, B) .
- if $\mu_k = \lambda_k$ for $k = 1, \dots, K$ then Uy_k is a μ_k -generalised-eigenvector of (A, B) for $k = 1, \dots, K$.

Proof. As in previous appendices, we convert from the GEP (A, B) to an eigenvalue problem for $M := B^{-1/2} A B^{-1/2}$ by defining $Z = B^{-1/2} U$, and $v_d = B^{1/2} u_d$.

We now check that the conditions and conclusions of Lemma 5.1 biject with the conditions and conclusions of this present lemma.

Indeed $(u_d)_d$ are B -orthonormal gevectors of (A, B) if and only if $(v_d)_d$ are orthonormal evecors of M ; the matrices C and then coincide and so does its eigenvectors and eigenvalues.

This proves the result. \square

We can now apply this to the Multi-view CCA problem, generalising the two-view case.

Lemma 5.2 (Interlacing for MCCA). *Let $(X^{(i)})_{i=1}^I$ be random vectors taking values in \mathbb{R}^{D_i} respectively, as in Section 2. Take arbitrary full-rank weight matrices $U^{(i)} \in \mathbb{R}^{D_i \times K}$ for $i \in \{1, \dots, I\}$ and define the corresponding transformed variables $Z^{(i)} = \langle U^{(i)}, X^{(i)} \rangle$. Then we have the element-wise inequalities*

$$\text{MCCA}_K(Z^{(i)}, \dots, Z^{(I)}) \leq \text{MCCA}_K(X^{(1)}, \dots, X^{(I)}) \quad (8)$$

Moreover simultaneous equality in each component holds if and only if there exist matrices $Y^{(i)} \in \mathbb{R}^{K \times K}$ for $i \in [I]$ such that the $(U^{(i)} Y^{(i)})_{i=1}^I$ are a set of top- K weights for the MCCA problem.

Proof. Let the matrices A, B be those from the MCCA GEP in Equation (II.31) defined by the input variables X . By definition, $\text{MCCA}_K(X^{(1)}, \dots, X^{(I)})$ is precisely the vector of the top- K such generalised eigenvalues.

Then the corresponding matrices defining the GEP for Z are block matrices \bar{A}, \bar{B} defined by the blocks

$$\begin{aligned} \bar{A}^{(ij)} &= \text{Cov}(Z^{(i)}, Z^{(j)}) = U^{(i)\top} \text{Cov}(X^{(i)}, X^{(j)}) U^{(j)} \\ \bar{B}^{(ii)} &= \text{Var}(Z^{(i)}) = U^{(i)\top} \text{Var}(X^{(i)}) U^{(i)} \end{aligned} \quad (9)$$

Now define the $D \times (KI)$ block diagonal matrix \tilde{U} to have diagonal blocks $U^{(i)}$. Then the definition from Equation (9) is equivalent to the block-matrix equations $\bar{A} = \bar{U}^T A \bar{U}$, $\bar{B} = \bar{U}^T B \bar{U}$, both in $\mathbb{R}^{(KI) \times (KI)}$. Finally, we define a normalised version $\hat{U} = \bar{U} \bar{B}^{-1/2}$ (possible because B positive definite and \bar{U} of full rank).

We can now apply the eigenvalue interlacing result of Corollary 5.1 to the GEP (A, B) and B -orthonormal matrix $\hat{U} \in \mathbb{R}^{D \times IK}$. Let the matrix $\bar{B}^{-1/2} \bar{A} \bar{B}^{-1/2} = \hat{U}^T A \hat{U}$ have top- K eigenvalues $\rho_1 \geq \dots \geq \rho_K$ with respective eigenvectors y_1, \dots, y_K . Then the $(\rho_k)_{k=1}^K$ are precisely the first K successive multi-view correlations between the $Z^{(i)}$. As before, the first K successive multi-view correlations ρ_k^* between the $X^{(i)}$ are precisely the first K generalised eigenvalues of the GEP

(A, B) . We therefore we have the element-wise inequalities $\rho_k \leq \rho_k^*$ for each $k = 1, \dots, K$.

Moreover, equality for each of the top- K multi-view correlations implies that $\hat{U}y_k$ is a generalised-eigenvector of the original GEP (A, B) for $k = 1, \dots, K$ (still by Corollary 5.1). Letting $Y^{(i)} = \begin{pmatrix} y_1^{(i)} & \dots & y_K^{(i)} \end{pmatrix}$ then gives the equality case statement.

□

References

- Adams, Rick et al. (n.d.). "Voxel-wise multivariate analysis of brain-psychosocial associations in adolescents reveals six latent dimensions of cognition and psychopathology". In: *Biological Psychiatry: Cognitive Neuroscience and Neuroimaging* ().
- Akaho, Shotaro (2006). "A kernel method for canonical correlation analysis". In: *arXiv preprint cs/0609071*.
- Ali, Alnur, Edgar Dobriban, and Ryan Tibshirani (2020). "The implicit regularization of stochastic gradient flow for least squares". In: *International conference on machine learning*. PMLR, pp. 233–244.
- Alpert, Mark I and Robert A Peterson (1972). "On the interpretation of canonical analysis". In: *Journal of marketing Research* 9.2, pp. 187–192.
- Altmann, Andre et al. (2023). "Tackling the dimensions in imaging genetics with CLUB-PLS". In: *arXiv preprint arXiv:2309.07352*.
- Amari, Shun-ichi (1993). "Backpropagation and stochastic gradient descent method". In: *Neurocomputing* 5.4-5, pp. 185–196.
- Andrew, Galen et al. (2013). "Deep canonical correlation analysis". In: *International conference on machine learning*. PMLR, pp. 1247–1255.
- Arora, Raman, Andrew Cotter, et al. (2012). "Stochastic optimization for PCA and PLS". In: *2012 50th Annual Allerton Conference on Communication, Control, and Computing (Allerton)*. IEEE, pp. 861–868.
- Arora, Raman, Poorya Mianjy, and Teodor Marinov (2016). "Stochastic optimization for multiview representation learning using partial least squares". In: *International Conference on Machine Learning*. PMLR, pp. 1786–1794.
- Ashburner, John et al. (2014). "SPM12 manual". In: *Wellcome Trust Centre for Neuroimaging, London, UK* 2464.4.

- Bach, Francis R and Michael I Jordan (2005). "A probabilistic interpretation of canonical correlation analysis". In: URL: <https://statistics.berkeley.edu/sites/default/files/tech-reports/688.pdf>.
- Balakrishnama, Suresh and Aravind Ganapathiraju (1998). "Linear discriminant analysis-a brief tutorial". In: *Institute for Signal and information Processing* 18.1998, pp. 1–8.
- Baldassarre, Luca, Janaina Mourao-Miranda, and Massimiliano Pontil (2012). "Structured sparsity models for brain decoding from fMRI data". In: *2012 Second International Workshop on Pattern Recognition in NeuroImaging*. IEEE, pp. 5–8.
- Balestriero, Randall, Mark Ibrahim, et al. (2023). "A Cookbook of Self-Supervised Learning". In: *arXiv preprint arXiv:2304.12210*.
- Balestriero, Randall and Yann LeCun (2022). "Contrastive and non-contrastive self-supervised learning recover global and local spectral embedding methods". In: *arXiv preprint arXiv:2205.11508*.
- Bardes, Adrien, Jean Ponce, and Yann LeCun (2021). "Vicreg: Variance-invariance-covariance regularization for self-supervised learning". In: *arXiv preprint arXiv:2105.04906*.
- Benton, Adrian et al. (2017). "Deep generalized canonical correlation analysis". In: *arXiv preprint arXiv:1702.02519*.
- Bhatia, Kush et al. (2018). "Gen-oja: Simple & efficient algorithm for streaming generalized eigenvector computation". In: *Advances in neural information processing systems* 31.
- Bhatia, Rajendra (1997). *Matrix Analysis*. Vol. 169. Graduate Texts in Mathematics. New York, NY: Springer. ISBN: 978-1-4612-6857-4 978-1-4612-0653-8. DOI: 10.1007/978-1-4612-0653-8. URL: <http://link.springer.com/10.1007/978-1-4612-0653-8> (visited on 03/21/2023).
- Biewald, Lukas (2020). *Experiment Tracking with Weights and Biases*. Software available from wandb.com. URL: <https://www.wandb.com/>.
- Bilenko, Natalia Y and Jack L Gallant (2016). "Pyrcca: regularized kernel canonical correlation analysis in python and its applications to neuroimaging". In: *Frontiers in neuroinformatics* 10, p. 49. DOI: 10.3389/fninf.2016.00049.
- Bogdan, Paul C et al. (2023). "ConnSearch: A framework for functional connectivity analysis designed for interpretability and effectiveness at limited sample sizes". In: *NeuroImage* 278, p. 120274.
- Bogdan, Ryan et al. (2017). "Imaging genetics and genomics in psychiatry: a critical review of progress and potential". In: *Biological psychiatry* 82.3, pp. 165–175.

- Borga, Magnus (1998). "Learning Multidimensional Signal Processing". eng. Publisher: Linköping University Electronic Press. PhD thesis. URL: <http://urn.kb.se/resolve?urn=urn:nbn:se:liu:diva-54341> (visited on 10/13/2022).
- Boyd, Stephen et al. (2011). "Distributed optimization and statistical learning via the alternating direction method of multipliers". In: *Foundations and Trends® in Machine learning* 3.1, pp. 1–122.
- Button, Katherine S et al. (2013). "Power failure: why small sample size undermines the reliability of neuroscience". In: *Nature reviews neuroscience* 14.5, pp. 365–376.
- Bzdok, Danilo, Thomas E Nichols, and Stephen M Smith (2019). "Towards algorithmic analytics for large-scale datasets". In: *Nature Machine Intelligence* 1.7, pp. 296–306.
- Bzdok, Danilo and B.T. Thomas Yeo (2017). "Inference in the age of big data: Future perspectives on neuroscience". In: *NeuroImage* 155, pp. 549–564. ISSN: 1053-8119. DOI: <https://doi.org/10.1016/j.neuroimage.2017.04.061>. URL: <https://www.sciencedirect.com/science/article/pii/S1053811917303816>.
- Carlsson, Marcus (Mar. 2021). "von Neumann's trace inequality for Hilbert–Schmidt operators". en. In: *Expositiones Mathematicae* 39.1, pp. 149–157. ISSN: 0723-0869. DOI: [10.1016/j.exmath.2020.05.001](https://doi.org/10.1016/j.exmath.2020.05.001). URL: <https://www.sciencedirect.com/science/article/pii/S0723086920300220> (visited on 01/04/2023).
- Carroll, J Douglas (1968). "Generalization of canonical correlation analysis to three or more sets of variables". In: *Proceedings of the 76th annual convention of the American Psychological Association*. Vol. 3. Washington, DC, pp. 227–228.
- Chang, Xiaobin, Tao Xiang, and Timothy M Hospedales (2018). "Scalable and effective deep CCA via soft decorrelation". In: *Proceedings of the IEEE Conference on Computer Vision and Pattern Recognition*, pp. 1488–1497.
- Chapman, James, Ana Lawry Aguila, and Lennie Wells (2022). "A Generalized EigenGame with Extensions to Multiview Representation Learning". In: *arXiv preprint arXiv:2211.11323*.
- Chapman, James and Hao-Ting Wang (2021). "CCA-Zoo: A collection of Regularized, Deep Learning based, Kernel, and Probabilistic CCA methods in a scikit-learn style framework". In: *Journal of Open Source Software* 6.68, p. 3823.
- Chapman, James and Lennie Wells (2023). "CCA with Shared Weights for Self-Supervised Learning". In: *NeurIPS 2023 Workshop: Self-Supervised Learning - Theory and Practice*. URL: <https://openreview.net/forum?id=7rYseRZ7Z3>.

- Chapman, James, Lennie Wells, and Ana Lawry Aguila (2023). *Efficient Algorithms for the CCA Family: Unconstrained Objectives with Unbiased Gradients*. arXiv: 2310.01012 [cs.LG].
- Chen, Man-Sheng et al. (2022). “Representation learning in multi-view clustering: A literature review”. In: *Data Science and Engineering* 7.3, pp. 225–241.
- Chen, Mengjie et al. (2013). “Sparse CCA via precision adjusted iterative thresholding”. In: *arXiv preprint arXiv:1311.6186*.
- Chen, Zehui et al. (2019). “On constrained nonconvex stochastic optimization: A case study for generalized eigenvalue decomposition”. In: *The 22nd International Conference on Artificial Intelligence and Statistics*. PMLR, pp. 916–925.
- Cheng, WC, PE Cheng, and M Liou (2013). “Group factor analysis for Alzheimer’s disease”. In: *Computational Mathematics Methods in Medicine* 2013, p. 428385. DOI: 10.1155/2013/428385.
- Chi, Eric C. et al. (2013). “Imaging genetics via sparse canonical correlation analysis”. In: *2013 IEEE 10th International Symposium on Biomedical Imaging*, pp. 740–743. DOI: 10.1109/ISBI.2013.6556581.
- Chun, Hyonho and Sündüz Keleş (2010). “Sparse partial least squares regression for simultaneous dimension reduction and variable selection”. In: *Journal of the Royal Statistical Society Series B: Statistical Methodology* 72.1, pp. 3–25.
- Cruciani, Federica et al. (2022). “What PLS can still do for Imaging Genetics in Alzheimer’s disease”. In: *2022 IEEE-EMBS International Conference on Biomedical and Health Informatics (BHI)*. IEEE, pp. 1–4.
- Cuingnet, Rémi et al. (2012). “Spatial and anatomical regularization of SVM: a general framework for neuroimaging data”. In: *IEEE transactions on pattern analysis and machine intelligence* 35.3, pp. 682–696.
- Curth, Alicia, Alan Jeffares, and Mihaela van der Schaar (2023). “A U-turn on Double Descent: Rethinking Parameter Counting in Statistical Learning”. In: *arXiv preprint arXiv:2310.18988*.
- Da Costa, Victor Guilherme Turrisi et al. (2022). “solo-learn: A Library of Self-supervised Methods for Visual Representation Learning.” In: *J. Mach. Learn. Res.* 23.56, pp. 1–6.
- De Pierrefeu, Amicie et al. (2017). “Structured sparse principal components analysis with the TV-elastic net penalty”. In: *IEEE transactions on medical imaging* 37.2, pp. 396–407.
- Demontis, Ditte et al. (Feb. 2023). “Genome-wide analyses of ADHD identify 27 risk loci, refine the genetic architecture and implicate several cognitive domains”. en. In: *Nat. Genet.* 55.2, pp. 198–208.

- Deng, Lingli et al. (2021). "Sparse PLS-based method for overlapping metabolite set enrichment analysis". In: *Journal of proteome research* 20.6, pp. 3204–3213.
- Dinga, Richard et al. (2019). "Evaluating the evidence for biotypes of depression: Methodological replication and extension of". In: *NeuroImage: Clinical* 22, p. 101796.
- Dohmatob, Elvis Dognima et al. (2014). "Benchmarking solvers for TV-L1 least-squares and logistic regression in brain imaging". In: *2014 International Workshop on Pattern Recognition in Neuroimaging*. IEEE, pp. 1–4.
- Drysdale, Andrew T et al. (2017). "Resting-state connectivity biomarkers define neurophysiological subtypes of depression". In: *Nature medicine* 23.1, pp. 28–38.
- Engl, Heinz Werner, Martin Hanke, and Andreas Neubauer (1996). *Regularization of inverse problems*. Vol. 375. Springer Science & Business Media.
- Ermolov, Aleksandr et al. (2021). "Whitening for self-supervised representation learning". In: *International Conference on Machine Learning*. PMLR, pp. 3015–3024.
- Euesden, Jack, Cathryn M. Lewis, and Paul F. O'Reilly (Dec. 2014). "PRSice: Polygenic Risk Score software". In: *Bioinformatics* 31.9, pp. 1466–1468. ISSN: 1367-4803. DOI: 10.1093/bioinformatics/btu848. eprint: https://academic.oup.com/bioinformatics/article-pdf/31/9/1466/50306478/bioinformatics_31_9_1466.pdf. URL: <https://doi.org/10.1093/bioinformatics/btu848>.
- Ferreira, Fabio S et al. (2022). "A hierarchical Bayesian model to find brain-behaviour associations in incomplete data sets". In: *NeuroImage* 249, p. 118854.
- Fischl, Bruce (Aug. 2012). "FreeSurfer". en. In: *Neuroimage* 62.2, pp. 774–781.
- Folstein, Marshal F, Susan E Folstein, and Paul R McHugh (1975). "“Mini-mental state”: a practical method for grading the cognitive state of patients for the clinician". In: *Journal of psychiatric research* 12.3, pp. 189–198.
- Fu, Xiao et al. (2017). "Scalable and flexible Max-Var generalized canonical correlation analysis via alternating optimization". In: *2017 IEEE International Conference on Acoustics, Speech and Signal Processing (ICASSP)*. IEEE, pp. 5855–5859.
- Galton, Francis (1907). "Vox populi". In: *Nature* 75.1949, pp. 450–451.
- Ge, Rong, Furong Huang, et al. (2015). *Escaping From Saddle Points — Online Stochastic Gradient for Tensor Decomposition*. arXiv: 1503.02101 [cs.LG].
- Ge, Rong, Chi Jin, Praneeth Netrapalli, et al. (2016). "Efficient algorithms for large-scale generalized eigenvector computation and canonical correlation analysis". In: *International Conference on Machine Learning*. PMLR, pp. 2741–2750.

- Ge, Rong, Chi Jin, and Yi Zheng (July 2017). "No Spurious Local Minima in Non-convex Low Rank Problems: A Unified Geometric Analysis". en. In: *Proceedings of the 34th International Conference on Machine Learning*. ISSN: 2640-3498. PMLR, pp. 1233–1242. URL: <https://proceedings.mlr.press/v70/ge17a.html> (visited on 05/16/2023).
- Gemp, Ian, Charlie Chen, and Brian McWilliams (2022). "The Generalized Eigenvalue Problem as a Nash Equilibrium". In: *arXiv preprint arXiv:2206.04993*.
- Gemp, Ian, Brian McWilliams, et al. (2021). *EigenGame Unloaded: When playing games is better than optimizing*. arXiv: 2102.04152 [stat.ML].
- Gemp, Ian M. et al. (2020). "EigenGame: PCA as a Nash Equilibrium". In: *CoRR abs/2010.00554*. arXiv: 2010 . 00554. URL: <https://arxiv.org/abs/2010.00554>.
- Genon, Sarah, Simon B Eickhoff, and Shahrzad Kharabian (2022). "Linking interindividual variability in brain structure to behaviour". In: *Nature Reviews Neuroscience* 23.5, pp. 307–318.
- Ghojogh, Benyamin, Fakhri Karray, and Mark Crowley (2019). "Eigenvalue and generalized eigenvalue problems: Tutorial". In: *arXiv preprint arXiv:1903.11240*.
- Golub, Gene H and Hongyuan Zha (1995). "The canonical correlations of matrix pairs and their numerical computation". In: *Linear algebra for signal processing*. Springer, pp. 27–49. DOI: 10.1007/978-1-4612-4228-4_3.
- Gönen, Mehmet and Ethem Alpaydin (2011). "Multiple kernel learning algorithms". In: *The Journal of Machine Learning Research* 12, pp. 2211–2268.
- Goyal, Priya et al. (2019). "Scaling and benchmarking self-supervised visual representation learning". In: *Proceedings of the ieee/cvf International Conference on computer vision*, pp. 6391–6400.
- Greenacre, Michael et al. (2022). "Principal component analysis". In: *Nature Reviews Methods Primers* 2.1, p. 100.
- Grosenick, Logan et al. (2013). "Interpretable whole-brain prediction analysis with GraphNet". In: *NeuroImage* 72, pp. 304–321.
- Gu, Fei and Hao Wu (2018). "Simultaneous canonical correlation analysis with invariant canonical loadings". In: *Behaviormetrika* 45, pp. 111–132.
- Guo, Wenzhong, Jianwen Wang, and Shiping Wang (2019). "Deep multimodal representation learning: A survey". In: *ieee Access* 7, pp. 63373–63394.
- Haemers, Willem H. (Sept. 1995). "Interlacing eigenvalues and graphs". en. In: *Linear Algebra and its Applications* 226-228, pp. 593–616. ISSN: 00243795. DOI: 10 . 1016/0024-3795(95)00199-2. URL: <https://linkinghub.elsevier.com/retrieve/pii/0024379595001992> (visited on 10/11/2022).

- Haroon, David R, Janaina Mourao-Miranda, et al. (2007). “Unsupervised analysis of fMRI data using kernel canonical correlation”. In: *NeuroImage* 37.4, pp. 1250–1259.
- Haroon, David R, Sandor Szedmak, and John Shawe-Taylor (2004). “Canonical correlation analysis: An overview with application to learning methods”. In: *Neural computation* 16.12, pp. 2639–2664. DOI: 10.1162/0899766042321814.
- Hastie, Trevor et al. (2009). *The elements of statistical learning: data mining, inference, and prediction*. Vol. 2. Springer.
- Helmer, Markus et al. (2020). “On stability of Canonical Correlation Analysis and Partial Least Squares with application to brain-behavior associations”. In: *bioRxiv*.
- Höskuldsson, Agnar (1988). “PLS regression methods”. In: *Journal of chemometrics* 2.3, pp. 211–228.
- Hotelling, Harold (1933). “Analysis of a complex of statistical variables into principal components.” In: *Journal of educational psychology* 24.6, p. 417.
- (1935). “Canonical correlation analysis (cca)”. In: *Journal of Educational Psychology*, p. 10.
- (1992). “Relations between two sets of variates”. In: *Breakthroughs in statistics*. Springer, pp. 162–190. DOI: 10.2307/2333955.
- ICML (2023). *ICML 2023*. URL: <https://icml.cc/Conferences/2023/Test-of-Time> (visited on 09/21/2023).
- Ij, H (2018). “Statistics versus machine learning”. In: *Nat Methods* 15.4, p. 233.
- International League Against Epilepsy Consortium on Complex Epilepsies (Dec. 2018). “Genome-wide mega-analysis identifies 16 loci and highlights diverse biological mechanisms in the common epilepsies”. en. In: *Nat. Commun.* 9.1, p. 5269.
- Jack Jr, Clifford R et al. (2008). “The Alzheimer’s disease neuroimaging initiative (ADNI): MRI methods”. In: *Journal of Magnetic Resonance Imaging: An Official Journal of the International Society for Magnetic Resonance in Medicine* 27.4, pp. 685–691.
- Johnstone, Iain M (2001). “On the distribution of the largest eigenvalue in principal components analysis”. In: *The Annals of statistics* 29.2, pp. 295–327.
- Kanai, Ryota and Geraint Rees (2011). “The structural basis of inter-individual differences in human behaviour and cognition”. In: *Nature Reviews Neuroscience* 12.4, pp. 231–242.
- Kanatsoulis, Charilaos I et al. (2018). “Structured SUMCOR multiview canonical correlation analysis for large-scale data”. In: *IEEE Transactions on Signal Processing* 67.2, pp. 306–319.

- Kettenring, Jon R (1971). "Canonical analysis of several sets of variables". In: *Biometrika* 58.3, pp. 433–451.
- Kim, Tae-Kyun, Shu-Fai Wong, and Roberto Cipolla (2007). "Tensor canonical correlation analysis for action classification". In: *2007 IEEE Conference on Computer Vision and Pattern Recognition*. IEEE, pp. 1–8.
- Kingma, Diederik P and Jimmy Ba (2014). "Adam: A method for stochastic optimization". In: *arXiv preprint arXiv:1412.6980*.
- Krishnan, Anjali et al. (2011). "Partial Least Squares (PLS) methods for neuroimaging: a tutorial and review". In: *Neuroimage* 56.2, pp. 455–475.
- Lambert, J C et al. (Dec. 2013). "Meta-analysis of 74,046 individuals identifies 11 new susceptibility loci for Alzheimer's disease". en. In: *Nat. Genet.* 45.12, pp. 1452–1458.
- Lawry Aguila, Ana, James Chapman, and Andre Altmann (2023). "Multi-modal Variational Autoencoders for Normative Modelling Across Multiple Imaging Modalities". In: *International Conference on Medical Image Computing and Computer-Assisted Intervention*. Springer Nature Switzerland Cham, pp. 425–434.
- Lê Cao, Kim-Anh et al. (2008). "A sparse PLS for variable selection when integrating omics data". In: *Statistical applications in genetics and molecular biology* 7.1.
- Le Floch, Édith et al. (2012). "Significant correlation between a set of genetic polymorphisms and a functional brain network revealed by feature selection and sparse Partial Least Squares". In: *NeuroImage* 63.1, pp. 11–24. ISSN: 1053-8119. DOI: <https://doi.org/10.1016/j.neuroimage.2012.06.061>. URL: <https://www.sciencedirect.com/science/article/pii/S1053811912006775>.
- Lindenbaum, Ofir et al. (2021). "L0-sparse canonical correlation analysis". In: *International Conference on Learning Representations*.
- Liu, Jingyu and Vince D Calhoun (2014). "A review of multivariate analyses in imaging genetics". In: *Frontiers in neuroinformatics* 8, p. 29.
- Liu, Zhangdaihong et al. (2022). "Improved Interpretability of Brain-Behavior CCA With Domain-Driven Dimension Reduction". In: *Frontiers in Neuroscience* 16, p. 851827.
- Lorenzi, Marco et al. (2017). "Secure multivariate large-scale multi-centric analysis through on-line learning: an imaging genetics case study". In: *12th International Symposium on Medical Information Processing and Analysis*. Vol. 10160. SPIE, pp. 347–353.
- Luo, Chunjie et al. (2018). "Cosine normalization: Using cosine similarity instead of dot product in neural networks". In: *Artificial Neural Networks and Machine Learning—ICANN 2018: 27th International Conference on Artificial Neural Networks*

- works, Rhodes, Greece, October 4-7, 2018, Proceedings, Part I* 27. Springer, pp. 382–391.
- Lyu, Qi et al. (2021). “Understanding latent correlation-based multiview learning and self-supervision: An identifiability perspective”. In: *arXiv preprint arXiv:2106.07115*.
- Ma, Zhuang, Yichao Lu, and Dean Foster (2015). “Finding linear structure in large datasets with scalable canonical correlation analysis”. In: *International conference on machine learning*. PMLR, pp. 169–178.
- Mackay, David John Cameron (1998). “Introduction to monte carlo methods”. In: *Learning in graphical models*. Springer, pp. 175–204.
- Mackey, Lester (2008). “Deflation methods for sparse PCA”. In: *Advances in neural information processing systems* 21.
- Mai, Qing and Xin Zhang (2019). “An iterative penalized least squares approach to sparse canonical correlation analysis”. In: *Biometrics* 75.3, pp. 734–744. doi: 10.1111/biom.13043.
- Matkovic, Andraz et al. (2023). “The contribution of diverse and stable functional connectivity edges to brain-behavior associations”. In: *bioRxiv*, pp. 2023–11.
- Matkovič, Andraž et al. (2023). “Static and dynamic fMRI-derived functional connectomes represent largely similar information”. In: *Network Neuroscience* 7.4, pp. 1266–1301.
- McIntosh, Anthony R (2021). “Comparison of Canonical Correlation and Partial Least Squares analyses of simulated and empirical data”. In: *arXiv preprint arXiv:2107.06867*.
- Meng, Zihang, Rudrasis Chakraborty, and Vikas Singh (2021). “An Online Riemannian PCA for Stochastic Canonical Correlation Analysis”. In: *Advances in Neural Information Processing Systems* 34, pp. 14056–14068.
- Meredith, William (1964). “Canonical correlations with fallible data”. In: *Psychometrika* 29.1, pp. 55–65.
- Michel, Vincent et al. (2011). “Total variation regularization for fMRI-based prediction of behavior”. In: *IEEE transactions on medical imaging* 30.7, pp. 1328–1340.
- Mihalik, Agoston, James Chapman, Rick A Adams, et al. (2022a). “Canonical correlation analysis and partial least squares for identifying brain-behaviour associations: a tutorial and a comparative study”. In: *Biological Psychiatry: Cognitive Neuroscience and Neuroimaging*.
- Mihalik, Agoston, James Chapman, Rick A. Adams, et al. (Aug. 2022b). “Canonical Correlation Analysis and Partial Least Squares for identifying brain-behaviour associations: a tutorial and a comparative study”. en. In: *Biological Psychiatry: Cognitive Neuroscience and Neuroimaging*. ISSN: 2451-9022. doi: 10.1016/

- j . bpsc . 2022 . 07 . 012. URL: <https://www.sciencedirect.com/science/article/pii/S2451902222001859> (visited on 08/29/2022).
- Mihalik, Agoston, Fabio S Ferreira, Michael Moutoussis, et al. (2020). "Multiple hold-outs with stability: Improving the generalizability of machine learning analyses of brain–behavior relationships". In: *Biological psychiatry* 87.4, pp. 368–376.
- Mihalik, Agoston, Fabio S Ferreira, Maria J Rosa, et al. (2019). "Brain-behaviour modes of covariation in healthy and clinically depressed young people". In: *Scientific reports* 9.1, pp. 1–11.
- Mills-Curran, William C (1988). "Calculation of eigenvector derivatives for structures with repeated eigenvalues". In: *AIAA journal* 26.7, pp. 867–871.
- Miranda, Lucas et al. (2021). "Systematic review of functional MRI applications for psychiatric disease subtyping". In: *Frontiers in Psychiatry* 12, p. 665536.
- Monteiro, João M et al. (2016). "A multiple hold-out framework for Sparse Partial Least Squares". In: *Journal of neuroscience methods* 271, pp. 182–194.
- Mullins, Niamh et al. (June 2021). "Genome-wide association study of more than 40,000 bipolar disorder cases provides new insights into the underlying biology". en. In: *Nat. Genet.* 53.6, pp. 817–829.
- Nalls, Mike A et al. (Dec. 2019). "Identification of novel risk loci, causal insights, and heritable risk for Parkinson's disease: a meta-analysis of genome-wide association studies". en. In: *Lancet Neurol.* 18.12, pp. 1091–1102.
- Nguyen, Nam D and Daifeng Wang (2020). "Multiview learning for understanding functional multiomics". In: *PLoS computational biology* 16.4, e1007677.
- OpenAI (2021). *ChatGPT: A Large-Scale Generative Model for Open-Domain Chat*. <https://github.com/openai/gpt-3>.
- Park, S, Eva Ceulemans, and Katrijn Van Deun (2023). "A critical assessment of sparse PCA (research): why (one should acknowledge that) weights are not loadings". In: *Behavior Research Methods*, pp. 1–20.
- Parkhomenko, Elena, David Tritchler, and Joseph Beyene (2009). "Sparse canonical correlation analysis with application to genomic data integration". In: *Statistical applications in genetics and molecular biology* 8.1, pp. 1–34. DOI: 10.2202/1544-6115.1406.
- Pearl, Judea (2009). *Causality*. Cambridge university press.
- Pedregosa, Fabian et al. (2011). "Scikit-learn: Machine learning in Python". In: *the Journal of machine Learning research* 12, pp. 2825–2830.
- Perekrestenko, Dmytro et al. (2018). "The universal approximation power of finite-width deep ReLU networks". In: *arXiv preprint arXiv:1806.01528*.

- Purcell, Shaun et al. (Sept. 2007). "PLINK: a tool set for whole-genome association and population-based linkage analyses". en. In: *Am. J. Hum. Genet.* 81.3, pp. 559–575.
- Qi, Jun and Javier Tejedor (2016). "Deep multi-view representation learning for multi-modal features of the schizophrenia and schizo-affective disorder". In: *2016 IEEE International Conference on Acoustics, Speech and Signal Processing (ICASSP)*. IEEE, pp. 952–956.
- Reichenbach, Hans (1956). *The direction of time*. Vol. 65. Univ of California Press.
- Rheenen, Wouter van et al. (Dec. 2021). "Common and rare variant association analyses in amyotrophic lateral sclerosis identify 15 risk loci with distinct genetic architectures and neuron-specific biology". en. In: *Nat. Genet.* 53.12, pp. 1636–1648.
- Riffenburgh, Robert Harry (1957). "Linear discriminant analysis". PhD thesis. Virginia Polytechnic Institute.
- Rosipal, Roman and Nicole Krämer (2005). "Overview and recent advances in partial least squares". In: *International Statistical and Optimization Perspectives Workshop" Subspace, Latent Structure and Feature Selection*". Springer, pp. 34–51.
- Rotman, Guy, Ivan Vulić, and Roi Reichart (2018). "Bridging languages through images with deep partial canonical correlation analysis". In: Association for Computational Linguistics.
- Rupnik, Jan and John Shawe-Taylor (2010). "Multi-view canonical correlation analysis". In: *Conference on data mining and data warehouses (SiKDD 2010)*. Vol. 473, pp. 1–4.
- Rypma, Bart and Mark D'Esposito (2001). "Age-related changes in brain-behaviour relationships: Evidence from event-related functional MRI studies". In: *European Journal of Cognitive Psychology* 13.1-2, pp. 235–256.
- Sansone, Emanuele and Robin Manhaeve (2022). "GEDI: GEnerative and DIscriminative Training for Self-Supervised Learning". In: *arXiv preprint arXiv:2212.13425*.
- Smith, Samuel L et al. (2021). "On the origin of implicit regularization in stochastic gradient descent". In: *arXiv preprint arXiv:2101.12176*.
- Smith, Stephen M et al. (2015). "A positive-negative mode of population covariation links brain connectivity, demographics and behavior". In: *Nature neuroscience* 18.11, p. 1565.
- Smith, Stephen M. and Thomas E. Nichols (2018). "Statistical Challenges in "Big Data" Human Neuroimaging". In: *Neuron* 97.2, pp. 263–268. ISSN: 0896-6273.

- DOI: <https://doi.org/10.1016/j.neuron.2017.12.018>. URL: <https://www.sciencedirect.com/science/article/pii/S0896627317311418>.
- Snoek, Cees GM et al. (2005). "Mediamill: Exploring news video archives based on learned semantics". In: *Proceedings of the 13th annual ACM international conference on Multimedia*, pp. 225–226.
- Somandepalli, Krishna et al. (2019). "Multimodal representation learning using deep multiset canonical correlation". In: *arXiv preprint arXiv:1904.01775*.
- Stewart, G. W. and Ji-Guang Sun (July 1990). *Matrix Perturbation Theory*. en. Google-Books-ID: bIYEogEACAAJ. ACADEMIC PressINC. ISBN: 978-1-4933-0199-7.
- Sudlow, Cathie et al. (2015). "UK biobank: an open access resource for identifying the causes of a wide range of complex diseases of middle and old age". In: *PLoS medicine* 12.3, e1001779.
- Sun, Liang, Shuiwang Ji, and Jieping Ye (2008). "A least squares formulation for canonical correlation analysis". In: *Proceedings of the 25th international conference on Machine learning*, pp. 1024–1031.
- Suo, Xiaotong et al. (2017). "Sparse canonical correlation analysis". In: *arXiv preprint arXiv:1705.10865*.
- Taquet, Maxime et al. (June 2021). "A structural brain network of genetic vulnerability to psychiatric illness". en. In: *Mol. Psychiatry* 26.6, pp. 2089–2100.
- Tenenhaus, Arthur and Michel Tenenhaus (2011). "Regularized generalized canonical correlation analysis". In: *Psychometrika* 76.2, p. 257. DOI: 10.1007/s11336-011-9206-8.
- Tipping, Michael E and Christopher M Bishop (1999). "Probabilistic principal component analysis". In: *Journal of the Royal Statistical Society Series B: Statistical Methodology* 61.3, pp. 611–622.
- Tong, Shengbang et al. (2023). "EMP-SSL: Towards Self-Supervised Learning in One Training Epoch". In: *arXiv preprint arXiv:2304.03977*.
- Townsend, Florence, James Chapman, and James Cole (Nov. 2023). *florencejt/fusilli: Fusilli v1.0.0*. Version v1.0.0. DOI: 10.5281/zenodo.10228564. URL: <https://doi.org/10.5281/zenodo.10228564>.
- Trubetskoy, Vassily et al. (Apr. 2022). "Mapping genomic loci implicates genes and synaptic biology in schizophrenia". en. In: *Nature* 604.7906, pp. 502–508.
- Tuzhilina, Elena, Leonardo Tozzi, and Trevor Hastie (2023). "Canonical correlation analysis in high dimensions with structured regularization". In: *Statistical modelling* 23.3, pp. 203–227.

- Uurtio, Viivi et al. (2017). "A tutorial on canonical correlation methods". In: *ACM Computing Surveys (CSUR)* 50.6, pp. 1–33.
- Van Essen, David C et al. (2013). "The WU-Minn human connectome project: an overview". In: *Neuroimage* 80, pp. 62–79.
- Vapnik, Vladimir (1999). *The nature of statistical learning theory*. Springer science & business media.
- Vaswani, Ashish et al. (2017). "Attention is all you need". In: *Advances in neural information processing systems* 30.
- Vinod, Hrishikesh D (1976). "Canonical ridge and econometrics of joint production". In: *Journal of econometrics* 4.2, pp. 147–166.
- Virtanen, Pauli et al. (2020). "SciPy 1.0: fundamental algorithms for scientific computing in Python". In: *Nature methods* 17.3, pp. 261–272.
- Waaijenborg, Sandra, Philip C Verselelewel de Witt Hamer, and Aeilko H Zwinderman (2008). "Quantifying the association between gene expressions and DNA-markers by penalized canonical correlation analysis". In: *Statistical applications in genetics and molecular biology* 7.1.
- Wang, Hao-Ting et al. (2018). "Finding the needle in high-dimensional haystack: A tutorial on canonical correlation analysis". In: *arXiv preprint arXiv:1812.02598*.
- (2020). "Finding the needle in a high-dimensional haystack: Canonical correlation analysis for neuroscientists". In: *NeuroImage* 216, p. 116745.
- Wang, Weiran, Raman Arora, Karen Livescu, and Jeff A Bilmes (2015). "Unsupervised learning of acoustic features via deep canonical correlation analysis". In: *2015 IEEE International Conference on Acoustics, Speech and Signal Processing (ICASSP)*. IEEE, pp. 4590–4594.
- Wang, Weiran, Raman Arora, Karen Livescu, and Nathan Srebro (2015). "Stochastic optimization for deep CCA via nonlinear orthogonal iterations". In: *2015 53rd Annual Allerton Conference on Communication, Control, and Computing (Allerton)*. IEEE, pp. 688–695.
- Wilms, Ines and Christophe Croux (2015). "Sparse canonical correlation analysis from a predictive point of view". In: *Biometrical Journal* 57.5, pp. 834–851.
- Witten, Daniela et al. (2013). "Package ‘pma’". In: *Genetics and Molecular Biology* 8.1, p. 28.
- Witten, Daniela M, Robert Tibshirani, and Trevor Hastie (2009). "A penalized matrix decomposition, with applications to sparse principal components and canonical correlation analysis". In: *Biostatistics* 10.3, pp. 515–534.
- Wold, Herman (1975). "Path models with latent variables: The NIPALS approach". In: *Quantitative sociology*. Elsevier, pp. 307–357.

- Yao, Yuan, Lorenzo Rosasco, and Andrea Caponnetto (2007). “On early stopping in gradient descent learning”. In: *Constructive Approximation* 26, pp. 289–315.
- Yeo, BT Thomas et al. (2011). “The organization of the human cerebral cortex estimated by intrinsic functional connectivity”. In: *Journal of neurophysiology*.
- Zbontar, Jure et al. (2021). “Barlow twins: Self-supervised learning via redundancy reduction”. In: *arXiv preprint arXiv:2103.03230*.
- Zhuang, Xiaowei, Zhengshi Yang, and Dietmar Cordes (2020). “A technical review of canonical correlation analysis for neuroscience applications”. In: *Human Brain Mapping* 41.13, pp. 3807–3833.
- Zong, Yongshuo, Oisin Mac Aodha, and Timothy Hospedales (2023). “Self-Supervised Multimodal Learning: A Survey”. In: *arXiv preprint arXiv:2304.01008*.
- Zou, Hui, Trevor Hastie, and Robert Tibshirani (2006). “Sparse principal component analysis”. In: *Journal of computational and graphical statistics* 15.2, pp. 265–286.
- Zou, Hui and Lingzhou Xue (2018). “A selective overview of sparse principal component analysis”. In: *Proceedings of the IEEE* 106.8, pp. 1311–1320.